

TR 3442J

STELLINGEN

BEHORENDE BIJ HET PROEFSCHRIFT

COMPUTER SIMULATIONS OF COLLOIDAL SUSPENSIONS

USING AN IMPROVED LATTICE-BOLTZMANN SCHEME

VAN M.W. HEEMELS

- i. Geluid kan, op korte tijden, een aanzienlijk oscillatorisch effect hebben op de collectieve dynamica van colloïdale deeltjes in evenwicht, echter, gemiddeld genomen is de invloed nul.
- ii. Colloïdale deeltjes in een suspensie hebben een extra geleidend effect op de voortplantingssnelheid van geluidsgolven door die suspensie.
- iii. De sterke afhankelijkheid van de lengteschaal van de viscositeit in verhouding tot de grootte van de colloïdale deeltjes suggereert dat de viscositeit in een zeer beperkte geometrie, bijvoorbeeld een dunne cilinder, lager is dan in een bulkvoorbeeld van eenzelfde suspensie.
- iv. Het feit dat daders van mishandeling en seksueel geweld de schadevergoeding, die zij hun slachtoffers moeten betalen, kunnen verhalen op hun WA-verzekering, suggereert ten onrechte dat deze bedoeld is voor schade die mensen elkaar aandoen bij geweldmisdrijven.
- v. Gezien de vaak scheve verhouding in wachttijden voor de sanitaire voorzieningen tussen vrouwen en mannen, zou het geen overbodige luxe zijn, als bij goed bezochte evenementen en gelegenheden het aantal van deze voorzieningen voor vrouwen het drievoudige is van dat voor mannen.
- vi. De mobiele telefoon is de methadon van de workaholic.
- vii. Het rijden van een scheve schaats kan het best voorkomen worden door een goed passende schoen.
- viii. Stellingen kun je schrijven na een flink aantal wijntjes, een proefschrift helaas niet.
- ix. Ieder mens draagt op elk moment de uitdrukking op zijn gezicht van wat hij op dat moment voelt, denkt en is.
- x. Anders denken zorgt ervoor dat je uiteindelijk anders gaat zijn.

PROPOSITIONS

- i. Sound may have, on short times, a large oscillating effect on the dynamics of colloidal particles in equilibrium, however, on average the effect is zero.
- ii. Colloidal particles in a suspension have an additional conducting effect on the speed of sound propagating through the suspension.
- iii. The strong dependence on the spatial length scales of the viscosity in relation to the size of the colloidal particles indicates that a colloidal suspension may have a somewhat lower viscosity in a confined geometry, for example a thin tube, than in a bulk sample of the same suspension.
- iv. The fact that offenders of mistreatment and sexual violation may claim the damages they have to pay their victims, from their indemnity insurance, wrongly suggests that this insurance is meant for damage from people injuring each other.
- v. Because of the often unbalanced waiting times for sanitary utilities between women and men, it would not be luxury if, at busy events and occasions, the amount of these utilities for women is the threefold of that of men.
- vi. The mobile telephone is the methadon of the workaholic.
- vii. Riding a crooked skate can be best prevented by a good fitting shoe.
- viii. You may write propositions after lots of wine, a PhD thesis unfortunately not.
- ix. Every person bears the expression on his face at every moment of what he feels, thinks and is.
- x. Start thinking differently eventually results in being differently.

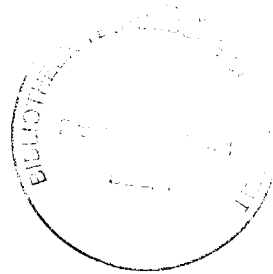
731174

3042/16g

3442

TR3442

COMPUTER SIMULATIONS
OF COLLOIDAL SUSPENSIONS
USING AN IMPROVED
LATTICE-BOLTZMANN SCHEME



PROEFSCHRIFT

ter verkrijging van de graad van doctor
aan de Technische Universiteit Delft,
op gezag van de Rector Magnificus prof. ir. K. F. Wakker,
in het openbaar te verdedigen ten overstaan van een commissie,
door het College voor Promoties aangewezen,
op maandag 13 december 1999 te 10:30 uur
door

Marleen Wilhelmina HEEMELS

natuurkundig ingenieur,
geboren te Roermond

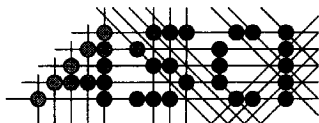
Dit proefschrift is goedgekeurd door de promotor: Prof. dr. S. W. de Leeuw

Toegevoegd promotor: Dr. ir. A. F. Bakker

Samenstelling promotiecommissie:

Rector Magnificus	voorzitter
Prof. dr. S.W. de Leeuw, promotor	Technische Universiteit Delft
Dr. ir. A.F. Bakker, toegevoegd promotor	Technische Universiteit Delft
Prof. dr. ir. H.E.A. van den Akker	Technische Universiteit Delft
Prof. dr. ir. J. Mellema	Universiteit Twente
Prof. ir. C.P.J.W. van Kruijsdijk	Technische Universiteit Delft
Dr. C.P. Lowe	Technische Universiteit Delft
Dr. M.H.J. Hagen	Unilever Research Port Sunlight, United Kingdom

Dr. C. P. Lowe heeft als begeleider in belangrijke mate aan de totstandkoming van het proefschrift bijgedragen.



Advanced School for Computing and Imaging

This work was carried out in graduate school ASCI.
ASCI dissertation series number 47.

ISBN 90-805120-2-8

subject headings: colloids / hydrodynamic interactions / computer simulation

Cover: Some lost colloidal particles, painted by Harry Pennekamp.

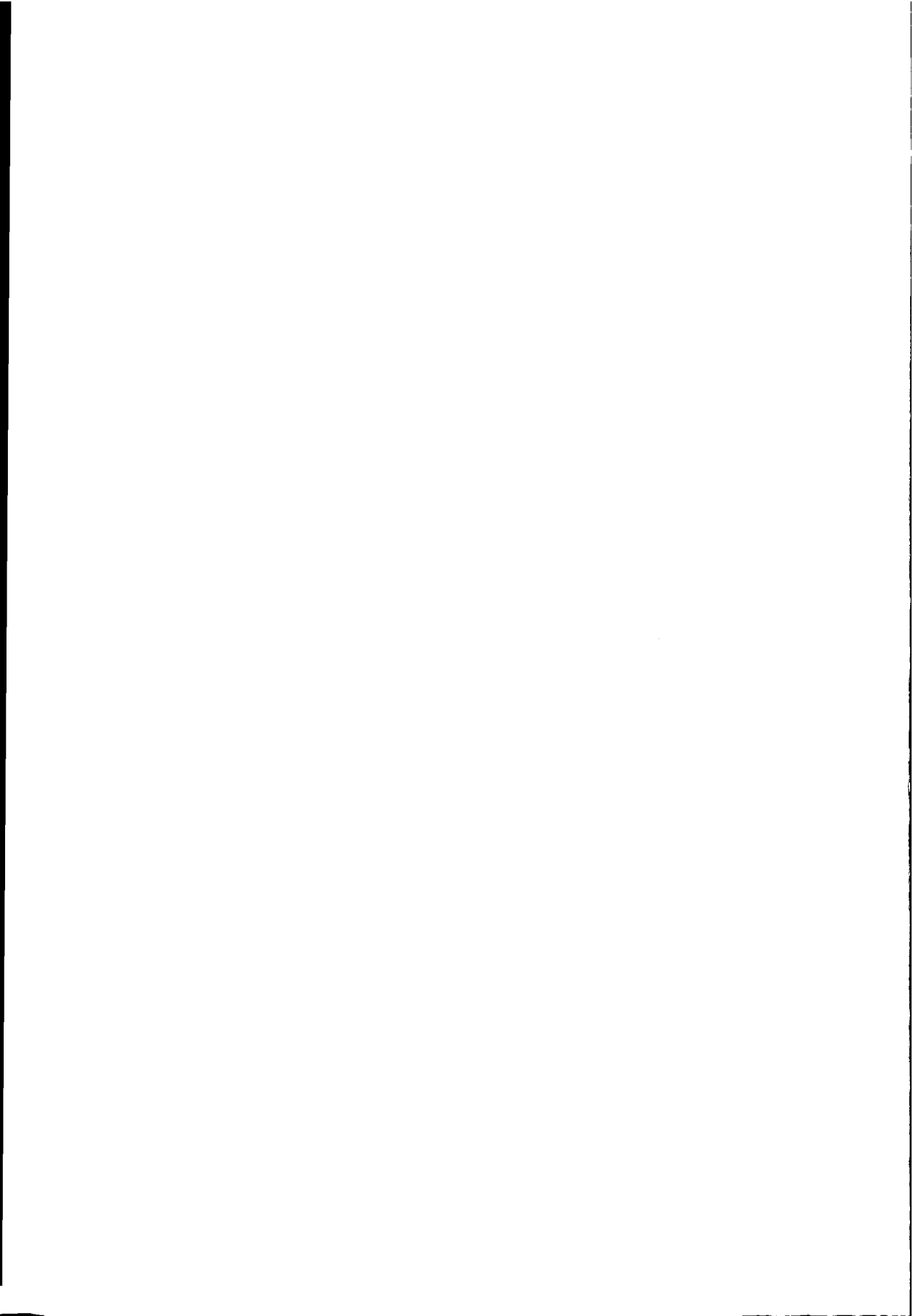
Printed by: PrintPartners Ipskamp B.V., Enschede.

Echte Beeselse die hubbe angere knôk,
die vechte mit eine echte Draak.
Het weijt doa as de hell,
de bliksem knettert en knalt flink
en de hagelwolke sjeure oet hun vel.
Mer, die Beeselse zin zô sterk wie Goliath,
veur niks en nemes bang...

Allein, auch eine Beeselse wet van te veure
noejts wie der ut precies môt doon.
En wen het ens sjitterend geit,
ken se daonoa neet geweun dinke:
"Ich dôt het weer net zoa wie veurige kier."
Dè vleger geit neet op.
Gistere war se zêkmer bienoa "total-loss"
en morges machtig, himmelhoch.
Det is het roadselechtige van ut leave.
Doe môs namelijk neet get doon,
mer het geit der ôm weam des se bûs
en doa geit het ôm.

Astrid Heemels, "ut leave", 1999.

To Harry,



Contents

List of symbols	9
1 Introduction to colloidal particle dynamics	13
1.1 Scope of the research	13
1.2 The dilute limit	15
1.3 Concentrated suspensions	17
1.3.1 Short time transport properties	18
1.3.2 Long time transport properties	18
1.4 Simulation methods	19
1.5 Outline of the thesis	23
Bibliography	24
2 Description of the lattice-Boltzmann model	27
2.1 Discrete velocity models	27
2.2 The lattice-Boltzmann equation	28
2.3 Integrating colloidal particles into the model fluid	32
2.4 Calculating transport coefficients	36
Bibliography	40
3 Simulation tools and equipment	41
3.1 Introduction	41
3.2 Basic algorithm	42
3.3 Computer Architecture	44
3.4 Storage Reduction	46
3.5 Parallelism	50
3.5.1 Linear domain decomposition	51
3.5.2 Performance results	51
3.6 Total Program	54
3.6.1 General remarks	54

3.6.2	Performance analysis	56
3.7	Conclusions	56
	Bibliography	58
4	Simulating solid colloidal particles	59
4.1	Introduction	59
4.2	Removing the effects of the internal fluid	61
4.3	Tests of the method	62
4.3.1	The frequency dependent rotational friction coefficient	62
4.3.2	The single particle velocity autocorrelation function	64
4.3.3	The viscosity of a concentrated suspension	68
4.4	Conclusions	71
	Bibliography	72
5	The high frequency viscosity of hard sphere colloidal suspensions	73
5.1	Introduction	73
5.2	The wave vector dependent viscosity	76
5.3	Calculating the wave vector dependent viscosity	77
5.4	Results	79
5.4.1	Typical decay of the correlation function	79
5.4.2	Determining the limiting suspension viscosity	80
5.4.3	The suspension viscosities for different volume fractions	81
5.4.4	The wave vector dependence of the viscosity	82
5.4.5	The viscosity of bimodal suspensions	83
5.5	Discussion	85
5.5.1	Monodisperse colloidal suspensions	85
5.5.2	Bidisperse colloidal suspensions	86
	Bibliography	88
6	The role sound plays in propagating hydrodynamic interactions	91
6.1	Introduction	91
6.1.1	The nature of hydrodynamic interactions	91
6.1.2	A single particle in a compressible fluid	92
6.1.3	Sound in a concentrated suspension	95
6.2	Calculating the current-current correlation function	97
6.3	Results	99
6.3.1	The effect of sound propagation on single particle motion	99
6.3.2	Calculating the interaction contribution	102
6.3.3	General features of the interaction correlation function	103
6.3.4	The frequency of the sound induced correlations	106
6.3.5	The initial amplitude of the correlations	108
6.3.6	The rate of decay of sound induced correlations	109
6.3.7	The effect of sound propagation on the wave vector dependent collective diffusion coefficient	110
6.4	Discussion	111

Contents

7

Bibliography	114
Summary	117
Samenvatting	121
Epilogue	125
Curriculum Vitae	127



List of symbols

***The most important ones. When in doubt look at context. Greek symbols are at the end of the list.**

Latin symbols

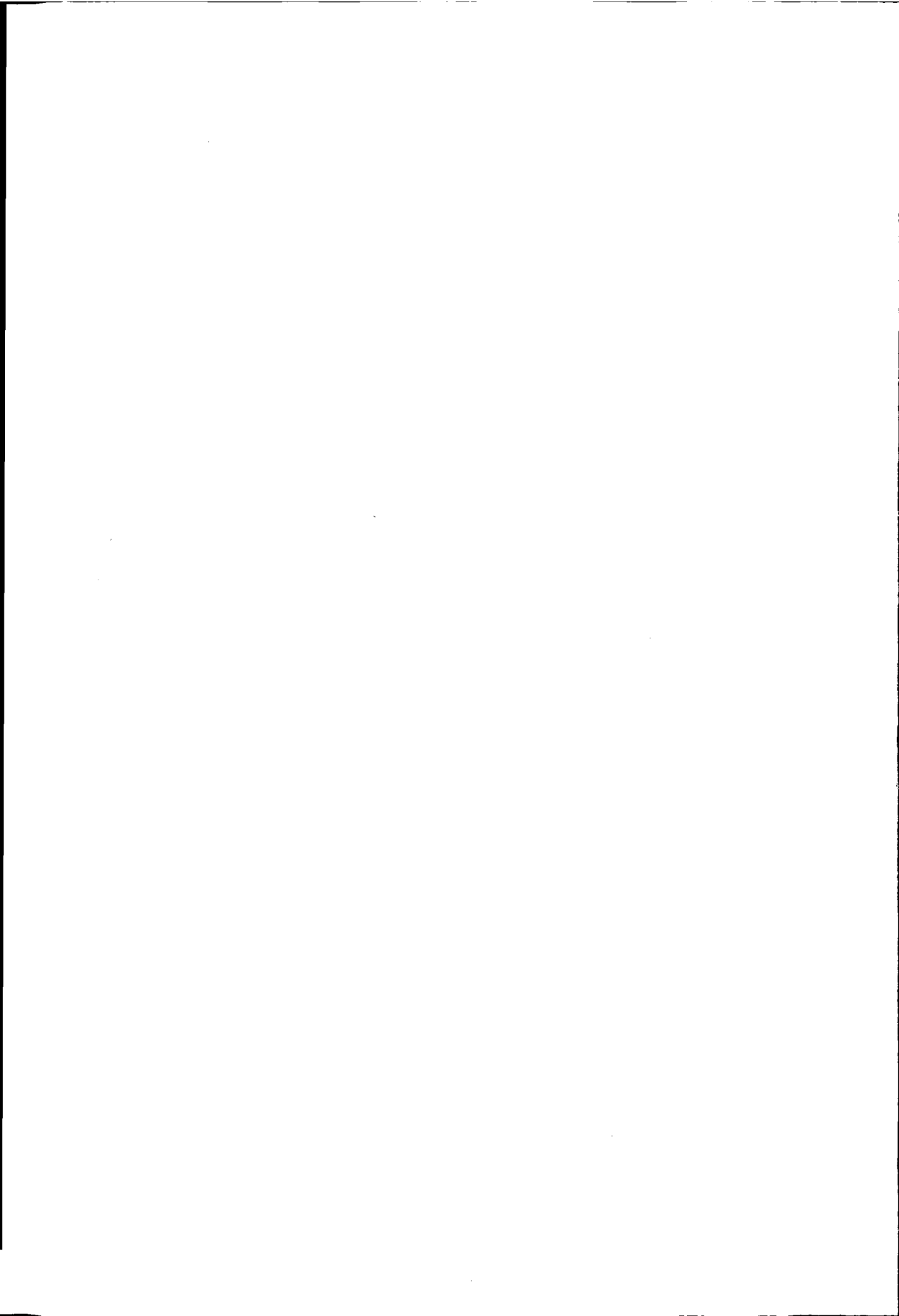
A^*	dimensionless amplitude
a	radius of the spherical colloidal particle
a_{eff}	effective, viscosity dependent, radius of the spherical colloidal particle
b	number of discrete lattice velocities
C	the velocity autocorrelation function
C_ν	a velocity correlation function to calculate the viscosity
\mathbf{c}_i	discrete velocity vector of direction i
\mathbf{c}_{ib}	discrete velocity vector of boundary link ib
c_s	speed of sound in the fluid or solvent
$c_{s\phi}$	speed of sound in the suspension
D	general diffusion coefficient, $D = D_s + D_c$
D_0	Stokes-Einstein diffusion coefficient
D_ϕ	short time suspension diffusion coefficient
D_ϕ^l	long time suspension diffusion coefficient
D_c	collective part of the diffusion coefficient in the limit of $k \rightarrow 0$
D_s	single particle or self-diffusion coefficient
\mathbf{D}_{ij}	mobility tensor of particle i and particle j
$E(n)$	efficiency of a n -processor system
\mathbf{f}	stochastic force acting on a Brownian particle
\mathbf{F}	total force acting on a colloidal particle
F	stochastic force acting on a colloidal particle
\mathbf{F}_x	external force acting on a colloidal particle
\mathbf{F}_{ib}	force acting on a boundary link of a colloidal particle
\mathbf{F}_r	friction force acting on a Brownian particle
I, \mathbf{I}	scalar or vector moment of inertia of a colloidal particle
I^*	effective moment of inertia of a colloidal particle

J	current-current correlation function
J_I	interaction velocity correlation function
\mathbf{j}	local momentum density of the lattice
k_B	Boltzmann's constant
k	wave vector
k_T	wave vector orthogonal to the velocity direction
k^*	dimensionless wave vector, $k^* = ka$
\mathcal{L}	linearized collision operator
m	mass of the colloidal particle
m^*	effective mass of the colloidal particle
N	number of colloidal particles
N_{int}	number of internal nodes inside a colloidal particle
n_i	particle velocity distribution function of direction i
n'_i	new particle velocity distribution function of direction i
n_{ib}	particle velocity distribution function of boundary link ib
n_0	equilibrium velocity distribution of the lattice
$P(r^N)$	Probability density of finding N colloidal particles in a state r^N
p	local pressure of the fluid
\mathbf{p}	colloidal particle momentum
\mathbf{r}	position vector of a lattice node
\mathbf{r}_0	position vector of the centre of the spherical colloidal particle
\mathbf{r}_{int}	position vector of the internal lattice nodes of a colloidal particle
\mathbf{r}_b	position vector of a boundary node
$S(\mathbf{k}, t)$	dynamic structure factor
$S(n)$	speedup factor for a n -processor system
T	temperature
$T(n)$	execution time for a n -processor system
\mathbf{T}	total torque acting on a colloidal particle
\mathbf{T}_x	external torque acting on a colloidal particle
\mathbf{T}_f	frequency dependent torque acting on a colloidal particle
t	time
tt	storage reduced plane index
TT	number of storage reduced planes
\mathbf{u}	flow velocity of the fluid or solvent
V	volume of the system
\mathbf{v}	linear velocity of a colloidal particle
v_0	(one component of the) initial velocity of a colloidal particle
\mathbf{v}_b	linear velocity of the boundary node
\mathbf{v}'	new linear velocity of a colloidal particle, $\mathbf{v}' = \mathbf{v}(t + 1)$
z	Laplace transform variable
z^*	dimensionless Laplace transform variable

.....

Greek symbols

α	- compressibility of the solvent, $\alpha = ac_s/\nu_0$ - as a subscript denotes one component of the coordinate axes
β	ratio of the bulk viscosity to the kinematic viscosity of the solvent, $\beta = \nu_B/\nu_0$ - as a subscript denotes one component of the coordinate axes
Γ_0	sound wave attenuation coefficient of the solvent, $\Gamma_0 = 4\nu_0/3 + \nu_B$
Γ_ϕ	sound wave attenuation coefficient of the suspension
γ	(general) friction coefficient
γ_r	rotational friction coefficient
γ_t	translational friction coefficient
γ_r^{int}	internal fluid contribution to the rotational friction coefficient
Δ	collision operator of the lattice nodes
δ	Dirac delta-function
ζ	relative volume fraction occupied by small spheres compared to the large spheres
η_0	solvent viscosity
η_B	bulk viscosity of the solvent
$\eta_B(\phi)$	bulk viscosity of the suspension
η_ϕ	short time suspension viscosity
η_ϕ^l	long time suspension viscosity
λ	eigenvalue of the collision operator \mathcal{L} , related to the viscosity
λ_B	eigenvalue of the collision operator \mathcal{L} , related to the bulk viscosity
ν_0	kinematic viscosity of the solvent
ν_B	kinematic bulk viscosity of the solvent
ν_ϕ	kinematic suspension viscosity
$\nu_{B\phi}$	kinematic bulk viscosity of the suspension
Π	local momentum flux density of the lattice
ρ	local density of the lattice
ρ_0	density of the solvent
ρ_ϕ	suspension density
ρ^*	ratio of the density of the solvent to the density of the colloidal particles
τ_B	Brownian time, $\tau_B = m/\gamma$
τ_H	hydrodynamical time, $\tau_H \sim \frac{a^2}{\nu_0} \sim \tau_B$
τ_P	Brownian time, $\tau_P = a^2/D_0$
τ_s	dimensionless sonic time scale, $\tau_s = tc_s/a$
τ_ν	dimensionless viscous time scale, $\tau_\nu = t\nu_0/a^2$
ϕ	volume fraction of the suspension
Ω	frequency of an applied external field
Ω^*	dimensionless frequency of an applied external field, $\Omega^* = \Omega a^2/\nu_0$
Ω_0	(constant) amplitude of the external field
$\Omega(r^N)$	Smoluchowski operator
ω	angular velocity of a colloidal particle
ω'	new angular velocity of a colloidal particle, $\omega' = \omega(t+1)$



1 Introduction to colloidal particle dynamics

1.1 Scope of the research

Suspensions of colloidal particles are ubiquitous in everyday life. Systems ranging from in vitro biological complexes, such as viruses, proteins, micelles and blood cells, to the latex pigments in water based paints belong to this class of particles. The fact that the sky appears blue can be regarded as consequence of the atmosphere being colloidal. Apart from aesthetics, colloids are also important in many industrial processes. Take for example the inks used in ball point pens or in high-speed printing presses. Each suspension owes its particular properties to its colloidal character. The characteristics of a suspension strongly depend on the sizes and types of the suspended particles. These properties are relatively straightforward to modify, thus the behaviour of a suspension can be “tuned” to suit a given application. So what is a colloidal suspension? A working definition might be as follows. A colloidal suspension consists of particles which are by molecular standards large (the colloidal particles) dispersed in a solvent. Colloidal particles are still, however, small enough to be influenced by the molecular nature of the solvent. One type of particle which fits into this category would be a grain of pollen. This can be considered as the first colloidal suspension to be studied experimentally. In 1828 the botanist Robert Brown observed pollen grains dispersed in water under a microscope [1, 2]. He noted that they displayed an erratic, jiggling motion. We now know that this is due to the effects of the rapid collisions the particles undergo with the (unseen) water molecules. It must be remembered, however, that even by the turn of the nineteenth century the atomic theory of matter was not universally accepted. It was in this context that Einstein turned his attention to “Brownian” motion [3, 4]. He showed theoretically that the motion of the suspended particles could be quantitatively understood in terms of a molecular description of the solvent.

Most colloidal suspensions encountered in practice, for instance the functional fluids described above, are rather complicated. They generally contain a polydisperse

collection of colloidal particles and additives. Simple "model" colloidal systems, for which the particle characteristics (shape, composition, size and size distribution) are well defined, provide a much more convenient basis for understanding the fundamental processes governing the behaviour of suspensions. Well characterized suspensions are now routinely synthesized and studied experimentally. Computer simulations provide a useful complement to these experimental studies. Using modern computational techniques, it is possible to simulate relatively simple colloidal suspensions to a high degree of accuracy. However, this is very computationally intensive even on state-of-the-art highly parallel computer systems. Nonetheless, relatively simple systems of the type often studied experimentally, can be simulated in a realistic manner. This serves as a useful aid to understand the fundamentals governing the behaviour of suspensions and for testing theories.

There is a surprising analogy between the equilibrium behavior of colloidal dispersions and that of simple atomic fluids [5]. The static or equilibrium properties of these systems can be derived from statistical mechanics in much the same way. This stands in stark contrast to the dynamic properties. From the dynamical point of view, the large size difference between the colloidal particles and the solvent molecules can lead to complex dynamical fluid behaviour. The dynamics of the colloidal particles are, for instance, characterized by processes occurring over a vast range of time scales, from picoseconds to seconds. Understanding the dynamics of the colloidal particles in suspensions implies understanding hydrodynamics in the solvent. That is, the flow fields induced by the particles as they move. From a practical point of view, the most important properties of suspensions are arguably those of dynamic origin. One notable example is the viscosity. This determines the ability of a suspension to flow. Furthermore, suspension viscosities strongly depend on the suspension's structure and can deviate substantially from that of the solvent in which the particles are dispersed. Mass transport in suspensions is characterized by the diffusion of the suspended particles as a consequence of Brownian motion. This is perhaps the process most extensively studied experimentally. If one is interested in understanding the fundamental processes occurring in colloidal suspensions, quite apart from intrinsic interest, mass transport studies form a vital link between computer simulations and experiment.

The main objectives of this research are twofold. Although it is feasible to study simple colloidal systems by computer simulation, there is still considerable scope for improving existing techniques. Improved techniques make it practical to study more realistic systems with existing computational resources. Part of this thesis is therefore concerned with algorithmic improvements. Specifically, we consider a relatively recent technique for simulating suspensions, the lattice-Boltzmann equation. The lattice-Boltzmann algorithm is in principle ideally suited to modern high performance computers in that it is intrinsically parallel. This means that one calculation can be subdivided into a number of sub-processes which can be assigned to separate processing elements without loss of generality or efficiency. The lattice-Boltzmann method nonetheless has its drawbacks. Notably it uses a lot of computer memory. For example, in a typical simulation a parallel processing element may need from

hundreds of Megabytes up to Gigabytes. To alleviate this problem we develop a novel storage reduction scheme, which saves more than 75% of the memory used in “traditional” lattice-Boltzmann simulations. The lattice-Boltzmann technique itself simulates the solvent in which colloidal particles are dispersed. To simulate suspensions, the colloidal particles themselves need to be incorporated. While considerable progress has been made in this area, an accurate and robust method for simulating impervious colloidal particles with the same density as the fluid is still lacking. We address this problem and describe a means of doing so.

The second objective we have is to apply these improved algorithms to try to further our understanding of suspensions. An interesting question is, under what conditions can general theories of the liquid state describe suspensions? We investigate this problem by studying the viscosity of suspensions as a function of the length scale on which one views them. Of course, for a simple liquid (on a macroscopic length scale) the viscosity is just a number. On what length scale is this true for a suspension? Having developed a novel technique for calculating the viscosity of suspensions, we apply the method to a more complex suspension, a binary mixture of colloidal particles of different sizes. This system is known experimentally to display very interesting rheological properties. Specifically, the introduction of a relatively low density of small colloidal particles can significantly reduce the viscosity of a suspension of larger particles. As one is often interested in tuning the viscous properties of suspensions, this effect is potentially extremely useful.

One respect in which we might expect suspensions to differ fundamentally from simple fluids is the nature of the interactions between the particles. In contrast to the inter-particle interactions in a simple fluid, the hydrodynamic interactions between particles in a suspension are time-dependent. The time regime during which these interactions propagate can now be probed experimentally. These experimental studies have stimulated interest in the role sound waves play. The lattice-Boltzmann method is ideally suited to examining this question because it models a compressible fluid. That is, sound propagates through the fluid in a realistic manner. By carefully studying the collective dynamics of a simple model suspension, our aim is to determine exactly what role sound does play.

1.2 The dilute limit

Because colloidal particles are large by molecular standards, most dynamical treatments make the simplifying assumption that the dynamics of the solvent, in which the particles are dispersed can be described at the continuum level. The “lumpiness” of the solvent, which is necessary to explain the random motion of the particles, is introduced in an effective way by making the equations of motion of the colloidal particles stochastic. Armed with such a view, it is possible to make considerable progress with the dilute limit. At the beginning of the century, Einstein considered the forces acting on the Brownian particles in a dilute suspension maintained in a dynamic equilibrium by some external field. These, he argued, can be split into two

components. The first is a hydrodynamic friction force, proportional to the drift velocity \mathbf{v} of the Brownian particles. This, continuum theory predicts, will be given by Stokes' Law, $\mathbf{F} = -\gamma\mathbf{v}$. For spherical particles of radius a the friction coefficient γ is given by $\gamma = 6\pi\eta_0 a$, with η_0 the fluid viscosity. The second force is a "thermodynamic" stochastic force $\mathbf{f}(t)$ which tries to restore the suspension to equilibrium. At the level of the Brownian particles, this results from the apparently random collisions of solvent molecules with the Brownian particle. By imposing the condition that, for a system in dynamic equilibrium, these forces sum to zero, Einstein was able to show that the value of the diffusion coefficient in the dilute limit, D_0 , is given by

$$D_0 = \frac{k_B T}{6\pi\eta_0 a} \quad (1.1)$$

where k_B is Boltzmann's constant and T the temperature. This is known as the Stokes-Einstein diffusion coefficient. Although Einstein's original derivation is by no means rigorous, it can be shown that equation 1.1 is exact, so long as the solvent can be described as a continuum Newtonian fluid and the velocity of the fluid adjacent to the surface of the particle equals the velocity of the particle itself (the "stick" boundary condition). By calculating the hydrodynamic flow field around a single large sphere, Einstein also derived the lowest order expression for the macroscopic viscosity of a colloidal suspension [6]

$$\eta_\phi = \eta_0 \left(1 + \frac{5}{2}\phi\right) \quad (1.2)$$

This result, valid to the first order in volume fraction, represents the increase in the suspension viscosity with respect to the solvent viscosity, due to the presence of mutually non-interacting spherical Brownian particles.

To gain some insight into the dynamic behaviour of Brownian particles in equilibrium we need an equation of motion. A phenomenological approach is to assume this takes the form of a Langevin equation. This basically takes the above idea of a random and frictional force further. The latter is assumed to be proportional to the instantaneous particle velocity $\mathbf{v}(t)$. Accordingly, the equation of motion for a colloidal particle takes the form

$$m \frac{d\mathbf{v}(t)}{dt} = -\gamma\mathbf{v}(t) + \mathbf{f}(t), \quad (1.3)$$

where m the mass of the Brownian particle. The correlation functions of the random force is assumed to be proportional to a delta function and uncorrelated with the velocity. In order to recover the correct equilibrium properties (for instance a Maxwellian distribution of velocities), this implies the following; the average of the random force is zero, *i.e.* $\langle \mathbf{f}(t) \rangle = 0$, while it is delta correlated in time with $\langle \mathbf{f}(t) \cdot \mathbf{f}(t') \rangle = G\delta(t - t')$, where $\delta(t)$ is the Dirac delta-function and $G = 3k_B T \gamma$. The equation can be solved for any statistical quantity we are interested in. One useful quantity is the velocity autocorrelation function (VACF), $C(t)$, defined as the

average of the product of instantaneous velocity with the velocity at a subsequent time t . The Langevin equation yields a VACF of the form:

$$C(t) = \langle v_\alpha(t)v_\alpha(0) \rangle = \frac{k_B T}{m} \exp(-t/\tau_B), \quad (1.4)$$

where the exponential decay is characterized by a "Brownian" time $\tau_B = m/\gamma$. For a spherical particle we therefore have

$$\tau_B = \frac{m}{6\pi\eta_0 a} \quad (1.5)$$

The velocity autocorrelation function gives information on the decay of velocity fluctuations. The characteristic time τ_B can therefore be interpreted as a typical time scale on which velocity fluctuations relax. Furthermore, the VACF can be related to the diffusion coefficient via the Green-Kubo relation

$$D = \int_0^\infty C(t) dt \quad (1.6)$$

In equation 1.6 it is implicitly assumed that the integral converges. Substituting the form of the VACF predicted by the Langevin equation into equation 1.6 we recover the Stokes-Einstein result for the diffusion coefficient. It is important to note that although the Langevin equation predicts the correct value for the diffusion coefficient of a spherical colloidal particle, it does not in general predict the dynamics correctly. The VACF is in fact not exponential. The assumption of a simple proportionality between the particle velocity and friction force is too simplistic [7]. A more general form of the Langevin equation is needed, which we will discuss in chapter 2.4. Nonetheless, the main conclusion, that velocity fluctuations decay in a time scale τ_B still holds. It should also be noted that the Green-Kubo relation is formal, and always holds, even if the velocity correlation function does not decay exponentially.

1.3 Concentrated suspensions

In the previous section only isolated particles have been considered and the colloidal suspension was described by one time scale parameter τ_B . This is only true in the dilute limit. For volume fractions of about 5% and higher, the typical separation between the surfaces of neighbouring particles becomes of the order of their diameter and the interactions between the Brownian particles become important. These inter-particle interactions are time-dependent and two different time scales can be distinguished. First of all there are the hydrodynamic interactions. These are indirect interactions between the Brownian particles due to the flow of the solvent. One measure for the hydrodynamical time τ_H is determined by the time it takes for a viscous shear-wave to propagate between two Brownian particles, *i.e.* $\tau_H \sim \frac{a^2}{\nu_0}$, where $\nu_0 (= \rho_0 \eta_0)$ is the kinematic viscosity of the solvent and ρ_0 the density. For most systems the Brownian time τ_B and the hydrodynamic time τ_H are of the same

order of magnitude, *i.e.* $\tau_H \approx \tau_B \sim 1ns$. The second time scale characterizes the direct (potential) interactions between the Brownian particles, for example Van der Waals or electrostatic forces. These interactions vary on a time scale typical of the time it takes a Brownian particle to diffuse over a distance equal to its own radius, *i.e.* $\tau_P = \frac{a^2}{D_0}$. This time scale is usually referred to as the Péclet time. As an example, for a particle of radius $0.1\mu m$ suspended in water the relaxation time τ_B is about $10^{-9}s$. By comparison, for the same system the Péclet time is of the order $10^{-3}s$. There is clearly a very large time scale separation between, on the one hand, the decay time for velocity fluctuations and the propagation of hydrodynamic interactions and, on the other, the diffusion of the Brownian particles themselves.

1.3.1 Short time transport properties

There is a substantial time regime $\tau_B, \tau_H \sim t \ll \tau_P$ (typically between 10^{-8} and $10^{-5}s$) during which velocity fluctuations relax and the hydrodynamic flow fields evolve. During this period the particle coordinates only vary by distances small compared to their size. For example, the $1nm$ colloidal particle discussed in the previous section only moves about one thousandth of its radius for times $t \sim \tau_B$. While velocity fluctuations decay the positions of the colloidal particles are essentially fixed in space. Within the time range $\tau_B \sim t \ll \tau_P$, we can therefore study the temporal evolution of the hydrodynamic interactions without the added complication of changes in particle configuration. These considerations allow us to define a "short time" $t < \tau_P$ within which considerable theoretical progress can be made. Exact solutions for the hydrodynamic interactions between pairs of spheres have been obtained [8, 9]. However, hydrodynamic interactions are not pairwise additive and many-body interactions cannot in general be neglected. By considering the hydrodynamical motion of one hard-sphere particle in a stationary field due to all other particles at rest, approximate solutions have been reported by Beenakker [10] and Beenakker and Mazur [11]. These workers obtained explicit expressions for the short time diffusion coefficient and the short time (or high frequency) viscosity up to volume fractions of 40%. Their values are in agreement with experiment [12, 13] up to relatively high volume fractions. The agreement between experiment and computer simulations, which solve the hydrodynamic equations numerically [14, 15], extends to remarkably high volume fractions. There is also, to a large degree, quantitative agreement as to the time dependence of the short time dynamics.

All the simulations described in this thesis apply to the short time scale. I consider the wave vector dependence both for the viscosity and diffusion. Also I consider the spatial and temporal evolution of the hydrodynamic interactions by investigating time-dependent correlations in particle motion.

1.3.2 Long time transport properties

At times $\tau_B \ll t \sim \tau_P$, there is an additional physical process to consider, involving the direct Brownian particle interactions (for example, in the case of hard spheres,

due to their direct collisions). Experimentally, the “transition” from short to long times ($t \gg \tau_P$) results in a reduction of the diffusion coefficient from its short time value D_ϕ to its long time value D_ϕ^l . For the viscosity, it results in an increase in the viscosity from its short time value η_ϕ to its long time value η_ϕ^l . The usual interpretation of this is that a particle’s neighbours exclude a certain volume of space to the particle and thus hinder its motion. This is reflected in the decrease in the diffusion coefficient. The fact that the motion is restricted by its neighbours hinders the ‘flow’ of the suspension and thus increase the viscosity. Understanding the long time regime for a suspension may be regarded as the most important goal. The true transport coefficients for a suspension, the viscosity or diffusion coefficient for instance, are the long time values. However, the short time transport coefficients set the natural time scale for processes occurring on the long time scale [16] and may make up a significant, if not dominant, contribution to the long time values. If we are ultimately interested in the long time properties, understanding the short time regime is an important step along the way.

1.4 Simulation methods

One way to extract information about colloids is to perform computer simulations [17]. Computer simulations are complementary to experimental and theoretical studies. In principle they are exact, *i.e.* they can be carried out to any desired degree of accuracy for a given model. They can be used to test assumptions made in approximate theories. A realistic and well tested model could predict the properties of particular suspensions before embarking on the expensive task of actually making them. Finally, computer simulations can be used to probe the behaviour of suspensions under conditions that are not easily achieved in experiments. Sometimes computer simulations can even allow us to predict new behaviour of suspensions and thereby act as a guide to both theoretical and experimental work.

There are several different simulation techniques that can be applied to study colloidal particle dynamics. Each technique has its own advantages and disadvantages. We begin a brief overview with the “brute force” approach; simulating the system at the atomic level using conventional Molecular Dynamics (MD). In an MD simulation one solves Newton’s equation of motion numerically for a system containing several hundreds up to several millions of molecules, in discrete time steps (see for instance references [17, 18]). For a simple fluid, a small number of atoms (100-10000) combined with the use of periodic boundary conditions is usually enough to approximate the behaviour of an infinite system. In the case of colloidal suspensions, however, the number of molecules needed to represent the solvent is prohibitively large compared to the number of colloidal particles. This means that to simulate a small number of colloidal particles, an astronomic number of solvent molecules are required. There are also problems in that the time scale on which the dynamics of a colloidal particle evolves is, by molecular standards, extremely long. Both the number of molecules and the number of time-steps over which the

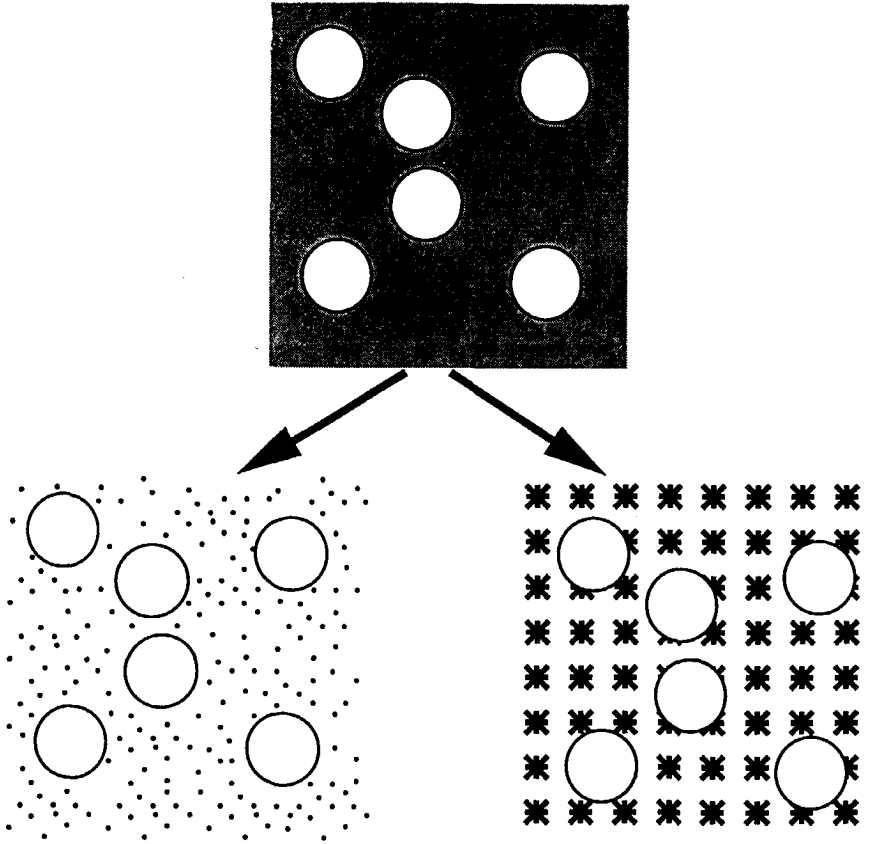


Figure 1.1: Models of a colloidal suspension. The dynamical properties of the large particles are insensitive to the detailed motions of the background fluid. So the continuum fluid of the top can be equally well replaced by a molecular solvent (lower left) or a lattice-Boltzmann fluid (lower right).

equations of motion must be integrated make MD very limited even as a means of studying short time colloidal dynamics. Recently a new technique, Dissipative Particle Dynamics (DPD) [19, 20], has been introduced which, by combining concepts from MD with certain features of the lattice-gas methods [21, 22, 23], attempts to surmount these problems. Lattice gases attempt to model the solvent discretely. The rules governing the motions of the particles are made as simple (and therefore computationally convenient) as possible while still generating fluid-like behaviour. Thus the particles have a discrete set of velocities which constrain their positions, at discrete times, to be located on a lattice. The problems with lattice gases, for the purpose of simulating suspensions, are two-fold. The method does not generate the correct thermodynamic behaviour and, for practical purposes, operates in the wrong range of parameters for a suspension (it does not well separate the time scales for velocity and positional relaxation for instance). DPD is conceptually similar, it sets out to mimic a generic fluid in as simple a way as possible, but is more MD-like in that the particles move continuously in space with a continuous set of velocities. The method, as originally proposed [19, 20], still failed to reproduce correct thermodynamic behaviour but a modified version, proposed by Espanol and Warren [24] was shown, in theory, to have a well defined canonical equilibrium state. The subsequent problem has been satisfying this condition in practice [25, 26]. While progress has been made on this point [27, 28], problems remain. The essence is calculating values for the transport coefficients of the model fluid over the full range of parameters [29, 30] and accurately incorporating colloidal particles into the scheme. Nonetheless, apparently successful simulations of suspensions have been reported using this method [31, 32]. In summary, DPD is a promising but as yet unproven approach for simulating suspensions.

If we do not proceed from a discrete or molecular level, we need to turn to theory and make some approximations. Following the pioneering work of Mori [33], it is possible to show that the equations of motion of the colloidal particles reduce to a generalized Langevin equation on time scales $t \sim t_B$, given the separation of time scales outlined above and starting from the molecular level. Further, the generalized Langevin equation reduces to the Smoluchowski equation on time scales $t \sim t \gg \tau_B$ [34]. According to the Smoluchowski equation, the evolution of the probability density $P(r^N, t)$, the probability of finding the N particles in a state $r^N = r_1, \dots, r_N$, is given by

$$\frac{dP(r^N, t)}{dt} = \Omega(r^N)P(r^N, t) \quad (1.7)$$

and $\Omega(r^N)$ is the Smoluchowski operator

$$\Omega(r^N) = \sum_{i,j=1}^N [k_B T \nabla_i + \mathbf{F}_i(r^N)] \cdot \mathbf{D}_{ij}(r^N) \cdot \nabla_j \quad (1.8)$$

Here $\mathbf{F}_i(r^N)$ is the total force on particle i , $\nabla_i = \partial/\partial r_i$, and \mathbf{D}_{ij} is the mobility tensor which gives the velocity change of particle i due to a force applied to particle j .

The mobility tensor is therefore a quantity that can be calculated hydrodynamically. Stokesian dynamics [35, 36] is based on solving the Smoluchowski equation numerically. It therefore probes the asymptotic time regime $t > \tau_p$. The mobility tensor is calculated and substituted into a discretized form of the Smoluchowski equation to update the particle positions. The details of the short time dynamics are essentially subsumed into the mobility tensor. The main problem with this approach is the complexity of calculating the instantaneous mobility tensor. Stokesian dynamics attempts to calculate the full mobility tensor as accurately as is practical (although still not exactly). Nonetheless, Brady and collaborators have made considerable progress understanding the properties of colloidal suspensions of spherical particles, in particular the rheology, using this method [36]. Because of the generally daunting task of calculating the mobility tensor, a computationally convenient simplification is to neglect the pair mobilities (*i.e.* let $\mathbf{D}_{i \neq j} = 0$) and set the self mobilities (*i.e.* \mathbf{D}_{ii} terms) all equal to a constant mean-field value D_{ii} . As the particles diffuse independently, the Smoluchowski equation then reduces to a much simpler form,

$$\frac{\partial P(\mathbf{r}^N, t)}{\partial t} = k_B T \langle D_{ii} \rangle \nabla_i \cdot \left[\nabla_i + \frac{\mathbf{F}_i(\mathbf{r}^N)}{k_B T} \right] P(\mathbf{r}^N, t) \quad (1.9)$$

We will refer to this as the “simplified Smoluchowski” equation. Solving this equation numerically forms the basis of the Brownian dynamics computer simulation technique. The problems with this approach are firstly that the mean field value the self mobility is related to the short time diffusion coefficient [16] and must therefore be calculated hydrodynamically within the short time approximation (although most workers do not follow this procedure). More seriously, it is not possible to know *a priori* how good an approximation equation 1.9 is. There is evidence that often it is often poor [37, 38, 16]. Because both Stokesian dynamics and Brownian dynamics operate on the time scale where Brownian motion of the particles dominates ($\sim 1ms$), long after the regime where the hydrodynamic interactions between the Brownian particles develop and velocities decay, they cannot give any information about these processes.

In this research the solvent is modelled by a lattice-Boltzmann model. This has its origins in lattice gases. It is essentially a “pre-averaged” lattice gas, dealing with distributions of particles rather than individual particles. These distributions evolve on a lattice in such a way that the behaviour of the system is governed by the continuum equations for a compressible fluid. It can essentially be regarded as a means of computing the time-dependent hydrodynamic interactions between particles, *i.e.* it probes the regime $t \sim \tau_B$. Because of the pre-averaging involved in going from a lattice gas to its Boltzmann equation, there are no spontaneous fluctuations in the system. They can be reinstated by simulating instead a fluctuating Boltzmann equation. This involves introducing local fluctuations in the stress. In this case one would be solving the generalized Langevin equation governing the dynamics of the suspension on the short time scale. The lattice-Boltzmann method could therefore in principle be used to probe the long time regime (simply by running it for times where the generalized Langevin equation reduces to the Smoluchowski equation used

in Stokesian dynamics). Whether it is a practical or efficient method to do so is an open question. There are problems. Introducing fluctuations in the way outlined above is not a totally satisfactory way of essentially introducing thermodynamics to the system (there is no rigorous equipartition for example). There is also the question as to whether or not makes computational sense to use a method which resolves τ_B when we have the option of integrating over this time scale by using Stokesian dynamics. Nonetheless, neither of these objections apply on the short time scale, for which the method has shown itself to be a very useful tool.

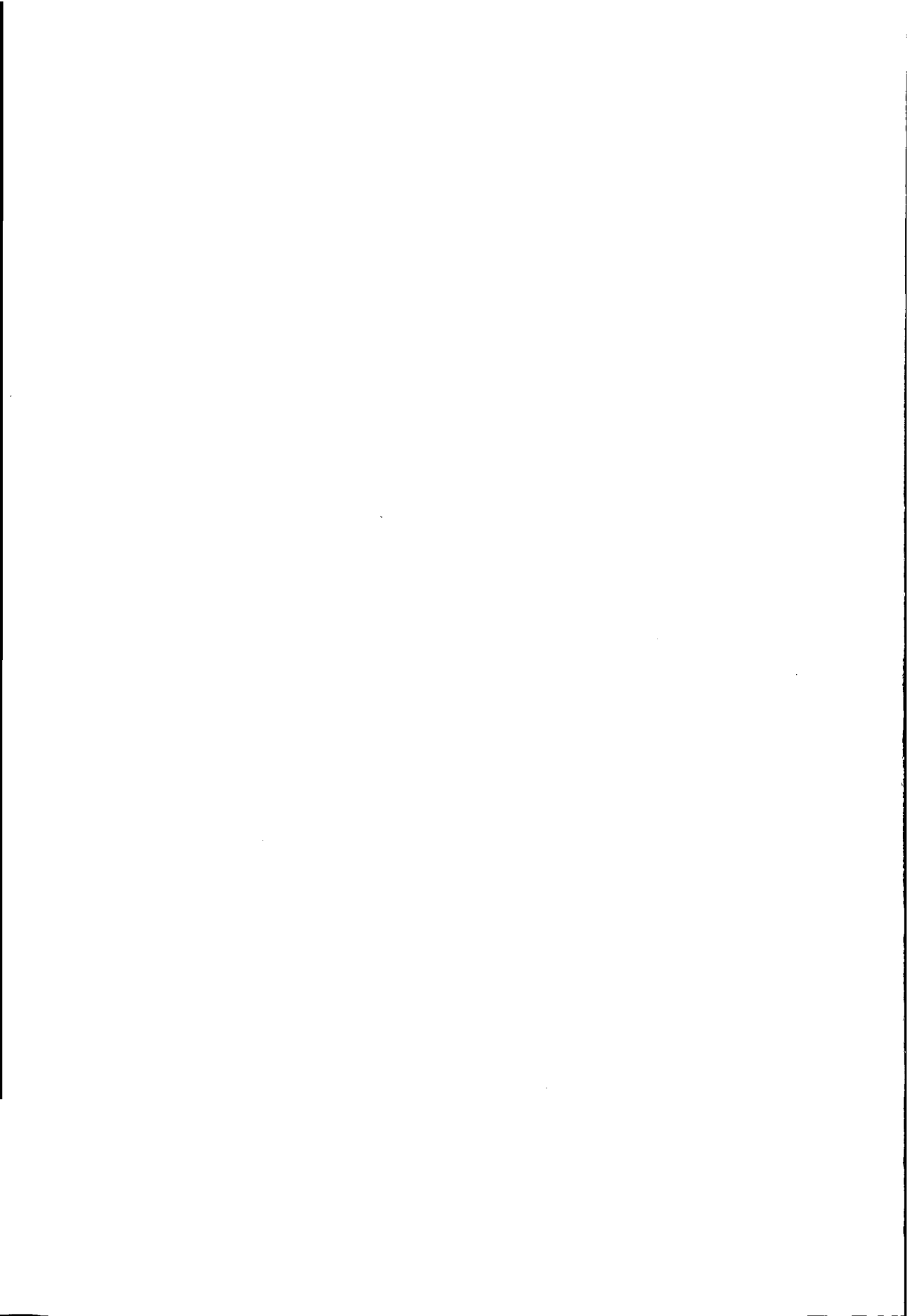
1.5 Outline of the thesis

The contents of this thesis can be outlined as follows. We begin, in chapter two, by describing in more detail the basic lattice-Boltzmann model we have used for simulating colloidal suspensions. Having considered the algorithm, in chapter three we describe a novel implementation which both utilizes high performance computing and introduces a new method to reduce the memory usage. Within the basic lattice-Boltzmann method there are still some undesirable features. Notably the existence of fluid inside and outside the colloidal particles. In chapter four we examine the limitations of this approach and describe and test a new method to simulate truly solid particles. With the computational and algorithmic wherewithall in place, in chapters five and six we turn to studying the dynamics of colloidal suspensions of hard spheres. In chapter five we calculate the suspension viscosity as a function of both the spatial length scale one considers and the volume fraction occupied by the colloidal particles. These results serve in the first place as a verification test of the implemented simulation model and besides to study the spatial length scale dependence of the viscosity. In addition, we consider the difference in viscosity of a suspension in which all the particles are the same and a similar suspension composed of two types of particles differing in size. We succeeded in observing the viscosity reduction and to our knowledge this is the first time this has been achieved in three dimensional simulations. The lattice-Boltzmann method is ideally suited to studying the temporal evolution of hydrodynamic interactions. Accordingly, in chapter six we study how these interactions develop and the mechanisms involved. In particular we examine the role sound plays in propagating interactions between the particles. Thus far the suggestion has been made that sound propagation might play an important role but it has not been made clear yet.

Bibliography

- [1] R. Brown, *Phil. Mag.* **4**, 161 (1828).
- [2] R. Brown, *Ann. Phys.* **14**, 294 (1828).
- [3] A. Einstein, *Ann. Physik* **17**, 549 (1905).
- [4] A. Einstein, *Ann. Physik* **19**, 371 (1906).
- [5] L. Onsager, *Chem. Rev.* **13**, 73 (1933).
- [6] A. Einstein, *Ann. Physik* **19**, 289 (1906).
- [7] B.J. Alder and T.E. Wainwright, *Phys. Rev. A* **1**, 18 (1970).
- [8] J. Happel and H. Brenner, *Low-Reynolds Number Hydrodynamics*. Prentice-Hall, Englewood Cliffs, New Jersey, (1965).
- [9] D.J. Jeffrey and Y. Onishi, *J. Fluid Mech.* **139**, 261 (1984).
- [10] C.W.J. Beenakker, *Physica A* **128**, 48 (1984).
- [11] C.W.J. Beenakker and P. Mazur, *Physica A* **126**, 349 (1984).
- [12] J.C. van der Werff, C.B. de Kruif, C. Blom and J. Mellema, *Phys. Rev. A* **39**, 795 (1989).
- [13] P.N. Pusey and W. van Meegen, *J. Phys. (Paris)* **44**, 258 (1983).
- [14] A.J.C. Ladd, *J. Chem. Phys.* **93**, 3484 (1990).
- [15] M.H.J. Hagen, D. Frenkel and C.P. Lowe, *Physica A*, in press (1999).
- [16] C.P. Lowe and A.J. Masters, *J. Chem. Phys.* (in press 1999).
- [17] M.P. Allen and D.J. Tildesley, *Computer simulation of liquids*. Pergamon Press, Oxford (1987).
- [18] D. Frenkel and B. Smit, *Understanding Molecular Simulation: From Algorithms to applications*. Boston (1996).
- [19] P.J. Hoogerbrugge and J.M.V.A. Koelman, *Europhys. Lett.* **19**, 155 (1992).
- [20] J.M.V.A. Koelman and P.J. Hoogerbrugge, *Europhys. Lett.* **21**, 363 (1992).
- [21] U. Frisch, B. Hasslacher and Y. Pomeau, *Phys. Rev. Lett* **56**, 1505 (1986).
- [22] D. d'Humières, P. Lallemand and U. Frisch, *Europhys. Lett.* **2**, 291 (1986).
- [23] S. Wolfram, *J. Stat. Phys.* **45**, 471 (1986).
- [24] P. Espanol and P. Warren, *Europhys. Lett.* **30**, 191 (1995).

- [25] C.A. Marsh and J.M. Yeomans, *Europhys. Lett.* **37**, 511 (1997).
- [26] K.E. Novik and P.V. Coveney, *J. Chem. Phys.* **109**, 7667 (1998).
- [27] I. Pagonabarraga, M.H.J. Hagen and D. Frenkel, *Europhys. Lett* **42**, 377 (1998).
- [28] C.P. Lowe, *Europhys. Lett.* **47**, 145 (1999).
- [29] C.A. Marsh, G. Backx and M.H. Ernst, *Europhys. Lett.* **38**, 411 (1997).
- [30] C.A. Marsh, G. Backx and M.H. Ernst, *Phys. Rev. E* **56**, 1676 (1997).
- [31] E.S. Boek and P. van der Schoot, *Int. J. of Modern Phys.* **9**, 1307 (1998).
- [32] E.S. Boek, P.V. Coveney, H.N.W. Lekkerkerker and P. van der Schoot, *Phys. Rev. E* **55**, 3124 (1997).
- [33] H. Mori, *Prog. Theor. Phys.* **34**, 399 (1965).
- [34] A.J. Masters, *Mol. Phys.* **57**, 303 (1986).
- [35] L.J. Durlofsky, J.F. Brady and G. Bossis, *J. Fluid Mech.* **180**, 21 (1987).
- [36] T.N. Phung, J.F. Brady and G. Bossis, *J. Fluid Mech.* **313**, 181 (1996).
- [37] K. Zahn, J.M. Mendez-Alcaraz and G. Maret, *Phys. Rev. Lett.* **79**, 175 (1997).
- [38] B. Rinn, K. Zahn, P. Maass and G. Maret, *Europhys. Lett.* **46** 537 (1999).



2 Description of the lattice-Boltzmann model

2.1 Discrete velocity models

The lattice-Boltzmann model, in historical terms at least, is closely related to lattice-gas cellular automaton (LGCA) model fluids. Lattice gas cellular automata are discrete velocity models introduced by Frisch, Hasslacher and Pomeau [1], with the aim of mimicking hydrodynamic behaviour using a system as simple as possible. As originally formulated, the lattice-gas consists of a collection of discrete particles moving on a two-dimensional (triangular or square) lattice. The state of the model fluid at any (discrete) time is specified by a set of Boolean variables describing whether a particle is (1) or is not (0) located at a given lattice node with a particular discrete velocity. Particles can only move to neighbouring lattice nodes in a limited number of directions. There can be at most one particle at a given node with a given velocity (the exclusion rule), consistent with the Boolean representation, and all nodes are updated synchronously. The time evolution of the LGCA consists of two steps (see figure 2.1). The first step is the propagation step, in which the particles are leaving a node towards the neighbouring nodes. The second step is the collision step, when the particles “collide” with other particles located at the same lattice node. The collisions conserve mass and momentum and retain the full symmetry of the lattice. At a macroscopic scale, the behaviour of the lattice gas is very close to the incompressible Navier-Stokes equations [2, 3, 4, 5]. The lattice-Boltzmann model is an adaption of lattice gas techniques [6, 7]. It can be considered as a “pre-averaged” version of the LGCA model fluid. This model retains the original macroscopic adherence to the Navier-Stokes equations but has a number of advantages. Because of the pre-averaging there are no fluctuations, the exclusion rule (which leads to certain unphysical properties in lattice gases) can be relaxed and there is greater freedom to specify the properties of the collision operator. The latter is important because the rate at which the collisions relax stress is related to the viscosity of the model fluid. The greater freedom one has in constructing

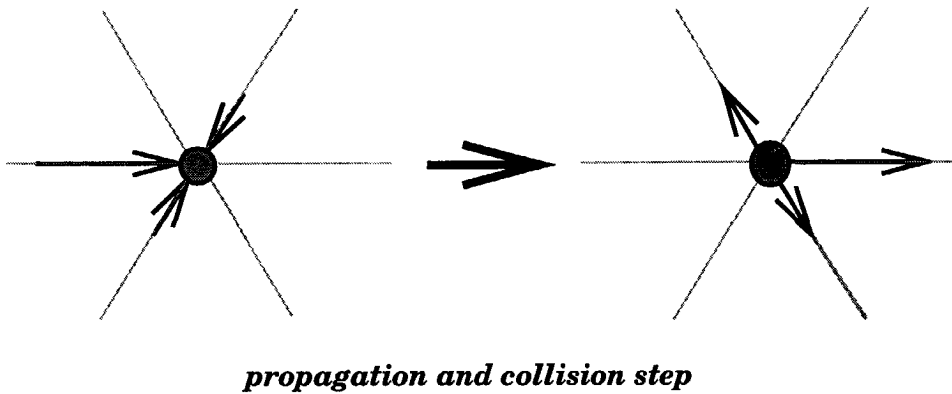


Figure 2.1: Example of a time-step in the two dimensional FHP lattice.

the collision operator at the Boltzmann level translates into the ability to vary the viscosity at will.

2.2 The lattice-Boltzmann equation

In the lattice-Boltzmann method, probabilities or, in lattice gas terms, average populations, substitute for discrete particles in the particle velocity distribution function $n_i(\mathbf{r}, t)$. This describes the number of particles at a particular node of the lattice \mathbf{r} , at a time t , with the velocity \mathbf{c}_i , where i stands for one of the possible velocities; \mathbf{r} and \mathbf{c}_i are discrete, whereas n_i is continuous. The hydrodynamic fields, mass density ρ , momentum density $\mathbf{j} = \rho \mathbf{u}$ (where \mathbf{u} is the flow velocity), and momentum flux $\mathbf{\Pi}$, are simply moments of this particle velocity distribution function $n_i(\mathbf{r}, t)$:

$$\rho = \sum_i n_i, \quad (2.1)$$

$$\mathbf{j} = \sum_i n_i \mathbf{c}_i, \quad (2.2)$$

$$\mathbf{\Pi} = \sum_i n_i \mathbf{c}_i \mathbf{c}_i. \quad (2.3)$$

The lattice used in this thesis is a three dimensional projection of the four dimensional Face-Centered Hyper Cubic (FCHC) lattice for which there are 18 velocities. The vectors spanning the particle motion in one time-step for this lattice are given in figure 2.2. A lower-dimensional model can be obtained by further projection. This FCHC model is used because three-dimensional Bravais lattices do not have enough symmetry to ensure that the hydrodynamic transport coefficients are isotropic.

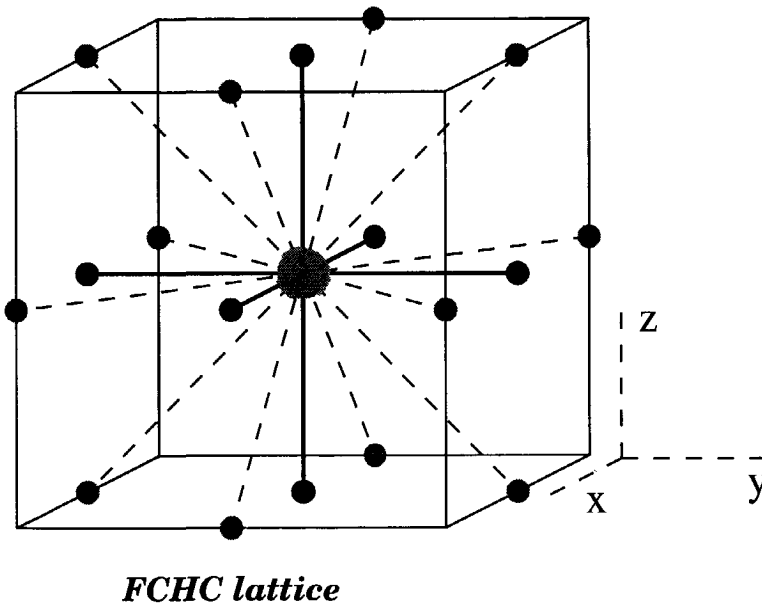


Figure 2.2: The 18 different velocity vectors (c_i) in the lattice-Boltzmann model. The solid lines represent velocity vectors used twice in the simulation, due to the projection from the four dimensional Face-Centered Hyper Cubic (FCHC) lattice.

The lattice-Boltzmann method involves an explicit solution of a discrete analogue of the Boltzmann equation [3]. Populations evolve in (discrete) time according to the propagation and collision rule given by

$$n_i(\mathbf{r} + \mathbf{c}_i, t + 1) = n_i(\mathbf{r}, t) + \Delta_i(\mathbf{r}, t), \quad (2.4)$$

where Δ_i is the change in n_i due to instantaneous collisions at the lattice nodes. The post-collisional distribution $n_i + \Delta_i$ is propagated for one time-step, in the direction \mathbf{c}_i . The collision operator $\Delta(n)$ depends on all the n_i 's at the node represented collectively by $n(\mathbf{r}, t)$; as with lattice gases, it is subject to the constraints of mass and momentum conservation. Exact expressions for the Boltzmann collision operator have been derived for several lattice-gas models [3, 6], by making use of the "molecular chaos" assumption (that the effect of the collision operator depends only on the instantaneous state of a node). However, such collision operators are complex and ill-suited to numerical simulation. A computationally more useful form for the collision operator can be constructed by linearizing the collision operator about the local equilibrium n^{eq} [8], *i.e.*

$$\Delta_i(n) = \Delta_i(n^{eq}) + \sum_j \mathcal{L}_{ij}(n_j - n_j^{eq}), \quad (2.5)$$

where \mathcal{L} is the linearized collision operator, and $\Delta_i(n^{eq}) = 0$ by definition. It is not necessary to calculate a particular \mathcal{L} ; rather it is sufficient to consider the general principles of conservation and symmetry and then to construct the eigenvalues and eigenvectors of \mathcal{L} . As a first step, the correct form of the equilibrium distribution must be established. We will give a brief outline of the procedure, for complete derivations of the equations below, the reader is encouraged to refer to the work of Ladd [9].

To determine the equilibrium distribution, the velocity distribution function is split into a local equilibrium part and a non-equilibrium part

$$n_i = n_i^{eq} + n_i^{neq}. \quad (2.6)$$

The equilibrium distribution is a collisional invariant (*i.e.* $\Delta_i(n^{eq}) = 0$). To achieve a constrained equilibrium distribution which will lead to the correct macroscopic fluid dynamics at the Euler level, *i.e.* non-dissipative hydrodynamics, the moments of the velocity distribution function must have the following form:

$$\rho = \sum_i n_i^{eq}, \quad (2.7)$$

$$\mathbf{j} = \sum_i n_i^{eq} \mathbf{c}_i, \quad (2.8)$$

$$\mathbf{\Pi}^{eq} = \sum_i n_i^{eq} \mathbf{c}_i \mathbf{c}_i = p\mathbf{I}, \quad (2.9)$$

with p the local pressure, $\mathbf{\Pi}^{eq}$ the non-dissipative part of the momentum flux and \mathbf{I} the unit tensor. The equilibrium distribution can be expressed as a series expansion

in powers of the flow velocity \mathbf{u} ,

$$n_i^{eq} = \rho[a_0^{c_i} + a_1^{c_i} \mathbf{u} \cdot \mathbf{c}_i + a_2^{c_i} \overline{\mathbf{u}\mathbf{u}} : \overline{\mathbf{c}_i \mathbf{c}_i} + a_3^{c_i} u^2], \quad (2.10)$$

where $\overline{\mathbf{u}\mathbf{u}} = \mathbf{u}\mathbf{u} - \frac{1}{3}u^2\mathbf{I}$ is the traceless part of $\mathbf{u}\mathbf{u}$; equation 2.10 has the same functional form as a small- u expansion of the Maxwell-Boltzmann distribution function. If we combine equation 2.10 and equation 2.7-2.9, supplemented with a condition to guarantee isotropy [9], then we can solve for all the coefficients in equation 2.10. The result of this is given in table 2.1. In these coefficients we have chosen the value for

i	0	1	2	3
a_i^1	$\frac{1}{12}$	$\frac{1}{6}$	$\frac{1}{4}$	$\frac{1}{6}$
$a_i^{\sqrt{2}}$	$\frac{1}{24}$	$\frac{1}{12}$	$\frac{1}{8}$	$\frac{1}{12}$

Table 2.1: The coefficients in the equilibrium distribution.

the speed of sound $c_s^2 = \frac{1}{2}$. Since the distribution function must always be positive, the speed of sound is bounded by the limits $\frac{1}{3} \leq c_s^2 \leq \frac{2}{3}$. The intermediate value $c_s^2 = \frac{1}{2}$ maximizes the stability with respect to variations in flow velocity and is used for all the work reported in this thesis.

Having constructed the local equilibrium distribution, we come to the relaxation of the non-equilibrium component of the local distribution. The collision operator conserves mass and momentum but relaxes the non-equilibrium part of the velocity distribution function, *i.e.* n_i^{neq} . The requirements on the eigenvalue equations of the collision operator concern only conservation of mass and momentum and isotropic relaxation of the stress tensor, where the eigenvalues λ and λ_B of the collision operator are related to the shear and bulk viscosities according

$$\eta_0 = -\frac{1}{6}\rho_0(2/\lambda + 1) \quad (2.11)$$

and the bulk viscosity is constant and not explicitly calculated in the lattice-Boltzmann method. The momentum flux density is then updated according to

$$\Pi'_{\alpha\beta} = \Pi_{\alpha\beta}^{eq} + (1 + \lambda)(\overline{\Pi}_{\alpha\beta} - \overline{\Pi}_{\alpha\beta}^{eq}) + \frac{1}{3}(1 + \lambda_B)(\Pi_{\gamma\gamma} - \Pi_{\gamma\gamma}^{eq})\delta_{\alpha\beta}, \quad (2.12)$$

The post-collision distribution, $n_i + \Delta_i(n)$, is determined by the requirement that the new populations are consistent with (2.1-2.3), so that

$$n_i + \Delta_i(n) = a_0^{c_i}\rho + a_1^{c_i}j_\alpha c_{i\alpha} + a_2^{c_i}\Pi'_{\alpha\beta}\overline{c_{i\alpha}c_{i\beta}} + a_3^{c_i}(\Pi'_{\alpha\alpha} - 3\rho c_s^2) \quad (2.13)$$

The procedure to update the lattice-Boltzmann equation therefore consists of the following steps. First one calculates the velocity moments $\rho, \mathbf{j}, \mathbf{\Pi}$ and the equilibrium momentum flux $\mathbf{\Pi}^{eq}$. From this the post-collision distribution can be calculated. This is then propagated according to equation 2.4. Following the usual Chapman-Enskog expansion procedure, the macroscopic behaviour of the system can be shown to be governed by the Navier-Stokes equations for an isothermal, compressible fluid.

In this thesis we will be concerned with colloidal particles in equilibrium. In this case a further convenient simplification of the lattice-Boltzmann scheme can be utilized. The relative magnitude of inertial forces compared to viscous forces acting on an object in a fluid flow can be characterized by the Reynolds number $Re = u^* l^* / \nu$, where u^* is a characteristic velocity and l^* a characteristic length. Taking u^* to be a typical thermal velocity (several $10m/s$) and l^* to be a particle diameter (typically $1\mu m$), we obtain the estimate $Re < 10^{-3}$ for a colloidal particle. Inertial forces are therefore negligible and the flow around the particles can be modelled within the “inertialess” creeping-flow regime. That is the convective term in the Navier-Stokes equations can be neglected ($\nabla \cdot \mathbf{u} = 0$). In lattice-Boltzmann simulations, it is the non-linear term in the equilibrium distribution that gives rise, at the macroscopic level, to the convective term. For creeping flow this can therefore be neglected, leading directly to a simpler equilibrium distribution.

$$n_i^{eq} = a_0^{c_i} \rho + a_1^{c_i} \mathbf{j} \cdot \mathbf{c}_i. \quad (2.14)$$

Finally, a further significant simplification of the algorithm occurs for the specific fluid viscosity $\nu_0 = \frac{1}{6}$. This corresponds with a relaxation to equilibrium in one time-step. This being the case, the output state of the collision operator does not depend on the non-equilibrium part of the distribution. This allows us to use a simplified collision operator

$$n_i + \Delta_i(n) = a_0^{c_i} \rho + a_1^{c_i} \mathbf{j} \cdot \mathbf{c}_i, \quad (2.15)$$

Formulated in these terms, the method can be implemented using less than half the number of floating-point operations required to solve equation 2.13. Furthermore, as we show in Chapter 3, by carefully constructing the collision operator a saving of more than a factor of four can be made in the amount of memory required for a given system size. Because of this convenient simplification, the majority of the simulations reported in this thesis are carried out using $\nu_0 = 1/6$ for the solvent. Although this may seem restrictive, in the creeping flow limit, and for time and length scales where the fluid behaves incompressibly, the viscosity becomes a relatively trivial parameter. In Chapter 6 however, where we study compressibility effects, this fixed choice of viscosity does turn out to be too restrictive and we use the full form of the collision operator so that we can vary the viscosity.

2.3 Integrating colloidal particles into the model fluid

In the lattice-Boltzmann model, colloidal particles are defined by a boundary surface (any size or shape), which cuts some of the links between lattice nodes. The fluid particle populations moving along these links interact with the solid surface via a perturbation assumed to act at a point halfway along the links. Thus a discrete representation of the particle surface is obtained, which becomes more precise as the particle, in terms of lattice units, gets larger (see figure 2.3).

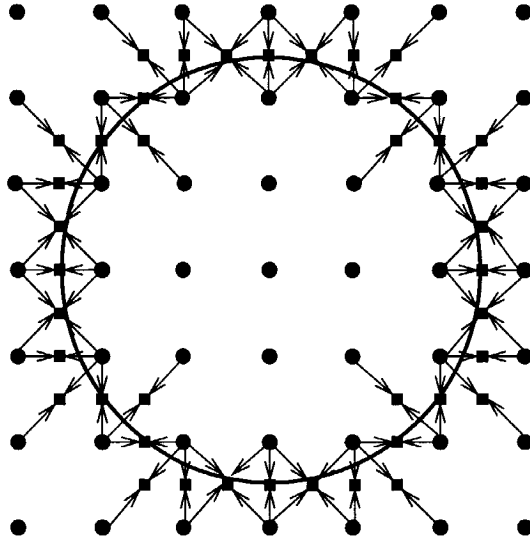


Figure 2.3: The discrete particle surface representation in a lattice-Boltzmann simulation for a sphere of radius 2.5 lattice spacings. The velocities along links cutting the surface are indicated by arrows. The locations of the boundary nodes are shown by squares and the lattice nodes by circles.

The motion of a colloidal particle is determined by forces and torques acting on it. These forces can be split into external, or non-hydrodynamic forces, and hydrodynamic forces. Non-hydrodynamic forces, for example attraction and/or repulsion between the particles due to an inter-particle potential, can be calculated separately, using standard techniques, and incorporated straightforwardly into the equations of motion. In contrast, the hydrodynamic forces are calculated from the velocity distributions themselves. This is essential because they characterize the interactions due to the flow fields induced in the solvent by the colloidal particles. These interactions are computed in the model by introducing additional update rules for the boundary-nodes. These update rules match the velocity of the Boltzmann fluid to the velocity of the solid particle surface, *i.e.* they impose the no-slip condition at the particle surface.

The implementation of the moving boundary rules is shown in figure 2.4. At each boundary node there are two incoming population densities n_1 and n_2 , corresponding to velocities \mathbf{c}_1 and \mathbf{c}_2 (where $\mathbf{c}_1 = -\mathbf{c}_2$). The location of the boundary is taken to be halfway between two lattice nodes. One of these lattice nodes is inside the solid object and the other outside and they are connected via a boundary link. We label the link which goes from inside to outside as ib and its partner as $-ib$. For a stationary boundary the populations are simply reflected back in the direction they came from [3, 10]. If the boundary is moving, the bounce-back rule is still applied, but some of the particles moving in the same direction as the solid object are allowed

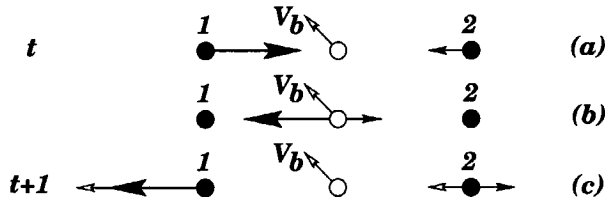


Figure 2.4: Illustration of the moving boundary rule. The solid circles represent the lattice nodes, the open circle the boundary node with its associated velocity vector. (a) Shows the densities n_1 and n_2 propagating in the direction of the boundary node. (b) Shows the intermediate step, reversing the densities at the location of the boundary node. (c) The reversed densities together with the projection of the boundary-velocity on the link of concern, propagate to the lattice nodes in reversed direction they came from. Hereafter the lattice nodes are updated.

to "leak" through in proportion to the boundary velocity. For the lattice-Boltzmann model these rules take the form

$$\begin{aligned} n_{-ib}(\mathbf{r}_b) &= n_{ib}(\mathbf{r}_b) - 4n_0(\rho)\mathbf{v}_b \cdot \mathbf{c}_{ib} \\ n_{ib}(\mathbf{r}_b) &= n_{-ib}(\mathbf{r}_b) + 4n_0(\rho)\mathbf{v}_b \cdot \mathbf{c}_{ib} \end{aligned} \quad (2.16)$$

where $n_0(\rho)$ is the equilibrium velocity distribution, \mathbf{v}_b is the local boundary velocity and \mathbf{r}_b is the vector connecting the center of mass of the object to the midpoint of the boundary link. These results are ensemble averages of earlier boundary node collision rules for lattice gases [11, 12]. The local boundary velocity is given by

$$\mathbf{v}_b = \mathbf{v} + \boldsymbol{\omega} \times \mathbf{r}_b, \quad (2.17)$$

with \mathbf{v} and $\boldsymbol{\omega}$ the linear and angular velocities respectively of the colloidal particle. The boundary node interactions, equations 2.16, conserve neither linear or angular momentum. Forces and torques must therefore act on the particle such that the correct conservation laws are recovered. The force on each individual boundary link, $\mathbf{F}_{ib}(\mathbf{r}_b)$, is related to the change of momentum and, assuming a time-step of unity, is given by

$$\mathbf{F}_{ib}(\mathbf{r}_b) = 2[n_{ib}(\mathbf{r}_b) - n_{-ib}(\mathbf{r}_b) - 4n_0(\rho)\mathbf{v}_b \cdot \mathbf{c}_{ib}]\mathbf{c}_{ib} \quad (2.18)$$

The total force and torque acting on the particle are obtained by summing these link forces, giving

$$\begin{aligned} \mathbf{F} &= \sum_{ib} \mathbf{F}_{ib}(\mathbf{r}_b) \\ \mathbf{T} &= \sum_{ib} \mathbf{F}_{ib}(\mathbf{r}_b) \times \mathbf{r}_b. \end{aligned} \quad (2.19)$$

The simplest way of updating the particle velocities is to use an Eulerian discretization of the equations of motion:

$$\begin{aligned}\mathbf{v}' &= \mathbf{v}(t+1) = \mathbf{v}(t) + \mathbf{F}/m \\ \omega' &= \omega(t+1) = \omega(t) + \mathbf{T}/I\end{aligned}\quad (2.20)$$

where m and I are the mass and moment of inertia of the particle, respectively. However using this scheme one matches the velocity of the fluid at the boundary with the 'old' velocity of the particle, rather than with the 'new' velocity. This makes the equations of motion inherently unstable. In order to suppress this instability, the density of the particle must be several times greater than the density of the fluid [9]. This is unrealistic because most colloidal suspensions have a density ratio of nearly unity (otherwise the particles would settle or float under the influence of gravity).

An alternative approach, described by Lowe *et al.* [13], is to match the 'new' velocity of the particle with the velocity at the boundary. The update rule is made self-consistent. To do so we express equation 2.17 in terms of the 'new' object velocity:

$$\mathbf{v}_b = \mathbf{v}' + \omega' \times \mathbf{r}_b, \quad (2.21)$$

where \mathbf{v}' and ω' indicate the 'new' object velocities. Substituting this modified expression for \mathbf{v}_b in equations 2.18 - 2.20 and solving the α -component of the linear and angular particle velocity results in

$$v'_\alpha = \frac{mv_\alpha(t) + 2 \sum_{ib} [n_{ib}(\mathbf{r}_b) - n_{-ib}(\mathbf{r}_b)] c_{ib\alpha}}{m + 8n_0(\rho) \sum_{ib} c_{ib\alpha} c_{ib\alpha}} \quad (2.22)$$

$$\omega'_\alpha = \frac{I\omega_\alpha + 2 \sum_{ib} [n_{ib}(\mathbf{r}_b) - n_{-ib}(\mathbf{r}_b)] (\mathbf{r}_b \times \mathbf{c}_{ib})_\alpha}{I + 8n_0(\rho) \sum_{ib} (\mathbf{r}_b \times \mathbf{c}_{ib})_\alpha (\mathbf{r}_b \times \mathbf{c}_{ib})_\alpha} \quad (2.23)$$

Using this rule the new fluid velocity at the boundary implies a force and torque on the object which, when incorporated into the equations of motion of the object, imply the same new velocity for the particle. Lowe *et al.* [13] reported that using this method it was possible to choose the density ratio freely - the algorithm is unconditionally stable. It is this approach with a density ratio of unity that is used in this thesis. Finally, it should be noted that using either of the above methods for integrating the equations of motion, imposing the stick boundary condition requires the presence of fluid both inside and outside the colloidal particles. The particles are essentially hollow spheres filled with fluid. This interior fluid is computationally convenient, since it avoids the necessity of creating and destroying fluid as the particle moves. However, it is an artefact. Real colloidal particles are not generally filled with fluid, they are impervious solid objects. In simulations of colloidal suspensions reported thus far, using this method, the presence of the internal fluid has not been reported as problematic. In Chapter 4 we consider to what extent this is justified, and suggest a modified approach negating any effects of the internal fluid.

2.4 Calculating transport coefficients

This thesis is concerned with hydrodynamic processes near equilibrium, corresponding to short times experimentally. Because matter is discrete, systems in equilibrium will undergo fluctuations about their equilibrium states. Fluctuations about the equilibrium state decay on the average according to the same hydrodynamic equations which describe the decay of the system from a non-equilibrium to the equilibrium state. The hydrodynamic equations govern the dynamics of the long-wavelength and low-frequency components of those fluctuations, and they determine the behaviour of dynamic equilibrium correlation functions. The point is that inhomogeneities in the densities of the particles, momentum or kinetic energy must be transported from one part of the fluid to another to achieve equilibrium. If we can probe the decay of these inhomogeneities, we have a means of probing the transport processes in the system. The lattice-Boltzmann method provides a method for doing this.

Starting from Newton's equations of motion, one can show that the dynamics of the colloidal particles can be written in the form of a generalized Langevin equation [16, 17, 18]. Considering one component of a particle i in a system of N particles the generalized Langevin equation (in the absence of propagative processes) takes the form

$$m \frac{dv_i(t)}{dt} = \sum_{j=1}^N \int_0^t \gamma_{ij}(t-s) v_j(s) ds + F_i(t) + F_{i\text{x}}(t) \quad (2.24)$$

Here the terms $\gamma_{ij}(t)$ are time-dependent friction coefficients, relating the force on particle i to the current and past velocity of particle j , and $F_{i\text{x}}$ is any external force acting on particle i . The term $F_i(t)$ is a stochastic force, similar to the random force in the simple Langevin equation (1.3). It again represents the cumulative effects of thermal collisions between the colloidal particles and solvent. In order to ensure that the correct equilibrium properties of the system are recovered, the statistical properties that the stochastic force must satisfy are now more complex [19], namely

$$\begin{aligned} \langle F_i(t) \rangle &= 0 \\ \langle F_i(t) v_j(t) \rangle &= 0 \\ \langle F_i(0) F_j(t) \rangle &= k_B T \gamma_{ij}(t) \end{aligned} \quad (2.25)$$

The "random" force is no longer delta function correlated. The generalized Langevin equation is quite formal because we do not know the friction coefficients. However, given an equation of motion for the solvent, they can, in principle, be calculated. The lattice-Boltzmann model can be summarized as a means of solving the generalized Langevin equation under the assumption that the dynamics of the fluid are governed by the Navier-Stokes equations. If we solve a fluctuating Boltzmann equation [9] we solve the stochastic differential equation (equation 2.24) in its entirety. Without fluctuations, we simply solve the dissipative equation one obtains from the generalized Langevin equation with the random force term neglected.

Following from the above, there are a number of ways we can extract transport coefficients for colloidal suspensions by using the lattice-Boltzmann equation. The most obvious is to solve the fluctuating Boltzmann equation and simply calculate the relevant correlation function. We have already seen that the diffusion coefficient is related to the time integral of a velocity correlation function (equation 1.6). There are similar Green-Kubo relations relating other transport coefficients to correlation functions. The viscosity of a pure fluid, for example, is related to the decay of equilibrium stress fluctuations. Specifically

$$\eta V k_B T = \int_0^\infty \left\langle \sum_{xy}^f(t) \sum_{xy}^f(0) \right\rangle dt, \quad (2.26)$$

where \sum^f is the fluid stress tensor, equivalent to the momentum flux density of the fluid (equation 2.3). Equation 2.26 can be applied to solid-fluid suspensions as well by including both the fluid stress tensor and the solid-fluid stress \sum^s , summed over all the solid particle surfaces. By integrating the stress-stress correlation functions the viscosity can be computed from equation 2.26.

While using a fluctuating Boltzmann equation and computing time correlation functions is the most obvious root for calculating transport coefficients, but there are alternatives [20]. We will discuss two of these here, in terms of the velocity auto-correlation function (although both approaches can be generalized). It is convenient to begin by taking the Laplace transform of equation 2.24 in the absence of external forces

$$m(z\tilde{v}_i(z) - v_{i0}) - \tilde{F}_i(z) = - \sum_j \tilde{\gamma}_{ij}(z)\tilde{v}_j(z), \quad (2.27)$$

where z is the Laplace transform variable, and v_{i0} is the initial velocity of particle i . Transformed quantities are indicated with a tilde. If we set $z = 0$ we find

$$mv_{i0} + \tilde{F}_i(0) = \sum_j \tilde{\gamma}_{ij}(0)\tilde{v}_j(0), \quad (2.28)$$

The N equations for the dynamics of the N particles in the system can be written as the matrix equation

$$mv_0 + \tilde{F}(0) = \tilde{\gamma}(0)\tilde{v}(0). \quad (2.29)$$

where v_0 and $\tilde{F}(0)$ are the vectors of initial velocities and Laplace transformed stochastic forces respectively. Inverting the equation and taking the product with v_0 we find

$$v_0\tilde{v}(0) = v_0\tilde{\gamma}(0)^{-1}(mv_0 + \tilde{F}(0)) \quad (2.30)$$

and averaging over all N particles

$$\frac{1}{N} \sum_i v_{i0}\tilde{v}_i(0) = \frac{1}{N} \sum_{ij} (\tilde{\gamma}(0)^{-1})_{ij} (mv_{i0}v_{j0} + v_{i0}\tilde{F}_j(0)) \quad (2.31)$$

If we now take the average over all thermal velocities, denoted $\langle \dots \rangle$, and note that for short-time diffusion the friction matrix γ *only* depends on the instantaneous positions of the particles, we find

$$\frac{1}{N} \sum_i \langle v_{i0} \tilde{v}_i(0) \rangle = \frac{1}{N} \sum_{ij} (\tilde{\gamma}(0)^{-1})_{ij} (m \langle v_{i0} v_{j0} \rangle + \langle v_{i0} \tilde{F}_{j0} \rangle) \quad (2.32)$$

In an equilibrium system we know from thermodynamics that $\langle v_{i0} v_{j0} \rangle = k_B T \delta_{ij} / m$ and by definition we have $\langle v_{i0} \tilde{F}_j(0) \rangle = 0$, hence, using the Green-Kubo relation between the velocity autocorrelation and the diffusion coefficient, we have

$$D = \frac{1}{N} \sum_i \langle v_{i0} \tilde{v}_i(0) \rangle = \frac{k_B T}{N} \sum_i (\tilde{\gamma}(0)^{-1})_{ii} = k_B T \langle D_{ii} \rangle, \quad (2.33)$$

By definition $\frac{1}{N} \sum_i (\tilde{\gamma}(0)^{-1})_{ii}$ is the average mobility $\langle D_{ii} \rangle$. This is known as the generalized Einstein relation. Now suppose we take the purely dissipative system where the fluctuating force term is zero (*i.e.* $\langle F_i(0) F_j(0) \rangle = 0$) and apply a constant external force $F_{i\mathbf{x}}$ to particle i . We expect that the system will come to a steady state whereby particle i has a constant velocity $v_{i\mathbf{x}}$. If the magnitude of the random force is zero but an external force acts on particle i the equation for the velocity of particle i from the set of equations 2.30 reduces, at low frequency, to

$$\tilde{v}(0) = \tilde{\gamma}(0)^{-1} \tilde{F}(0) \quad (2.34)$$

If we substitute for low frequency Laplace transform we find

$$\frac{v_{i\mathbf{x}}}{F_{i\mathbf{x}}} = (\tilde{\gamma}(0)^{-1})_{ii} \quad (2.35)$$

So, by applying a constant force to particle i and calculating the steady response we can calculate the value of the mobility for particle i . By repeating such a calculation for each particle in the system we can calculate the average mobility and so, by making use of the generalized Einstein equation, calculate the diffusion coefficient.

The argument outlined above shows how we can calculate the diffusion coefficient from the purely dissipative system *i.e.* without the need for fluctuations. There is another route for doing so which follows along the lines of Onsager's regression hypothesis. The decay of a fluctuation we impose on the dissipative system should be the same as the decay of a spontaneous fluctuation in a real system. To see this, let us return to the generalized Langevin equation. If we take the Laplace transformed equations of motion for the purely dissipative system, at low frequencies we have

$$v_0 \tilde{v}(0) = m v_0 \tilde{\gamma}(0)^{-1} v_0 \quad (2.36)$$

or in terms of individual particles

$$\frac{1}{N} \sum_i v_{i0} \tilde{v}_i(0) = \frac{1}{N} \sum_{ij} (\tilde{\gamma}(0)^{-1})_{ij} m v_{i0} v_{j0}. \quad (2.37)$$

Suppose we now *specify* the properties of the initial velocities such that the equilibrium condition $m \langle v_{i0} v_{j0} \rangle = k_B T \delta_{ij}$ is satisfied (denoted [...]), then we find that

$$\frac{k_B T}{N} \sum_i (\tilde{\gamma}(0)^{-1})_{ii} = \frac{1}{N} \sum_i [v_{i0} \tilde{v}_i(0)] \quad (2.38)$$

If we calculate the quantity on the right hand side then, comparing with equation 2.33 derived for the “real” fluctuating system, then this is clearly equal to the diffusion coefficient. This latter approach has the advantages that it allows us to calculate the diffusion coefficient in the dissipative system without the need to average over thermal fluctuations, and without having to explicitly evaluate the mobility on a particle by particle basis. It effectively evaluates the average mobility in one simulation.

Bibliography

- [1] U. Frisch, B. Hasslacher and Y. Pomeau, *Phys. Rev. Lett.* **30**, 1505 (1986).
- [2] S. Wolfram, *J. Stat. Phys.* **45**, 471 (1986).
- [3] U. Frisch, D. d'Humières, B. Hasslacher, P. Lallemand, Y. Pomeau and J. -P. Rivet, *Complex Systems* **1**, 649 (1987).
- [4] L. Kadanoff, G. McNamara and G. Zanetti, *Phys. Rev. A* **40**, 4527 (1989).
- [5] G. Zanetti, *Phys. Rev. A* **40**, 1539 (1989).
- [6] G. McNamara and G. Zanetti, *Phys. Rev. Lett.* **61**, 2332 (1988).
- [7] F. Higuera and J. Jimenez, *Europhys. Lett.* **9** (7), 663 (1989).
- [8] F. Higuera, S. Succi and R. Benzi, *Europhys. Lett.* **9**, 345 (1989).
- [9] A. J. C. Ladd, *J. Fluid Mech.* **271**, 285 (1994).
- [10] R. Cornubert, D. d'Humières, & C. D. Levermore, *Physica D* **47**, 241 (1991).
- [11] A. J. C. Ladd & D. Frenkel, *Cellular Automata and Modeling of Complex Physical Systems* (ed. P. Manneville, N. Boccara, G. Y. Vichniac & R. Bidaux), Springer (1989).
- [12] A. J. C. Ladd, *Computer Simulation in Materials Science* (ed. M. Meyer & V. Pontikis), Kluwer (1991).
- [13] C. P. Lowe, D. Frenkel, and A. J. Masters, *J. Chem. Phys.* **103**, 1582 (1995).
- [14] J. P. Hansen and I. R. McDonald, *Theory of simple liquids*, Academic Press Limited, 2nd edition (1990).
- [15] B. J. Alder and T. E. Wainwright, *Phys. Rev. A* **1**, 18 (1970).
- [16] H. Mori, *Prog. Theor. Phys.* **34**, 399 (1965).
- [17] B.J. Berne and G.D. Harp, *Adv. Chem. Phys.* **17**, 63 (1970).
- [18] J.M. Deutch and I. Oppenheim, *Faraday Discuss. Chem. Soc.* **83**, 1 (1987).
- [19] M. Medina-Noyola, *Faraday Discuss. Chem. Soc.* **83**, 21 (1987).
- [20] M. Hagen, *Diffusion of Confined Colloidal Particles*, PhD Thesis, Faculteit Scheikunde Universiteit Utrecht en FOM-Instituut voor Atoom- en Molecuulfysica Amsterdam (1997).

3 Simulation tools and equipment

3.1 Introduction

This chapter deals with algorithmic considerations to reduce the computational costs required to perform the lattice-Boltzmann simulations described in the subsequent chapters. The computational cost depends on the size and number of time-steps of the simulation system involved. Generally speaking, the size of the system determines the accuracy of the results, whereas the number of time-steps represents the time evolution of the physical quantities. As we shall see in later chapters, these two considerations are also, to some extent, linked. There are two main reasons why large system sizes are generally required. One is that the many-body colloidal particle interactions are long ranged in nature, so systems containing large numbers of colloidal particles are needed to minimize finite size effects [1, 2]. The second is that the size of the model colloidal particles, relative to the lattice spacing, determines the spatial resolution of the simulation. To capture hydrodynamic effects with sufficient accuracy we may need to use large representations of the colloidal particles. Again, this translates, in computational terms, into a need for a large system. The limitations on the size of a lattice-Boltzmann simulation system are, however, closely related to the limitations on the computer capacities. Large scale lattice-Boltzmann simulations consist of typically several tens of thousands of colloidal particles. This is very demanding both in computing time and in memory usage.

To solve the problem of computational costs we tried both to improve the algorithm and increase the computational power. A serious disadvantage of the lattice-Boltzmann algorithm is its memory usage. The problem space uses large amounts of storage capacities [3] both on main memory and on disk. For large scale simulations memory can become a serious problem. By carefully analysing the algorithm it appears that often less than 25% of the original data has to be kept in memory. This appeared to be possible by making use of the properties of the collision operator and by starting the simulation time-step at a different point. We shall show how this works by analysing the algorithm steps in terms of processor operations.

During the course of the research reported here, the computational power avail-

able increased due to continuous developments in hardware. New and faster computers became available. However, the simulation of colloidal suspensions, still requires large supercomputers. The current top performance is still time consuming and many calculations of scientific and technological relevance are still impractical. Increasing hardware performance is achieved in two independent ways; by the development of faster technology and by utilising parallelism. Whereas faster technology is used to scale up the performance of a sequential computer, parallelism is used to bring "many hands make light work" into practice. The nature of the lattice-Boltzmann algorithm is highly parallel and can be exploited on most computer topologies. In order to optimise the performance and reduce the necessary computing time to a minimum, the lattice-Boltzmann computer program should be written such that the hardware capacities are fully exploited.

This chapter is organised as follows. We start with an explanation of the sequence of steps involved in the algorithm. In section 3.3 the efficiency of the sequential algorithm on a single processor will be considered. Section 3.4 will describe a modification to the conventional algorithm that considerably reduces the demand on computer memory. The degree of parallelisation and performance of a parallel computer system is discussed in section 3.5. Finally, the performance of the current computer program is described.

3.2 Basic algorithm

As we already explained in section 2.2, the time evolution of the lattice-Boltzmann model fluid consists of a propagation and a collision step. In practice, the **propagation** step consists of collecting, for every node in the system, the 18 floating point values of the distribution functions, n_i , from the nearest neighbour nodes. From this we calculate the velocity moments $\rho, \mathbf{j}, \mathbf{\Pi}$ and $\mathbf{\Pi}^{eq}$, according the equations 2.7-2.12 described in chapter 2. The **collision** step updates the nodes in the system, again in terms of 18 floating point numbers, towards their new populations according equation 2.13 from chapter 2. Both steps affect all nodes in the system and can be performed in any random sequence, provided that for every single node, the propagation step precedes the collision step.

On the other hand, the colloidal particles add two more steps to the basic algorithm. One of these involves the **update of the colloidal particle velocities** for the next time step. For the modified algorithm, without internal fluid, this will be done according equation 4.5 and 4.6 from chapter 4 accompanied with the associated treatment of the internal nodes. For the standard model with internal fluid the equations 2.22 and 2.23 will be used from chapter 2. Notably, this step has to be carried out before the moving boundary rules can be applied and affects all the velocity distributions to and from the boundary nodes in the system. The other step, concerning the integration of the colloidal particles, is applying the **moving boundary rules** on both directions of all the boundary nodes from all colloidal particles. After the moving boundary conditions are applied, the propagation step

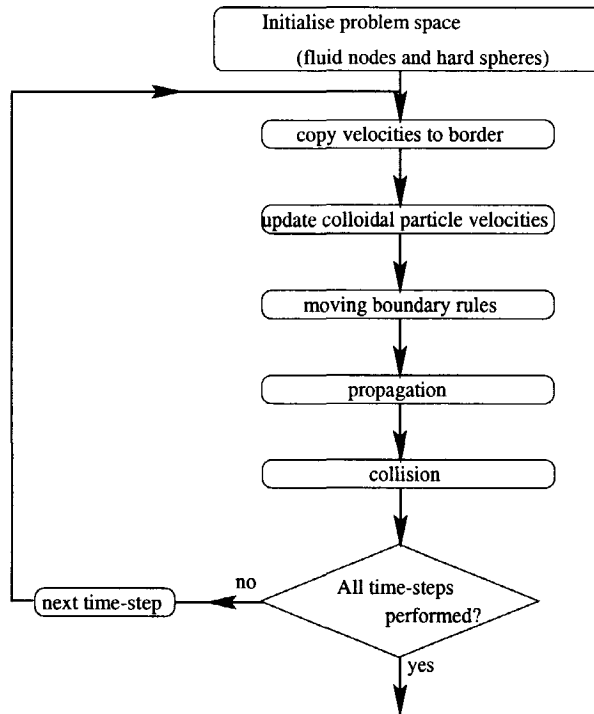


Figure 3.1: Schematic overview of the implementation of the conventional algorithm.

and collision step may update all nodes in the system towards their new state.

These four steps contain the body or inner loop of the calculational scheme. Fig. 3.1 displays a schematic overview of this basic algorithm, containing the steps in the right order. The calculations used in this numerical scheme are mainly floating point calculations, supplied with predefined address-lists where possible, e.g. boundary links, internal nodes, fluid nodes if desired. However, for the simulation of colloidal suspensions we are dealing with large system sizes. The memory required to describe the fluid state in terms of 18 floating point numbers per node can really be prohibitively large in this conventional algorithm. Therefore we implemented an improved storage technique, described in section 3.4.

There is one step left over from fig. 3.1 and that is dealing with the finite size of the simulation box. This we call **copy velocities to border**. To simulate a (pseudo) infinitely large system, periodic boundary conditions are used. This means that the original problem space is surrounded by identical copies of itself. In order to efficiently implement these periodic boundary conditions, extra layers (halos) of nodes are added to the boundaries of the system. The values of each boundary node is copied into a corresponding halo node, such that the nodes with directions pointing outside the system can collide with the nodes of the opposite sides. When

using a parallel computer (see section 3.5.1), the halos act as communication buffers and contain information of the nodes at neighbouring processor boards.

3.3 Computer Architecture

The match between the computer architecture to be selected and the algorithm to be used, importantly determines the performance of the simulation system. To optimise this performance against costs we either can search for commercially available computers and benchmark our algorithm, or, as an alternative, design and build a computer ourselves, the architecture of which is tailored to the algorithm involved. These two cases will be considered in this section.

The computational characteristics of the lattice-Boltzmann simulations are used to choose possible candidates from the large variety of available computers. First of all, lattice-Boltzmann simulations of colloidal suspensions require a large memory to store all their fluid- and colloidal particle information to avoid time consuming swapping to disk. Secondly, the operations on the data are standard Single Precision (SP) and Double Precision (DP) floating point operations, such as add, subtract and multiply, and integer address calculations. Because DP floating point operations require twice as much storage as SP floating point operations, this implies a two times smaller maximum system size. Therefore the performance of DP floating point operations is important for the selection of the computer system. Thirdly, the calculational scheme is memory intensive, that is only a few operations are involved on all data. Therefore the usage of cache memory at the processor level is important for the total performance of the simulation.

In general the choice for a RISC processor instead of a CISC processor is clearly justified. A RISC processor is made to do only simple calculations at a high processing rate. One of the characteristics of a RISC architecture is its load/store mechanism, made to obtain maximum processor-memory speed. The load and store operations are made independent of processor operations which allows for instruction pipelining. Such a processor operates merely on registers, which additionally reduces the instruction set. Fast cache memories reduce memory excesses by holding frequently used data and instructions close to the processor. The instructions and data use separate buses. A (build-in) floating point processor is also required and a high clock speed is an obvious advantage.

Furthermore there are trivial other conditions that limit the number of candidates in our choice for a suitable computer for Lattice Boltzmann simulations. These are the available budget to purchase, lease or rent such a computer, the maximum turn-around-time allowed for a simulation and the local availability of such a computer in the research group. Once such a computer is selected, the implementation of the algorithm can still be tuned to the hardware architecture of the computer. Also the programming language used to implement the algorithm may depend on the efficiency of the available compilers.

We started by using the available workstations in our group and performed

lattice-Boltzmann simulations on three RISC processor types, *i.e.* MIPS R4000, R5000 and R10000. These three processors are representative of the technological improvements in workstations over the last five years. The improvements in processor technology and thus in simulation time are clear from the results shown in figure 3.2.

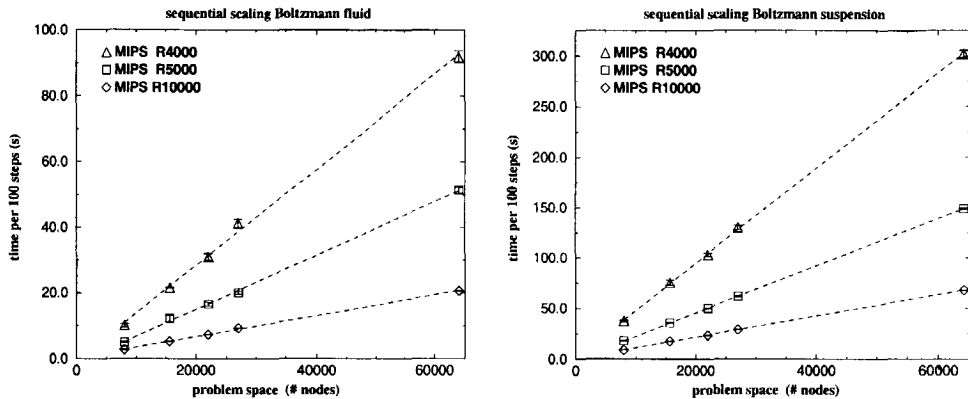


Figure 3.2: Processor speed plotted as a function of problem size for a Boltzmann fluid (left) and for a colloidal suspension(right).

As an alternative, when both performance and costs do not meet the requirements, and thus the simulations can not be carried out, designing and building a special-purpose computer can be considered. If the infrastructure locally allows you to do so, the advantages of building your own computer are enormous. Multiple memory sections, data paths and arithmetic operators can be exploited to use pipelined and parallel operations tailored to the algorithm involved. Also word lengths and memory sizes can be tuned to optimize the performance and the accuracy of the simulation. The newest commercially available hardware components at the chip- or board level can be used to speed up the calculations and to minimize the cost/performance ratio. Commercially available Computer Aided Design software packages allow efficient design, building, testing and maintenance of such a special purpose computer. This approach has been successfully demonstrated over the last 20 years in our group. Cost/performance ratio improvements of two orders of magnitude were shown for molecular dynamics, Monte Carlo Ising spin simulations and Cellular Automata systems [4, 5, 8, 9, 10, 11]. As we can state that modern commercially available super computers are good candidates for our simulations and they are available to us, we will only consider commercially available computers during the rest of this thesis.

3.4 Storage Reduction

As we already mentioned, large scale lattice-Boltzmann simulations of colloidal suspensions demand large amounts of computer memory. To give a feeling for the size of numbers we are dealing with consider the following. A typical system size we want to simulate contains for example 20000 colloidal particles, with a radius of 4.5 lattice spacings and intermediate volume fraction of 25%, we need a simulation box of over 300^3 nodes which corresponds with 30 Mb nodes. Nodes consist of 18 floating point numbers each to describe their flow state, requiring 2.2 Gb to describe just the fluid state. The particles in this case occupy another 120 Mb storage for their boundary links. Here the problem space requires in total about 2.3 Gb main memory from its processor and thus it seems unavoidable that these simulations require very expensive hardware.

However, by carefully analysing the collision operator we have found a way to greatly reduce the demand for memory. The method is based on the properties of the collision operator and, to our knowledge, has not been described before. Storage reduction is particularly effective when the collision operator is described by equation 2.15, with which most of our simulations are carried out (see chapter 2). In this case the mass ρ and the three components of momentum \mathbf{j} are calculated. Then, using only those four values, in addition to the constant values for a_0 and a_1 , the new velocity distributions n_i can be calculated, representing the new states of the fluid sites. This makes an important storage reduction of the configuration space possible. Storing the four intermediate data rather than the usual 18 values of the output state leads to a storage reduction factor of $4/18$, which is better than a factor of four. Therefore, the collision step is split into two steps: A **pre-collision** step where the four values of ρ and momentum \mathbf{j} are calculated and a **post-collision** step where the 18 new populations are computed from these four values. A time-step now starts with the post-collision step. To update the fluid state this is followed by the propagation step and ends with the pre-collision, where only ρ and the three components of \mathbf{j} are kept in memory. However, when (moving) boundaries are involved, as is the case in colloidal suspensions, the interaction between fluid and colloidal particles needs to be calculated (see 3.2). In that case, we will need some of the 18 values of n_i for the boundary nodes involved. These can only be obtained by the post-collision operation, which would destroy the storage reduction effect. To overcome this problem we allocate a small portion of memory where only a small part of configuration space is stored with their 18 n_i values. During a time-step we sweep through configuration space in one direction and do all calculations plane by plane. By choosing a plane to expand into the detailed configuration space, we still can both use the storage reduction scheme and efficiently allow (moving) boundary conditions in our simulations.

The data storage is organised such that the required information is efficiently retrieved from memory. A closer look at the FCHC-lattice shows that it is convenient to define three different sets of velocity directions: a *top*, a *middle* and a *bottom* set (see fig. 3.3). Five directions are pointing up to nodes in the upper layer (the top

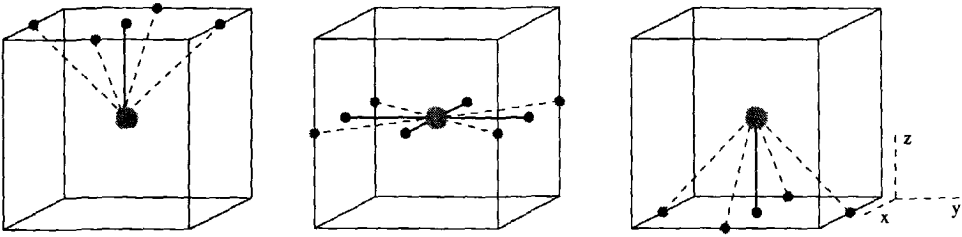


Figure 3.3: Top, middle and bottom set of the FCHC lattice.

set top), five directions are pointing down to the lower layer (the bottom set bot) and the eight other directions lie in the middle plane pointing to the nodes situated in the same plane (the middle set mid). Each site in a plane interacts with sites in the two neighbouring planes in addition to sites in the same plane. Hence the problem space is divided in planes each consisting of a top , bot and mid part, indexed by a stepping variable tt (numbered from top to bottom). That is, the top set $top(tt)$ of the current plane tt interacts with the bottom set $bot(tt - 1)$ of the plane $tt - 1$, indicating the preceding plane. The bottom set $bot(tt)$ of the current plane interacts with the next top set $top(tt + 1)$ to be handled, corresponding to the plane with index $tt + 1$, the middle set $mid(tt)$ with the current middle set $mid(tt)$. The small portion of additional memory that is required to keep these populations amounts, per site in a plane, to 5 locations for $bot(tt - 1)$, 5 locations for $top(tt)$, 8 locations for $mid(tt)$, 5 locations for $bot(tt)$ and 5 locations for $top(tt + 1)$.

At the start of each sweep or time-step, we calculate the new velocity and angular velocity of each colloidal particle by summing over the velocity distributions n_i concerning their boundary nodes. At this time the storage is in reduced state and therefore this operation needs a small partial post-collision operation. Furthermore, for each plane, we can pre-calculate a list for all three sets, *i.e.* $toplist(tt)$, $midlist(tt)$ and $botlist(tt)$, containing boundary node position, velocity direction and population for that plane. These lists are then used to perform the moving boundary rules, resulting in a preparation step that takes the effect of the boundary interactions into account. This step is required before the propagation step can be performed for all sites in the system. Figure 3.4 displays the storage reduced algorithmic procedure in terms of high level algorithm steps.

By contrast, we need a more detailed description to deal with the separated and independent top , mid and bot sets. To serve as a visual guide we give a schematic overview of the data flow in figure 3.5. This illustrates the update of the planes, utilizing the storage reduced algorithm, in a system of four planes. The steps are as follows. Starting updating the sites in the planes, we apply the post-collision step for the first plane, where $tt = 0$, for the following sets $bot(-1)$, $top(0)$, $mid(0)$, $bot(0)$ and $top(1)$. For this we are using the reduced storage information from the plane(-1), the plane(0) and the plane(1). Due to periodic boundary conditions, plane(-1) is

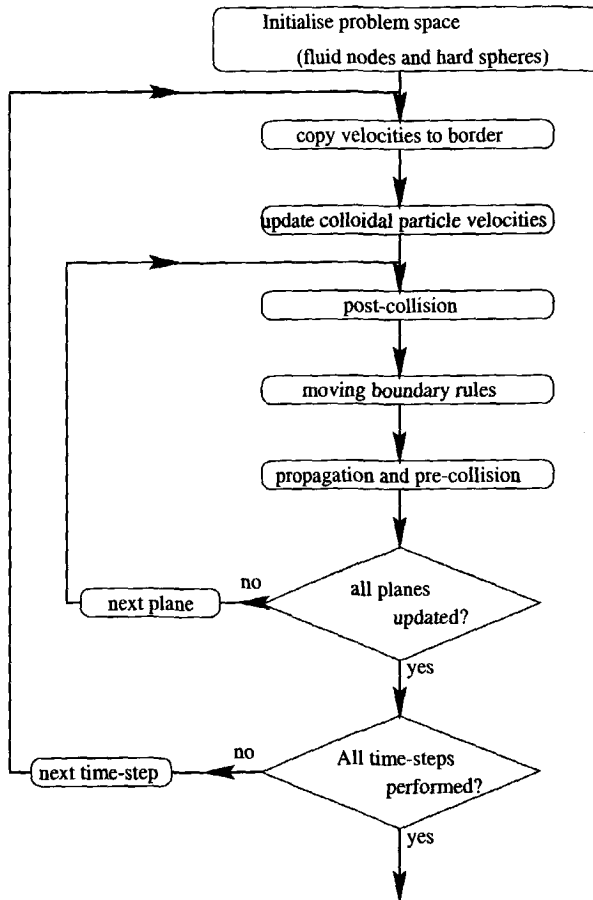


Figure 3.4: Schematic overview of the algorithm steps and their sequence taken in the storage reduced algorithm.

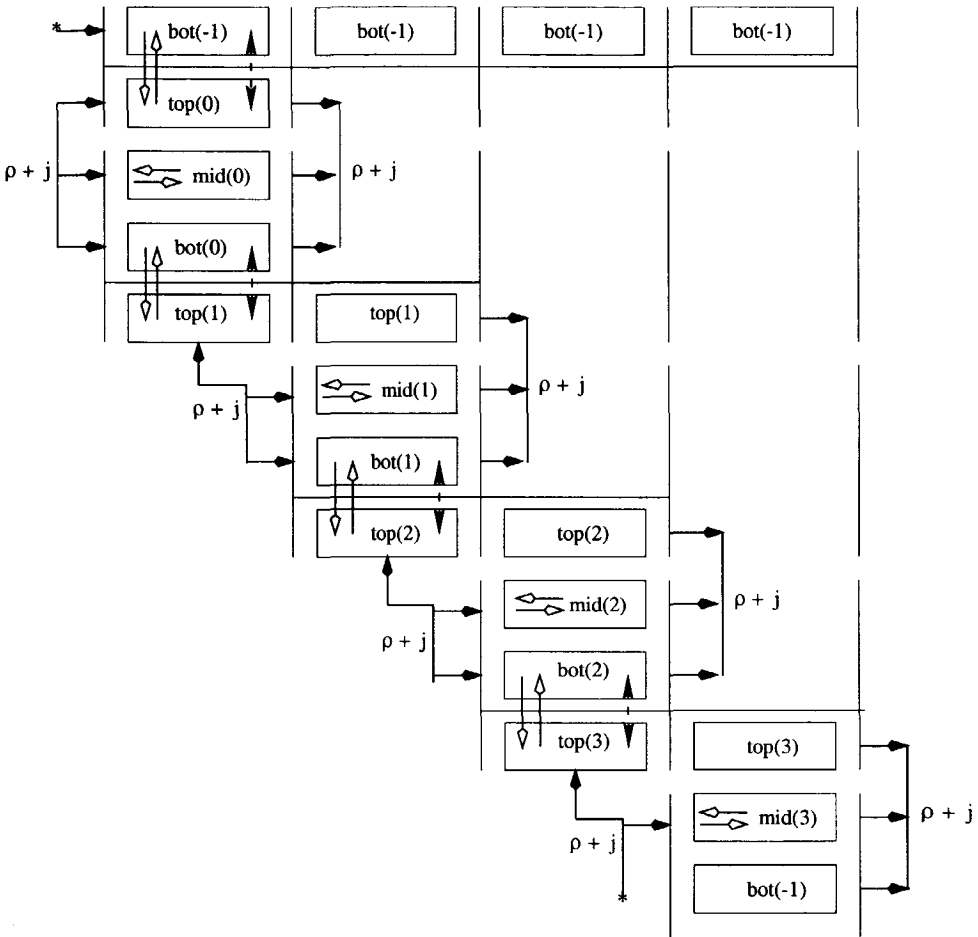


Figure 3.5: Data flow diagram for updating the planes in the storage reduced algorithm for a system consisting of four planes. The symbols $bot(tt)$, $mid(tt)$ and $top(tt)$ represent the independent plane sets. Adjacent planes are indexed consecutively. The planes are updated consecutively, starting from plane(0) to plane(3) so that the course of time is from left to right in the figure. The black arrows represent the data flow from and back to the reduced configuration storage. The open arrows represent the moving boundary interactions and the dashed arrows represent the propagation of data.

equal to $\text{plane}(TT-1)$, where TT is the total number of planes in configuration space. Next, the pre-calculated lists, the $\text{toplist}(0)$ and $\text{botlist}(-1)$ are used to account for the (moving) boundary effects in both $\text{bot}(-1)$ and $\text{top}(0)$ and then both $\text{bot}(-1)$ and $\text{top}(0)$ are propagated, just by swapping the pointers of the $\text{bot}(-1)$ and $\text{top}(0)$ plane sets. Next $\text{midlist}(0)$ is used for performing the (moving) boundary interactions in plane set $\text{mid}(0)$, and then the propagation step is carried out at once by proper addressing the velocities in $\text{mid}(0)$ during the pre-collision operations. Thereafter, both $\text{botlist}(0)$ and $\text{toplist}(1)$ are used to account for the (moving) boundary interactions in both $\text{bot}(0)$ and $\text{top}(1)$. Both $\text{bot}(0)$ and $\text{top}(1)$ are now propagated, just by swapping the pointers of the $\text{bot}(0)$ and $\text{top}(1)$ plane sets. From $\text{top}(0)$, $\text{mid}(0)$ and $\text{bot}(0)$ plane sets, we now apply the pre-collision step and thus overwrite the storage reduced data with their new states for $\text{plane}(0)$, *i.e.* the resulting 4 data per site in reduced storage format.

To update the next plane a similar procedure is repeated where tt is incremented. First the post-collision operations for $\text{mid}(tt)$, $\text{bot}(tt)$ and $\text{top}(tt+1)$ are carried out. Next the pre-calculated lists $\text{midlist}(tt)$, $\text{botlist}(tt)$ and $\text{toplist}(tt+1)$ are used to account for the (moving) boundary interactions. The pointers to $\text{bot}(tt)$ and $\text{top}(tt+1)$ are then swapped for the propagation step, and finally $\text{top}(tt)$, $\text{mid}(tt)$ and $\text{bot}(tt)$ are used to calculate the pre-collision step and, with that, the newly updated $\text{plane}(tt)$ is restored in the reduced storage space. In the last cycle, when updating the $\text{bot}(TT-1)$ plane part, we replace this plane set by $\text{bot}(-1)$ because of periodic boundary conditions. This plane set was already taken care of in the first cycle.

3.5 Parallelism

One primary advantage of the lattice-Boltzmann scheme is its suitability for parallel computing. Because exotic technology is required to speed up sequential computer architectures, parallel computer systems are the only way to speed up the calculations at modest costs. In general, when the nature of the problem to be solved allows a decomposition of the calculations, a parallel calculational scheme will speed up the calculations. In the lattice-Boltzmann scheme a simultaneous update or time-step of all fluid nodes is allowed, simply just by performing the sequence of algorithm steps for every node simultaneously. Besides, the information needed to update a node is contained by its 18 nearest neighbouring nodes. All of them are separated by equal distances, because of the underlying structured grid topology, and this ensures that only local environment calculations are necessary. The simultaneous update of the lattice nodes and the local environment characteristics are responsible for the highly parallel and scalable nature of the lattice-Boltzmann algorithm. Furthermore, splitting the calculations up into equally sized smaller parts, corresponds to decomposing problem space into equally sized slices to be updated. Such a domain decomposition appears to be applicable in every extent to the lattice-Boltzmann scheme. Since the Boltzmann-scheme has a structured grid topology, domain de-

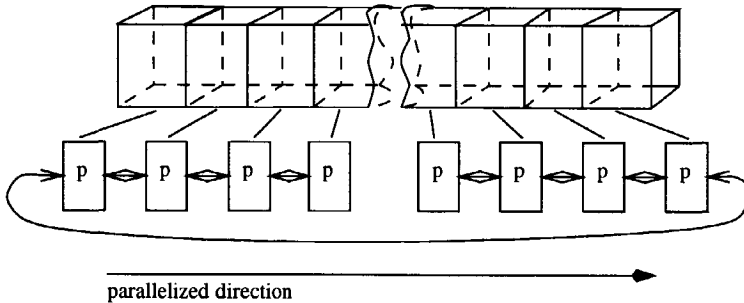


Figure 3.6: The LPA concept; Each slice of the problem space is calculated parallel on a separate processor.

composition into equally sized sub-parts will result in a load balanced application. The simplest approach is a one-dimensional, or linear domain decomposition. To start with, we chose this straightforward approach and examined the efficiency of the parallel program on two parallel computers, detailed below.

3.5.1 Linear domain decomposition

An obvious decomposition of the problem space is to subdivide it into equally sized slices in just one dimension. Each slice is then assigned to a separate processor, which computes the new states of the nodes independently for each domain. As the interaction distance of the lattice nodes is smaller than or equal to the slice dimension, information is only required from the local processor and at most the two neighbouring processors. Such a one-dimensional communication topology, illustrated in figure 3.6, is called The Linear Processor Array (LPA). Because of the very small interaction distance inherent in the lattice-Boltzmann algorithm this LPA communication topology should lead to a high degree of inherent parallel scalability.

Furthermore, the parallel algorithm contains the same steps as the storage reduced algorithm (see figure 3.4) except that the interprocessor communication takes place at the boundary of each slice. Here the populations from neighbouring nodes need to be copied from adjacent domains. This implies that the halos, previously used for periodic boundary conditions, now hold, in the parallelized direction, copies of the boundary nodes of neighbouring domains. After updating the domains on each processor, a synchronous communication step takes place between all neighbouring processors.

3.5.2 Performance results

The simulations described in this thesis were performed on two different parallel computers. Before showing their scalability results it is useful to consider the fol-

lowing. The speedup factor is defined as follows.

$$S(n) = T(1)/T(n) \quad (3.1)$$

With $T(1)$ the sequential execution time on a uniprocessor and $T(n)$ the parallel execution time for an n -processor system. There are still a lot of current definitions for the speedup performance of a parallel system. For example, consider the fixed-load speedup. This includes the famous (at least in the world of parallel computing) Amdahl's law [12], whereby the speedup factor is upper-bounded asymptotically by the sequential portion of the program. The idea is that the parallel portion of the program is evenly distributed by n processors, resulting in a reduced time, while the sequential part cannot be divided among the processors and therefore becomes dominant. In other words the communication overhead increases faster than the machine size and will, due to communication limits, eventually restrict the performance even if the sequential fraction is small. One of the major shortcomings in applying Amdahl's law is that the fixed load prevents scalability in performance. Although the sequential bottleneck is a serious problem in time critical-applications, in accuracy-critical applications we wish to solve the largest problem size as possible on a larger machine with about the same execution time as for solving a smaller problem on a smaller machine. Therefore fixed-time speedups are a more appropriate measure of performance [13]. In scalability analysis, one can increase the machine size and problem size proportionally to maintain the system efficiency at an equal level. The system efficiency for a n -processor system is defined by [14]

$$E(n) = \frac{S(n)}{n} = \frac{T(1)}{nT(n)} \quad (3.2)$$

Efficiency is an indication of the actual degree of scalable speedup performance. In the ideal case, we want a workload that grows linearly with the machine size. If the workload grows exponentially, the system is considered poorly scalable. In this case the efficiency or speedup is restricted by exceeding memory and I/O limits. Hence, exponential workload growth might not be feasible due to memory shortage or I/O bounds. A parallel system can be used to solve arbitrarily large problems in a fixed time if and only if its workload pattern is allowed to grow linearly. In practice, an algorithm must fit within the resource constraints and is considered efficient only if it can be cost effectively implemented. Also the match between the implementation of the parallel algorithm and the computer architecture contributes another important factor to the performance. Here we measured the system efficiency for two given parallel computer systems, indicating to what degree the n processors are fully utilized during execution.

We start by analysing the scalable parallel system efficiency, on the DEMOS [4, 5, 6] and the Cray T3E [7]. The DEMOS (DElft MOlecular dynamics Simulator), is a special-purpose computer that can be used for speeding up local environment problems with a low cost/performance ratio. The Cray T3E is a large Massive Parallel Processing (MPP) system that could also be used for a three dimensional domain decomposition. Using a linear domain decomposition appears efficient enough

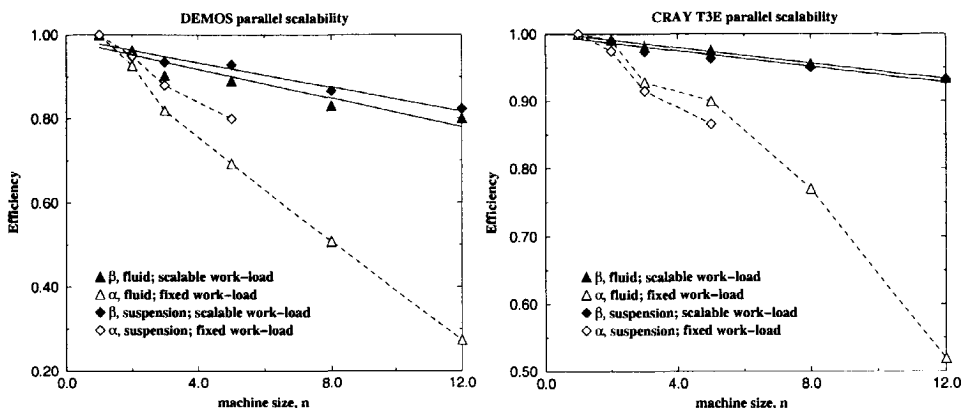


Figure 3.7: The system efficiency plotted as a function of machine size for a Boltzmann fluid (triangles) and for a Boltzmann colloid (diamonds). The left figure refers to the DEMOS and the right figure shows the CRAY T3E performance. The dashed lines represent fixed-load performance while the solid lines denote fixed-time performance, or scalable performance. The figure shows that when problem size grows linear with machine size, the performance stays still high.

throughout this research and thus a more complex decomposition has not yet been necessary.

For both parallel systems we plotted the system efficiency, as defined above, as a function of the number of processors. As we are interested in the communication overhead, we kept the system sizes small in relation to the number of processors. This corresponds to a maximum surface-to-volume ratio of the domain decomposition and therefore a worst case scalability. We calculated both the run times according to the fixed-load speedup model and the fixed-time speedup model. For the fixed-time speedup we allow the system size to grow linearly with the number of processors. The results are shown in figure 3.7, left for the DEMOS and right for the CRAY T3E. The fixed-load curves are denoted by dashed lines whereas the scaled-load curves are denoted by solid lines. For a constant workload we see that the efficiency curves drop rapidly (curves α). The figure also shows that, for both a lattice-Boltzmann fluid and a lattice-Boltzmann suspension, the efficiency curves are almost flat as the workload increases linearly with the machine size (curves β). This means that the ratio of communication overhead and workload is very low for lattice-Boltzmann simulations, indicating a high degree of parallel scalability. When the problem space is not exactly divisible by the number of processor elements, inefficient asynchronous communication is encountered. This may account for small fluctuations about linearity. Another consideration is that, using the storage reduction scheme, the scalability with problem size is optimized for cubic systems. The ordered planes, see section 3.4, must be perpendicular to the direction of slicing.

This is highly favourable for simulating cubic systems. If the system is not cubic the performance may be degraded.

3.6 Total Program

3.6.1 General remarks

The performance (or long term objective) of parallel computing must be assessed, not only on the grounds of system scalability, but also on the implementation of the parallel program. The portability of the code, the scalability of the code in practice, the program options and flexibility for future development are also important considerations.

The lattice-Boltzmann program developed as part of this research can simulate many kinds of complex, (dense) colloidal suspensions. The program is robust enough that the user need not to be an expert to run the parallel code. Regarding the portability, the code has been written entirely in ansi-C, making full use of the concepts such as dynamic data structures and pointers. Thus a well structured and maintainable code has been obtained. The code also provides the user with architecture-independent software which runs on a sequential machine, a workstation cluster, or a massively parallel system.

In practice, the numerical scheme utilizes massively parallel systems economically and in a scalable way. One small restriction with our code is that, to minimize the communication overhead, one colloidal particle can only occupy a maximum of two processors. This may degrade the performance in a number of cases. There is always a restriction, for instance, on the maximum number of processors. For large particles this may be problematic. Another point concerns the ordered passage through planes, utilized as part of the memory reduced algorithm. In combination with a linear domain decomposition, this means that a cubic system is optimal. For non-cubic systems we would expect the performance to be somewhat poorer. In practice, this is not a major problem. It is rarely necessary to use a non-cubic system.

At the same time the program contains a lot of flexibility and options for future expansion. First, the measurement of any physical quantity can easily be incorporated in the program. Second, the program supports real-time visualisation, implemented by a controlling program. This program has only the tasks of organising data files for visualisation and handling the (parallel) simulation data. Because of its limited workload, it offers a fast response for visualisation by continually checking updated files. Within the framework of the code, the simulation of mixtures of particles and particles with different sizes and shapes is also possible. The basic structure of the algorithm is identical. We therefore expect no influence on the parallel efficiency if we switch to simulating these more complicated colloidal systems. This remains , however, to be investigated.

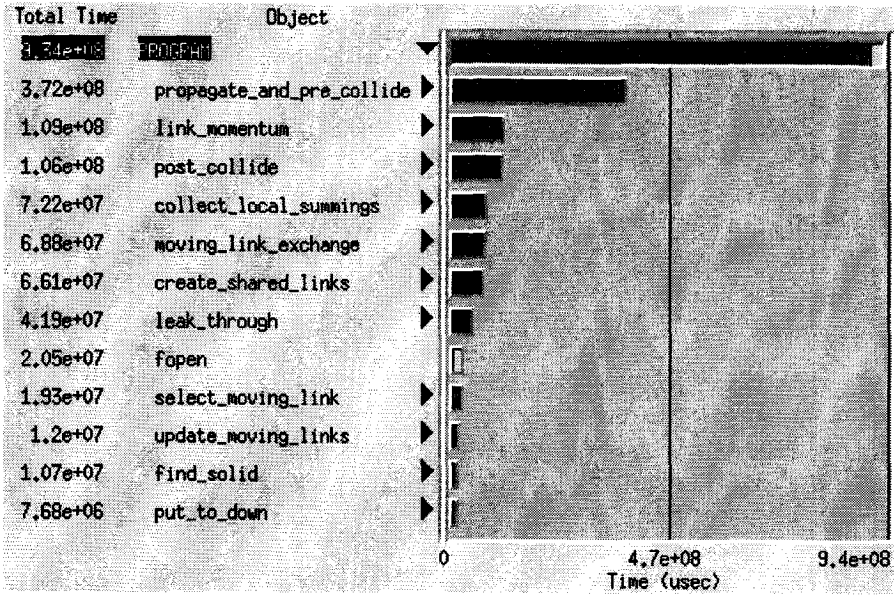


Figure 3.8: Time spent in indicated routines measured in micro seconds.

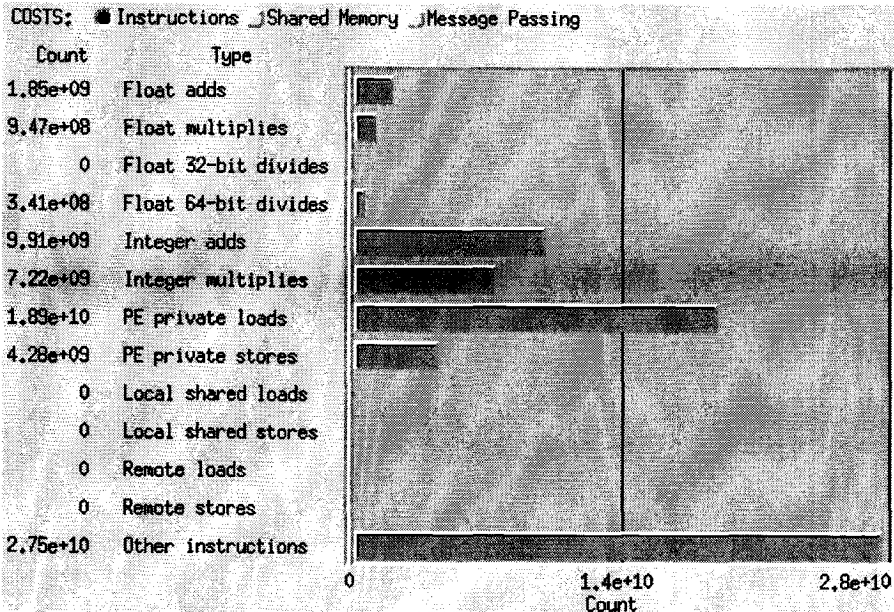


Figure 3.9: The computational costs spread over the different number of instructions.

3.6.2 Performance analysis

As we have detailed, the implementation of the lattice-Boltzmann scheme consists of several separate routines (figure 3.4). The inner loop calculations concern the update of fluid sites plane by plane. A detailed description of the calculations in a plane are given in section 3.4. In addition, the particle coordinates and velocities must also be updated once per time-step, along with the extra populations at the boundary. We examined the efficiency of the program running on the Cray T3E with the *apprentice* tool from CRAY RESEARCH. *Apprentice* is an X Window System tool designed for CRAY T3E systems to find anomalies and inefficiencies in a parallel program. The graphical output is shown in figure 3.8 and 3.9. To summarize, it appears that there is almost no time (0.12%) lost for communication overhead. The same holds for the amount of I/O time (0.04%). However, unfortunately a lot of time (74%) is spent on loading instructions and data caches, while only a small percentage (24%) of the total time is used for executing work instructions. This percentage appears the same for both lattice-Boltzmann fluids and suspensions. The same is true for the sequential program. Another point concerns the multiple integer calculations. These are a consequence of indirect addressing via pointers. This would be much faster using direct addressing. Unfortunately this overrides the idea of well structured and maintainable code. The sections of code consuming the largest proportion of the total time, including subordinate code and routines called, are `propagate_and_pre_collide` and `update_solids`. If the time spent in the routine `propagate_and_pre_collide` could be decreased by a more efficient usage of data caches and instruction registers this could provide a considerable speed up of the total simulation time. The routine `update_solids` updates the new solid velocities by visiting the populations of the boundaries (calculated by `link_momentum`) and by collecting data from neighbouring processors (collected via `collect_local_summings`). There is no obvious way to speeding up this particular routine.

3.7 Conclusions

We have described a new improved storage technique for lattice-Boltzmann simulations. This storage reduced algorithm performs strictly the same calculations as the conventional algorithm but in a more memory efficient way. By alleviating the problem of huge memory demand for large simulations, this method allows the maximum system size to increase by a factor four. Using this storage reduction method, it is possible to simulate large scale concentrated suspensions, containing up to 1 million colloidal particles (corresponding to a storage of nearly 7 Gb instead of about 30Gb for the conventional algorithm). For the more general case, for which the fluid viscosity can be varied, the reduced storage technique is still useful. However, the storage reduction will be a factor of two instead of four. This is still worthwhile. We demonstrated the method's suitability for parallel computing by examining the parallel performance for the storage reduced algorithm. This showed the expected high degree of scalability. The current computer code is extremely parallel, *i.e.* al-

most no communication is involved. However, unfortunately the cache of the Cray T3E appears to be used very inefficiently. This drawback remains to be solved by programming in a way that fully exploits the capacities of the Cray T3E. Considering the use of Fortran is a possible option. This should alleviate the problem of the large number of integer address calculations generated by C. Using the novel memory algorithm imposes no further restrictions with respect to the size and shape of the colloidal particles. It only requires a small amount of extra work to prepare the new velocities of the colloidal particles. As we have seen, this is, in computational terms, negligible compared to propagation and collision of the lattice-Boltzmann fluid.

Bibliography

- [1] A.J.C. Ladd, *J. Chem. Phys.* **93**, 3483 (1990).
- [2] A.J.C. Ladd, *Physical Review Letters*, **76** (8), 1392 (1996).
- [3] A.F. Bakker and M.W. Heemels, *Storage reduction in lattice-Boltzmann simulations*, Proceedings of the second annual conference of the Advanced School for Computing and Imaging, 21 (1996).
- [4] A.F. Bakker and C. Bruin, in *Special Purpose Computers* (ed. B.J. Alder), Boston: Academic Press (1988).
- [5] A.F. Bakker, G.H. Gilmer, M.H. Grabow and K. Thompson, *Journal of Computational Physics*, **90** (2), 313-335 (1990).
- [6] H.J.M. van Grol, *TRAFFIC ASSIGNMENT PROBLEMS solved by SPECIAL PURPOSE HARDWARE with emphasis on real time applications*, PhD Thesis, Computational Physics, TU Delft (1992).
- [7] CRAYT3E, Online, <http://www.cray.com/t3e> or <http://www.sgi.com/t3e>.
- [8] A. Hoogland, A. Compagner and H.W.J. Blöte, in *Special Purpose Computers* (ed. B.J. Alder), Boston: Academic Press (1988).
- [9] J.A. Herweijer, *A special-purpose computer for lattice gasses*, MSc Thesis, Computational Physics, TU Delft (1991).
- [10] W.T.J. Dekker, *The Cellular Automata Special Purpose Computer*, MSc Thesis, Computational Physics, TU Delft (1992).
- [11] A.F. Bakker, F. Berwald, J.V. Beckers, M.T.C. Elhorst, M.J. Haye, M.W. Heemels, S.W. de Leeuw, M.J. Neefs and M. van der Plas, *DEMOS: a simple parallel architecture for molecular simulations*, Proceedings of the first annual conference of the Advanced School for Computing and Imaging, 252 (1995).
- [12] G.M. Amdahl, Proceedings AFIPS Conference, Reston VA., 483 (1967).
- [13] J.L. Gustafson, D. Rover, S. Elbert and M. Carter, *J. Para. Distr. Computing*, 11 (1991).
- [14] K. Hwang, *Advanced Computer Architecture: parallelism, scalability, Programmability*, McGraw-Hill (1993).

4 Simulating solid colloidal particles

4.1 Introduction

Because of the complexity of hydrodynamic interactions between the particles in a suspension, the properties of suspensions are generally difficult to predict theoretically or to calculate numerically. In the hybrid lattice-Boltzmann solid particle model the time-dependent hydrodynamic interactions and motions of the particles emerge quite naturally from the dynamics of the model fluid. As such, it represents a useful tool for studying suspensions numerically. In this respect it has two particular strengths both related to the fact that the velocity fields in the fluid evolve with the correct time dependence *i.e.* it avoids the approximation of pseudo steady states. This means, firstly, that the technique can be used to probe the time-dependent nature of the interactions between the particles [1, 2]. Secondly, it can be used to study the effects of inertia on suspensions [3] (that is, particulate flows where the Reynolds number is not negligible). The latter becomes important if, for example, the particles are large ($\gg 1\mu\text{m}$) or the suspension is very far from equilibrium (a common occurrence during the processing).

In this chapter the point we address is the following. Because the approach outlined in section 2.3 requires fluid both inside and outside the object it cannot be regarded *a priori* as representing a truly solid particle. It actually describes the dynamics of a hollow shell, of mass m and moment of inertia I , filled with fluid. Now, it may be that the behaviour of these two systems is broadly similar, in which case the presence of the internal fluid is not problematic. Indeed, the method outlined in section 2.3 (which we will subsequently refer to as the “original” method) has been successfully applied in several studies. By investigating the influence of the internal fluid on the dynamics of a single spherical particle undergoing periodic rotational motion, Ladd [4] showed the following. For high values of the frequency Ω ($\Omega \gg \nu_0/a^2$, where ν_0 is the kinematic viscosity of the fluid and a the particle radius), the internal fluid makes no contribution and the particle displays behaviour characteristic of a solid sphere with moment of inertia I . For low frequency motion ($\Omega \ll \nu_0/a$) the internal fluid contributes essentially as a rigid body and the particle

displays behaviour characteristic of a solid particle with an effective moment of inertia, I^* , comprising the moment of inertia of the shell and the moment of inertia of internal fluid. For a sphere this gives

$$I^* = I + \sum_{\mathbf{r}_{int}} bn_0 |\mathbf{r}_{int} - \mathbf{r}_0|^2 \quad (4.1)$$

Here b is the number of discrete velocities, n_0 the zero velocity distribution, \mathbf{r}_0 the position vector of the centre of the sphere and \mathbf{r}_{int} the position vectors of all the N_{int} lattice nodes inside the object. By analogy, for translational motion we would expect a particle to behave as if it had a mass m at high frequencies, but an effective mass $m^* = m + N_{int}bn_0$ at low frequencies. This is not particularly satisfactory because the ratio of the density of the fluid to the density of a colloidal particle, ρ^* , plays an important role in the dynamics. It influences the inertial time scale (the characteristic time it takes the particle to respond to changes in the velocity of the fluid surrounding it). If one is interested in the effects of inertia it would be preferable to get this right. Furthermore, the parameter ρ^* does not vary much in real suspensions. It always takes a value close to unity otherwise the particles would separate out under the effects of gravity. If we try to simulate a neutrally buoyant particle ($\rho^* = 1$) using the original approach then at best we can choose between setting $m = 0$ and having the correct low-frequency behaviour, or setting $m = N_{int}bn_0$ and having the correct high frequency behaviour. Our aim in this chapter is therefore to develop and test a modified algorithm that is free of these artefacts.

Given the above, it is unsurprising that attempts have been made to develop a scheme for simulating colloidal particles that does not involve internal fluid [3, 5, 6]. To our knowledge, none of these methods is completely satisfactory as they do not conserve both mass and momentum. There is also the question, do we actually want to get rid of the internal fluid or keep it, but get rid of its contribution to the effective particle mass and moment of inertia? Dispensing with it altogether actually creates a new problem. That is, as the particle moves over the lattice some nodes that were external become internal and vice versa. If the nodes inside the particle are undefined (*i.e.* there is no internal fluid) we then face problems. In particular how do we define the state of an "exposed" node *i.e.* a node that was inside the particle but suddenly becomes part of the system [3]. Taking this into consideration, the second of the two options above, keeping the internal fluid but mitigating its effects, is probably preferable as it limits these problems. It is this approach that we pursue here.

This chapter is organized as follows. We start by describing a modified algorithm that should remove the effects of the internal fluid. By focusing on the motion of an isolated sphere in a compressible fluid we compare the new method against both the original method and theory. Finally, we conclude the chapter by studying the effects of the internal fluid on the viscosity of a many particle system. Again we compare the new and original algorithms against known results.

4.2 Removing the effects of the internal fluid

The method we propose to minimize the effects of the internal fluid and the reasoning behind it, proceed along the following lines. Suppose the internal fluid is at rest. In this case it is straightforward to see that, using the original method (equation 2.19), summed over the entire object the internal fluid contributes no nett force or torque. Consequently it does not enter into the equations of motion. Making use of this fact we therefore adopt a two stage process. The first stage is to impose the condition that the internal fluid remains at rest. To this end, at the start each time step we reset all the distribution functions inside a particle $n_i(\mathbf{r}_{int}, t)$ to values characteristic of a fluid at rest *i.e.*

$$n_i(\mathbf{r}_{int}, t)' = \frac{\sum_{\mathbf{r}_{int}} \sum_i n_i(\mathbf{r}, t)}{bN_{int}} \quad (4.2)$$

The value of this constant ensures conservation of mass (all mass inside the particle is equally redistributed, thus dissipating any sound propagation within the particle). This step does not conserve linear or angular momentum. However, if the changes in linear and angular momentum, resulting from step 1, are interpreted as inducing an external force and torque on the particle

$$\begin{aligned} \mathbf{F}_x &= - \sum_{\mathbf{r}_{int}} \sum_{\mathbf{c}_i} \left(n_i(\mathbf{r}_{int}, t)' - n_i(\mathbf{r}_{int}, t) \right) \mathbf{c}_i \\ \mathbf{T}_x &= - \sum_{\mathbf{r}_{int}} \sum_{\mathbf{c}_i} \left(n_i(\mathbf{r}_{int}, t)' - n_i(\mathbf{r}_{int}, t) \right) (\mathbf{r} - \mathbf{r}_o) \times \mathbf{c}_i \end{aligned} \quad (4.3)$$

and these additional forces and torques are included in equation 2.19, so that we have

$$\begin{aligned} \mathbf{F} &= \sum_{ib} \mathbf{F}_{ib}(\mathbf{r}_b) + \mathbf{F}_x \\ \mathbf{T} &= \sum_{ib} \mathbf{F}_{ib}(\mathbf{r}_b) \times \mathbf{r}_b + \mathbf{T}_x \end{aligned} \quad (4.4)$$

then, over a full time-step, both linear and angular momenta are conserved. Following the same procedure described in 2.3, we then find for the α component of the new linear and angular velocities, \mathbf{v}' and ω'

$$v'_\alpha = \frac{\frac{F_{x\alpha}}{m} + mv_\alpha(t) + 2 \sum_{ib} [n_{ib}(\mathbf{r}_b) - n_{-ib}(\mathbf{r}_b)] c_{ib\alpha}}{m + 8n_0(\rho) \sum_{ib} c_{ib\alpha} c_{ib\alpha}} \quad (4.5)$$

$$\omega'_\alpha = \frac{\frac{T_{x\alpha}}{I} + I\omega_\alpha + 2 \sum_{ib} [n_{ib}(\mathbf{r}_b) - n_{-ib}(\mathbf{r}_b)] (\mathbf{r}_b \times \mathbf{c}_{ib})_\alpha}{I + 8n_0(\rho) \sum_{ib} (\mathbf{r}_b \times \mathbf{c}_{ib})_\alpha (\mathbf{r}_b \times \mathbf{c}_{ib})_\alpha} \quad (4.6)$$

This second step ends with updating the state of the system in the usual manner from $t \rightarrow t + \Delta t$. The internal fluid adjacent to the shell of the particle will generally not now be at rest (because of the intervening boundary collisions). However, on

the subsequent step we will apply the first operation again. The second step can therefore be interpreted as transferring the momentum that would, using the original method, have been transferred into the internal fluid back to the shell - where it belongs. In essence, we preserve Ladd's original method for imposing the stick boundary condition but apply a small correction preventing momentum transfer to the interior fluid. The internal fluid thus has no linear or angular momentum and does not contribute to the equations of motion.

If we consider a colloidal particle that is to move on the lattice, the method we outlined above, because it keeps the internal fluid, provides a convenient point at which to do so. This point is immediately prior to applying the first operation. The reason for this is the following. The normal bounce back rule (step two) applies the stick boundary condition to both the exterior and interior of the solid-fluid interface. Thus, at this point in the algorithm, nodes adjacent to the boundary, both inside and outside, will be set to the correct velocity. Therefore, if a particle moves and a node originally inside the object is now outside, it will, to a good approximation, be in the correct state. Using the method outlined above a particle moving over the lattice can be dealt with quite simply. No costly special procedure is needed to identify and deal with nodes that enter or exit the interior of the object. This is in contrast to approaches which remove the internal fluid completely [3].

4.3 Tests of the method

As a test of the method outlined above we consider three different dynamic properties of colloidal systems. Our aim is to apply the original method and establish the role of the interior fluid. Then we apply the new method for comparative purposes. Specifically we have calculated the following. Firstly, we have calculated the frequency dependent rotational friction coefficient of an isolated colloidal sphere. This is the same problem considered by Ladd [4]. Secondly, we have calculated the single particle velocity autocorrelation function for a colloidal sphere. In contrast to rotation, sound propagation (related to mass conservation) influences this quantity. Finally we consider a transport property, the viscosity of a concentrated suspension of colloidal hard spheres. For the first two cases there is an analytic result to compare with. For the third we can compare with accurate numerical values, calculated using multipole methods [7], or theory, valid at low to intermediate volume fractions. In all the simulations we report here, the shell mass and moment of inertia (m and I) are set to values characteristic of a solid sphere with the same density as the density of the fluid. Thus, if the effects of the internal fluid can be neglected, we are simulating neutrally buoyant particles.

4.3.1 The frequency dependent rotational friction coefficient

If we consider one Fourier component of the velocity of a particle executing some arbitrary time-dependent rotational motion, *i.e.* $\omega(t) = \Omega_0 \cos(\Omega t)$, then the fluid

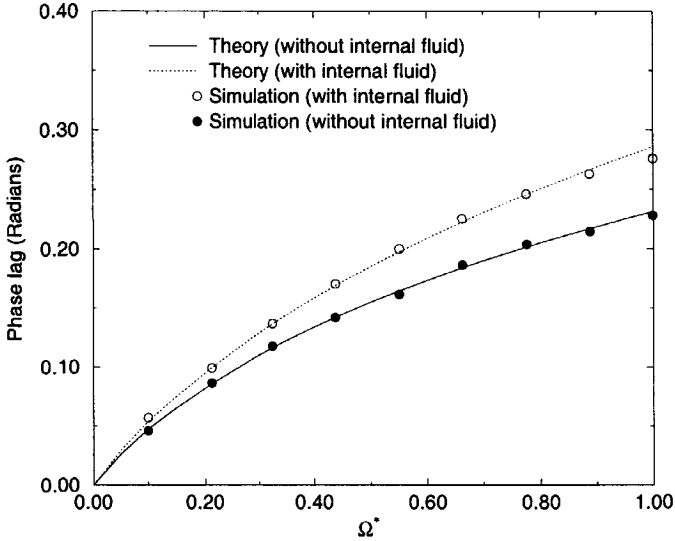


Figure 4.1: Phase lag between the external torque required to maintain an imposed periodic angular velocity and the angular velocity itself. The results are for a sphere of radius 4.5 lattice units

will exert a frequency dependent torque $T_f(\Omega)$ on the particle with the general form

$$T_f(\Omega) = \Omega_0 \gamma_r(\Omega) \quad (4.7)$$

where $\gamma_r(\Omega)$ is a frequency dependent rotational friction coefficient. The time-dependent motion of a single spherical particle can be analyzed theoretically in considerable detail. By assuming that the dynamics of the fluid can be described by the Navier-Stokes equations for an incompressible fluid (in the limit of zero Reynolds number) and that a stick boundary condition applies at the solid-fluid interface, this problem can be solved [8] analytically. For a particle suspended in a fluid of viscosity η_0 and density ρ_0 the result for the friction coefficient γ_r is

$$\gamma_r(\Omega^*) = -\gamma_r(0) \left(1 - \frac{i\Omega^*}{3(1 + \sqrt{-i\Omega^*})} \right) \quad (4.8)$$

where $\Omega^* = \Omega a^2 / \nu_0$, $\nu_0 = \eta_0 / \rho_0$ is the kinematic viscosity of the fluid and $\gamma_r(0) = 8\pi\eta_0 a^3$ is the zero frequency rotational friction coefficient. If the spherical particle is not solid but filled with fluid, there is an additional contribution to the friction coefficient coming from the internal fluid $\gamma_r^{int}(\Omega)$. At low values of the reduced frequency, $\Omega^* \ll 1$, this contribution takes the form

$$\gamma_r^{int}(\Omega^*) = \frac{\gamma_r(0)}{15} \Omega^* \left(i - \frac{\Omega^*}{35} \right) \quad (4.9)$$

The first term simply represents the inertial force of the internal fluid acting as a rigid body. Numerically, it is straightforward to calculate $\gamma_r(\Omega)$. We simply impose a cosinusoidal velocity on the particle and calculate the in phase and out of phase components of the torque exerted on the particle by the fluid. These are then conveniently expressed in terms of a magnitude and phase shift. The results we obtained for the phase shift (the dominant effect at low frequencies) are plotted in figure 4.1, along with the analytical result for a solid sphere (equation 4.8) and the asymptotic result for a fluid filled sphere. The calculation was performed using both the method described in chapter 2 (“with internal fluid”) and using the modified method we outlined above (denoted “without internal fluid”, although this method could more correctly be described as using a passive internal fluid). As figure 4.1 shows, for the simulations with the internal fluid, the inertial contribution at low frequencies is clearly visible. Just as Ladd concluded [4] at low frequencies, the particle behaves as a solid sphere with a moment of inertia equal to that of the shell plus that of the equivalent volume of fluid undergoing rigid body rotation. In contrast, using the modified method we described above, there is no additional inertial contribution and the data follow the theoretical curve for a solid object with a moment of inertia simply equal to the assigned moment of inertia I . Thus, from the point of view of rotation, the method we outlined above succeeds in its objective of removing the effects of the internal fluid.

4.3.2 The single particle velocity autocorrelation function

We now turn to translational motion, where, this time, we will consider the velocity autocorrelation function (VACF). In a real colloidal suspension a colloidal particle experiences rapid collisions with the solvent molecule, giving it a fluctuating thermal velocity. The VACF, or $C(t)$, is defined as an average over these fluctuations, $C(t) = \langle v_\alpha(0)v_\alpha(t) \rangle$, where $v_\alpha(t)$ is one component of the instantaneous thermal velocity. In our lattice-Boltzmann model we have no spontaneous velocity fluctuations. However if we impose a velocity fluctuation then, according to Onsager’s regression hypothesis, the subsequent decay of our fluctuation will be identical to the average thermal decay in a real system. To analyze the decay of an imposed velocity fluctuation, in the same way that we defined a rotational friction coefficient, we define a translational frequency dependent friction coefficient $\gamma_t(\Omega)$. $\gamma_t(\Omega)$ characterizes the force acting on a particle undergoing simple periodic translational motion with frequency Ω . Since the function $\gamma_t(\Omega)$ connects the velocity to its derivative, it can be used to define an equation of motion. In terms of Fourier components, the velocity of the particle satisfies the equation

$$v_\alpha(\Omega) = \frac{F_{x_\alpha}(\Omega)/m}{-i\Omega + \gamma_t(\Omega)/m} \quad (4.10)$$

where $F_{x_\alpha}(\Omega)$ is the Fourier transform of any time-dependent external forces acting on the particle. If we consider a particle impulsively accelerated to a velocity v_0 at

$t = 0$, *i.e.* $F_{x_\alpha}(\Omega) = mv_0$, then

$$\frac{v_\alpha(\Omega)}{v_0} = \frac{1}{-i\Omega + \gamma_t(\Omega)/m} \quad (4.11)$$

This can be related to the Fourier transform of the “true” VACF (see chapter 2),

$$\frac{v_\alpha(\Omega)}{v_0} = \frac{C(\omega)}{C(t=0)} = \frac{m}{k_B T} C(\Omega) \quad (4.12)$$

where T is the temperature and k_B is Boltzmann’s constant. We have also used the equipartition condition to identify $C(t=0) = k_B T/m$. So, if we know $\gamma_t(\Omega)$ then, with the aid of equation 4.11, equation 4.12 and an inverse transformation, we can calculate the velocity autocorrelation function. For a single spherical particle $\gamma_t(\Omega)$ can be calculated analytically. Assuming that the motion of the fluid is described by the compressible Navier-Stokes equations and that a stick boundary condition applies at the solid/fluid interface, this calculation yields [9, 10]

$$\gamma_t(\Omega) = 2\gamma_t(0)\alpha^2 \frac{(1 + \alpha + \frac{1}{9}\alpha^2)B - \frac{1}{9}\beta^2 A}{\beta^2 A + 2\alpha^2 B} \quad (4.13)$$

with

$$\begin{aligned} A &= 1 + \alpha + \frac{1}{3}\alpha^2 \\ B &= 1 + \beta + \frac{1}{3}\beta^2 \\ \alpha &= -ia\sqrt{\Omega/\nu_0} \\ \beta &= \frac{ia\Omega}{\sqrt{(c_s^2 - i\Omega(\frac{4}{3}\nu_0 + \nu_B))}} \end{aligned} \quad (4.14)$$

Here $\gamma_t(0) (= 6\pi\eta_0 a)$ is the zero frequency translational friction coefficient, $\nu_B = \eta_B/\rho_0$, where η_B is the bulk viscosity of the fluid, ρ_0 the density of the fluid and c_s is the speed of sound through the fluid. The latter two quantities are associated with the speed and rate of damping of the sound wave generated by a moving particle respectively (see chapter 6). Comparisons have been made between theoretical and numerical values, calculated using the lattice-Boltzmann model [4], for the VACF of a single spherical colloidal particle. However, the comparison was made against theory derived using the additional assumption that the fluid is incompressible (the compressible result, equation 4.13, reduces to the incompressible result in the limit $\beta \rightarrow 0$ *i.e.* the speed of sound going to infinity). The lattice-Boltzmann approach simulates a compressible fluid, sound propagates through the model fluid at a finite speed. Although the effects of compressibility are limited to high frequencies, $\Omega \sim c_s/a$ [10], a comparison with the full compressible result, notably at short times, is more appropriate.

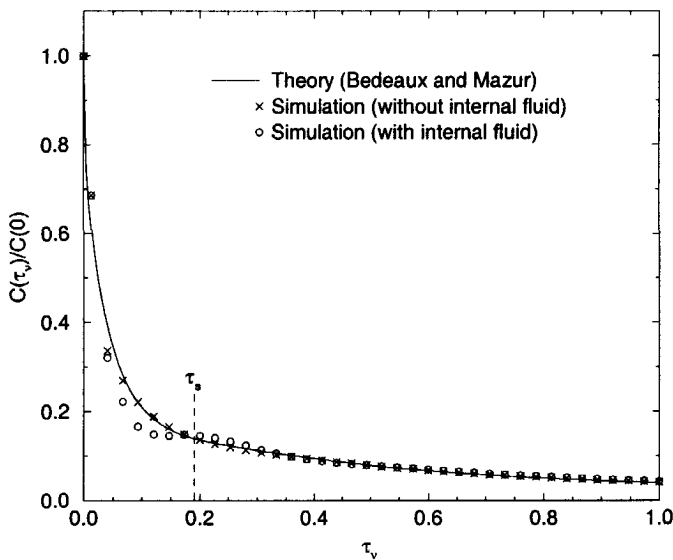


Figure 4.2: The normalised velocity autocorrelation function for a particle of radius 2.5 lattice spacings. For comparative purposes the theoretical result from Bedeaux and Mazur is also shown.

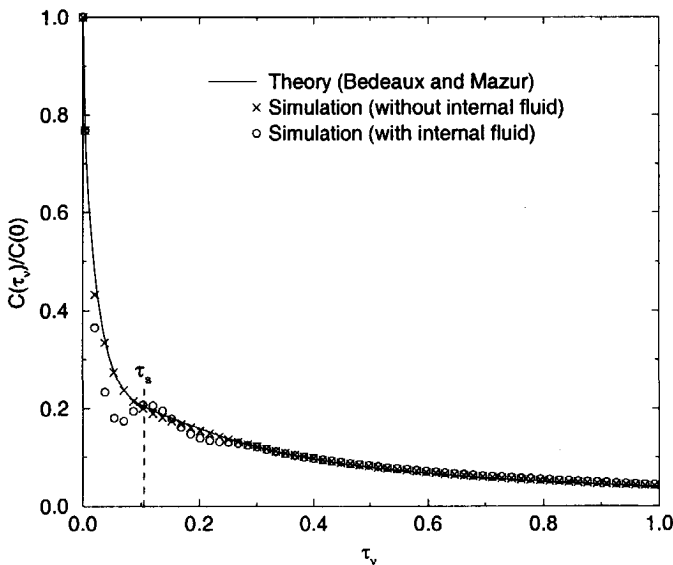


Figure 4.3: The normalised velocity autocorrelation function for a particle of radius 4.5 lattice spacings. For comparative purposes the theoretical result from Bedeaux and Mazur is also shown. Note that the effects of the internal fluid are more pronounced whereas the simulation using the new approach is nearer to the theoretical result.

Numerically, we have calculated the normalized velocity autocorrelation function along the lines outlined above (equation 4.12). Starting with a fluid at rest and a spherical particle with a velocity v_0 , we allowed the system to evolve in time and from the subsequent velocity of the particle, $v(t)$, we calculate the normalized velocity autocorrelation function $v(t)/v_0$. We performed the same procedure for particles of radius 2.5 and 4.5 lattice sites using a cubic system with periodic boundary conditions applied at the faces of the simulation box. We only calculated the VACF up until times less than the time it takes a sound wave to pass between the central particle and its nearest periodic image. Thus, the results are free from any finite size effects. In figure 4.2 we have plotted the normalized velocity autocorrelation function, as a function of the viscous time $\tau_\nu = t\nu_0/a^2$, calculated by using the original method and using the modified method outlined above. For the results plotted in figure 4.2 the radius of the solid particle was 2.5 lattice sites. Also plotted in figure 4.2 is the theoretical result for a compressible fluid, calculated by substituting appropriate values for the transport coefficients into equation 4.13 and transforming the frequency dependent VACF into the time domain. In lattice units, such that the time-step density of the fluid and lattice spacing are all unity, the values of the transport coefficients were $\nu_0 = 1/6$, $c_s = 1/\sqrt{2}$ and $\nu_B = 1/30$. In figure 4.3 we show the same plot for data obtained using the identical fluid, but this time using a sphere of radius 4.5 lattice sites. Examining figure 4.2 we see that the VACF calculated using our new method ("without internal fluid") follows the theoretical curve more closely than does the curve calculated using the original method. With the internal fluid present, the VACF lies initially below the theoretical curve then subsequently above it. It displays weak oscillations about the true result. This is almost certainly an effect of sound propagation inside the colloidal particle. To support this hypothesis, the time it takes a sound wave to travel one particle diameter is also shown in the plot ($\tau_s = c_s/a$). As we can see, it corresponds to an artificial maximum in the VACF. Turning to the plot for the sphere of radius 4.5 lattice units (figure 4.3), the oscillations about the correct result for the simulation with internal fluid are now, compared to the case of radius 2.5, more pronounced. Again the first artificial maximum occurs at a time commensurate with a sound wave travelling one diameter through the fluid (τ_s) - consistent with our remark above, that these oscillations are an artefact of sound propagation back and forth through the internal fluid. Given the fact that we are using a bigger representation of the sphere we should get a more accurate answer. The spatial resolution of the simulation has been increased. However, the artificial oscillations we observe are more pronounced. At short times we are further away from the true result. The reason for this is that, by moving from a sphere of radius 2.5 to 4.5, we have, in dimensionless terms decreased the compressibility. Sound waves are dissipated proportionately more slowly. In contrast, the simulation in which we have attempted to remove the effects of the internal fluid, on going from a radius of 2.5 to 4.5 just gives a result nearer to the theoretical curve. This is the behaviour we would expect for a truly solid particle. On the whole, the agreement between the theoretical result and the simulations with the effects of the internal fluid removed is very good. Particularly so given the extremely rapid initial

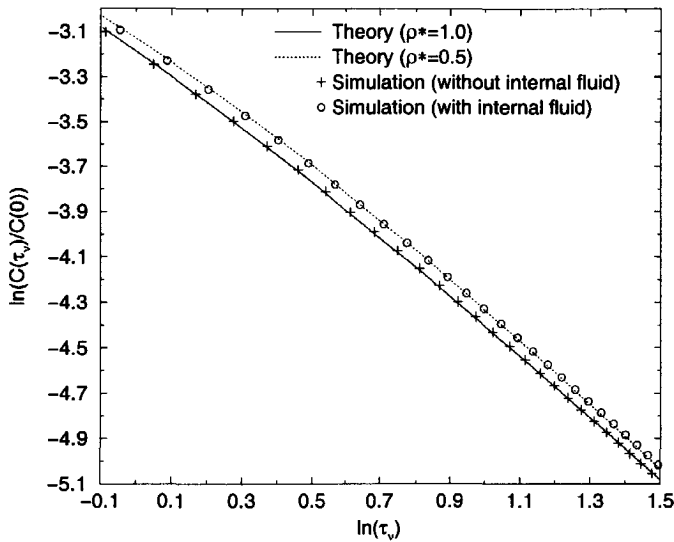


Figure 4.4: The normalised velocity autocorrelation function at long times, calculated using a particle of radius 2.5 lattice spacings. The long time effects of the internal fluid are clearly visible as the simulation results “with internal fluid” follow the theoretical curve for a particle with twice the density of the fluid. By contrast, the results obtained using the modified method described here follow the theoretical result for a neutrally buoyant particle

decay of the function relative to one time step. Turning to longer times, after the oscillations induced by the internal fluid have died away, figures 4.2 and 4.3 suggest that either method is adequate. However, on closer examination we find this is not true. In figure 4.4 we have plotted, in log-log form, the decay of the VACF at longer times for a particle of radius 2.5. It is clear that, with the internal fluid present, the results follow the theoretical curve for a particle with mass ratio $\rho^* = 0.5$. Again, as with rotation, the internal fluid is contributing, at low frequencies (or in this case long times), a rigid body inertial term to the equations of motion. In contrast, using the approach we outlined above, the results follow the (correct) curve for a neutrally buoyant particle. Again our method seems to successfully reproduce the dynamics of a solid particle.

4.3.3 The viscosity of a concentrated suspension

Whereas for generalized rotational and translational motion, considered above, the internal fluid causes only a relatively minor perturbation to the dynamics of the particle, we now turn to what may be a more serious problem: The influence this may, in turn, have on the transport coefficients. Specifically, we consider the viscosity of a concentrated suspension. There are various ways to calculate this quantity.

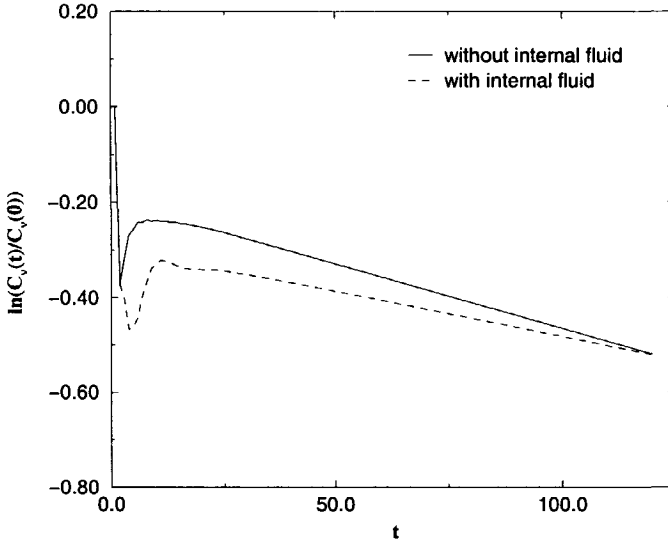


Figure 4.5: Log-linear plot of the correlation function $C_\nu(t)$ as a function of time. The data refer to a simulation of a system of 1956 spheres of nominal radius 2.5 lattice units, with a volume fraction of 25%. Note that the simulations with and without internal fluid give different rates of decay. In addition, the initial transients are less pronounced using the novel algorithm we describe here. The reduced wave vector (ka) was equal to 0.2.

Probably the most convenient way is by studying the decay of an initial transverse sinusoidal velocity perturbation [11] $v_{ix}(0) = \sin(kr_{iy})$, where $v_{ix}(0)$ is the x component of the velocity of particle i and r_{iy} the y component of its position vector. If we calculate the subsequent velocity of $v_{ix}(t)$ of the N particles in the system, then according to classic hydrodynamics [12]

$$C_\nu(t) = \frac{1}{N} \left\langle \sum_{i=1}^N v_{ix}(0)v_{ix}(t) \right\rangle = \frac{1}{N} \left(\sum_{i=1}^N v_{ix}^2(0) \right) \exp(-k^2 \nu_\phi t) \quad (4.15)$$

where the angular brackets denote an average over all possible configurations of the N particles and ν_ϕ is the kinematic viscosity of the suspension. As discussed at greater length in chapter 5, we only expect equation 4.15 to apply on length scales long compared to the length scale defined by the particles themselves *i.e.* $k \ll 2\pi/a$.

The decay of this correlation function has been reported elsewhere [11]. In fig 4.5 the typical decay of the correlation function is plotted in log-linear form. The figure clearly shows that the results using the original and the new algorithm give different values for ν_ϕ . These particular results are for a suspension consisting of 1956 spheres, at a volume fraction of $\phi = 0.25$ and the function has been averaged over 10 independent configurations. The dimensionless wave vector $k^* = ka$ was equal to 0.2. In the simulation the radius of one sphere was nominally equal to 2.5 lat-

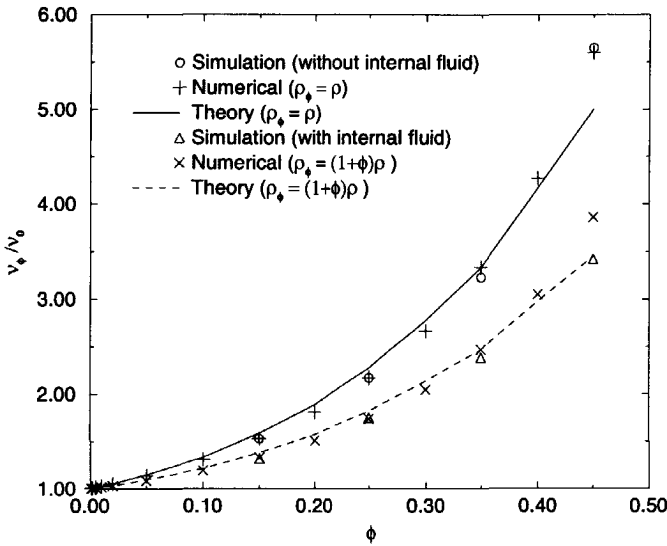


Figure 4.6: The high frequency suspension viscosity, ν_ϕ/ν_0 , calculated at four different volume fractions $\phi = 0.15, 0.25, 0.35$ and 0.45 , both with the algorithm without internal fluid (circles) and with internal fluid (upward triangles). The solid line is the theory from Beenakker and the dashed line represents this theory adapted for the internal fluid algorithm. The + and \times symbols represent numerical multipole expansions, respectively for the neutral buoyant viscosity values and the internal fluid algorithm

tice spacings. The point here is that using this method we calculate the kinematic viscosity of the suspension. This is related to the suspension viscosity, η_ϕ , so long as we know the density, by $\eta_\phi = \rho\nu_\phi$. But what should we take for the density? If the particles are neutrally buoyant we expect that the density of a suspension, regardless of the volume fraction, will be equal to the density of the solvent, so

$$\frac{\nu_\phi}{\nu} = \frac{\eta_\phi}{\eta_0} \quad (4.16)$$

If, however, we set the shell mass such that the particles are nominally neutrally buoyant, but the internal fluid contributes an equivalent mass to the particles (assuming that it is the low frequency mass that is relevant) then the density of the suspension ρ_ϕ , at volume fraction ϕ , will effectively differ from the solvent density as $\rho_\phi = (1 + \phi)\rho_0$. This being the case, we would expect

$$\frac{\eta_\phi}{\eta_0} = \frac{(1 + \phi)\nu_\phi}{\nu} \quad (4.17)$$

Using the methodology outlined above (and described in more detail in chapter 5 or reference [11]), we have calculated the kinematic viscosity of a suspension of

hard spheres as a function of volume fraction. In figure 4.6 we have plotted ν_ϕ/ν_0 as a function of volume fraction for nominally neutrally buoyant particles, simulated using Ladd's original method ("with internal fluid") and using the modified method we outlined above ("without internal fluid"). Also plotted in figure 4.6 are theoretical predictions (based on an expansion up to second order in the volume fraction [13]) for the kinematic viscosity of a suspension of neutrally buoyant particles and accurate numerical values calculated by Ladd [7]. As we see from the figure, whereas the data calculated using the modified method agree with theoretical and numerical values for the viscosity of a suspension of neutrally buoyant particles, data calculated using the original method do not. They clearly follow the curve $\nu_\phi/\nu_0 = \eta_\phi/(1 + \phi)\eta_0$. The internal fluid is therefore contributing to the effective density of the suspension (equation 4.17) and the kinematic viscosity is increasingly underestimated with increasing volume fraction.

4.4 Conclusions

We have described a method for simulating truly solid colloidal particles within the lattice-Boltzmann framework. Unlike other methods that have been proposed, our method strictly adheres to the microscopic conservation laws for mass and momentum. For computational convenience our approach keeps the internal fluid inherent in Ladd's original model. However, by transferring linear and angular momentum, that would otherwise have been transported to the internal fluid, back to the shell of the particle, we recover the dynamics of a truly solid particle. We demonstrated this by showing that the correct time-dependent rotational and translation dynamics of a solid particle were recovered. To our knowledge, the theoretical result for the VACF of a colloidal particle suspended in a compressible fluid has not been tested before. Thus, our simulations could equally well be regarded as a test of the theory rather than vice versa. Either way, the agreement was excellent. For the simulations where the internal fluid reacted passively, we reached the same conclusion as Ladd. At low frequencies, or long times, the internal fluid contributes an additional rigid body inertia to the motion of the particles. By considering the viscosity of a concentrated suspension, we showed that this additional inertia leads to a suspension with an effective density greater than one would expect for a suspension of colloidal particles with the same density of the fluid. This means that the kinematic viscosity and viscosity do not display the same dependence on volume fraction, as they should. Using our modified method, the correct equivalence was recovered.

Bibliography

- [1] A.J.C. Ladd, *Phys. Rev. Lett.* **70**, 1339 (1993).
- [2] C.P. Lowe and D. Frenkel, *Phys. Rev* **E54**, 2704 (1996).
- [3] C.K. Aidun, Y. Lu and E.J. Ding, *J. Fluid Mech.* **373**, 287 (1998).
- [4] A.J.C. Ladd, *J. Fluid Mech.* **271**, 311 (1994).
- [5] D. Qi, *J. Fluid Mech.* **385**, 41 (1999).
- [6] C.K. Aidun, Y. Lu and E.J. Ding, *J. of Stat Phys.* **81**, Nos. 1/2, 49 (1995).
- [7] A.J.C. Ladd, *J. Chem. Phys.* **93**, 3483 (1990).
- [8] L.D. Landau and E.M. Lifshitz, *Fluid Mechanics* (Addison-Wesley), London (1959).
- [9] R. Zwanzig and M. Bixon, *Phys. Rev.* **A2**, 2005 (1970).
- [10] D. Bedeaux and P. Mazur, *Physica* **78**, 505 (1974).
- [11] M.W. Heemels, A.F. Bakker and C.P. Lowe, *Prog. Colloid Polym. Sci.* **110** (1998).
- [12] J.-P. Hansen and I. R. McDonald, "*The theory of simple liquids*", Academic Press, London (1986).
- [13] C.W.J. Beenakker, *Physica* **128A**, 48 (1984).

5 The high frequency viscosity of hard sphere colloidal suspensions

5.1 Introduction

Probably the most important dynamical property of a colloidal suspension is its viscosity. The viscosity characterizes the flow properties of the suspension. For example, if one has a colloidal suspension flowing through a tube of circular cross-section of radius R , the mass Q of suspension passing per unit time through any cross-section of the pipe (the discharge) should, one would expect, be given by the usual Poiseuille equation [1] but with the kinematic viscosity of the suspension ν_ϕ replacing the solvent viscosity,

$$Q = \frac{\pi \Delta}{8\nu_\phi} R^4 \quad (5.1)$$

This of course assumes that the radius of the pipe is sufficiently large compared to the size of the colloidal particles so that, on the scale of the pipe, the suspension appears homogeneous. One of the notable characteristics of a suspension is that its viscosity ν_ϕ is greater than the viscosity of the solvent ν_0 . This enhancement of the viscosity depends strongly on the volume fraction ϕ occupied by the colloidal particles. For a suspension of colloidal spheres, Einstein derived the relation between ν_ϕ and ν_0 to first order in the volume fraction [2]

$$\frac{\nu_\phi}{\nu_0} = 1 + \frac{5}{2}\phi + O(\phi^2) \quad (5.2)$$

Higher order corrections depend on the non-hydrodynamic interactions between the particles. The model most widely studied theoretically is the monodisperse suspension of hard spheres. For this system the quadratic term has subsequently been evaluated by several authors [3, 4, 5]. This analysis shows that equation 5.2 is only valid at very low volume fractions. Taking higher order terms into account Beenakker and Mazur [6] succeeded in predicting the viscosity of suspensions of

hard spheres up to moderate to high volume fractions ($\phi \sim 0.40$) where equation 5.2 is totally inadequate. The monodisperse suspension of hard spheres is not just a theoretical abstraction. It can also, to good approximation, be studied experimentally [7] and has thus come to represent something of a benchmark system. There is therefore excellent experimental and theoretical data on the monodisperse hard sphere system which, up to moderate to high volume fractions, are in very good agreement. The viscosity of a suspension has also been calculated numerically up to volume fractions $\phi = 0.45$, and again the agreement is very good. One question that remains, however, is on what length scale can the suspension be treated as a simple Newtonian fluid characterized by the suspension viscosity. We mentioned above the example of predicting the flow of a suspension through a tube. What happens if the diameter of the tube is not very much greater than the size of the colloidal particles? Because colloidal particles are atomically very large, it is not uncommon to come across suspensions flowing in geometries that are not characterized by length scales very large compared to the size of the particles composing the suspension. A good example would be your blood vessels, their diameter is not vastly greater than the cells dispersed in the blood they carry. One of our main objectives here is therefore to study on what length scales a colloidal suspension can be regarded as simply a fluid characterized by the suspension viscosity.

Although the monodisperse suspension of hard spheres is certainly the most widely studied and best understood system, it is rarely typical for suspensions encountered in practice. It is very difficult to synthesize a truly monodisperse suspension. Even the "monodisperse" suspensions studied experimentally and compared with monodisperse theory display a polydispersity of typically 5%. In general, suspensions of particles that could be regarded as approximating hard spheres will be significantly polydisperse due either to deliberate mixing, aggregation or vagueries in the synthesizing procedure. Neither are the effects of polydispersity limited to dynamical quantities. The effect of polydispersity on the equilibrium properties of colloidal suspensions is still a significant question [8, 9, 10], particularly when and whether such systems are thermodynamically stable. This will not concern us here. We are more interested in the following remarkable property of polydisperse suspensions. If one takes a dense suspension and replaces a certain fraction of the colloidal particles with smaller particles, such that the total volume occupied by the solvent remains the same, the resulting suspension can have a significantly lower viscosity. This effect can be technologically very useful because it offers a route for producing very dense suspensions (useful if the colloidal particles are pigments for example), without paying the price of impractically high viscosity.

The viscosity of a suspension will depend on the composition, the volume fraction occupied by the colloidal particles and the nature of the interactions between the particles. Even if all these quantities are fixed, the viscosity further depends on the frequency (or time scale) [7] and the shear rates [11] one is considering. It is therefore important to be clear about which regime one is addressing. In this chapter we consider the limit of low shear rates and high frequency. The limit of low shear rates means that we can assume that the suspension has its equilibrium structure.

By taking the limit of high frequencies we can neglect the “collisions” between the suspended particles. These collisions are driven by Brownian motion and are responsible for the long-time (or low frequency) contribution to the viscosity. The only relevant effects in the high frequency regime are the hydrodynamic interactions between the suspended particles. These hydrodynamic interactions are a result of momentum transfer through the fluid and between the colloidal particles. The true, low frequency, Newtonian viscosity η_ϕ^l , *i.e.* the viscosity that would be measured from a steady shear experiment, consists of a short-time contribution η_ϕ (due to hydrodynamic interactions) plus a long-time, or Brownian, contribution $\eta_B(\phi)$ (due to the effects of Brownian motion). By definition we have:

$$\eta_\phi^l = \eta_\phi + \eta_B(\phi) \quad (5.3)$$

Other than at very high volume fractions, ($> 40\%$ [14]), the high frequency component is the dominant contribution to the Newtonian viscosity ($\eta_\phi \gg \eta_B(\phi)$). At even higher volume fractions, the high frequency viscosity remains a significant contribution to the Newtonian viscosity. It is also worth pointing out that there are very successful theories for predicting the Brownian contribution to the Newtonian viscosity based on solving the simplified Smoluchowski equation [12, 13] (discussed in section 1.4). These theories necessarily introduce further approximations because solving even the simplified Smoluchowski equation to all orders in ϕ is impractical. An analytical approach also becomes more problematic if one wishes to generalize to suspensions of particles other than spheres. Alternatively, the simplified Smoluchowski equation can be solved numerically using Brownian dynamics, in which case there is no restriction on the applicability of the approach. There is, therefore, an approximate computational method for calculating the Brownian contribution to the viscosity. It does not, however, resolve the high frequency component. If we can develop a good method for calculating the high frequency viscosity we can, using a two stage approach, calculate the two contributions separately and obtain the true Newtonian viscosity of any suspension. It should be added that the validity of this approach depends on the assumption that the simplified Smoluchowski equation is a good approximation to the full Smoluchowski equation. There is evidence that it may not be [14].

Following the preceding discussions, our aims in this chapter are three-fold. The first is simply to find a convenient way of extracting the high frequency viscosity from a lattice-Boltzmann simulation. The second is to establish on what length scales a suspension may be expected to behave like a simple Newtonian fluid. Finally, we wish to begin to examine the effects of polydispersity by considering a bimodal suspension of hard spheres. This system has been studied theoretically by Jones [15]. We also note that, whereas extensive calculations of the viscosity of monodisperse suspensions of hard spheres have been reported using Stokesian Dynamics [11], simulations of bimodal suspensions have been limited to two-dimensional systems of disks [16].

5.2 The wave vector dependent viscosity

To see where the high frequency regime dominates the suspension viscosity in terms of length scales, it is necessary to consider the quantitative contributions to the viscosity from the two different time scales involved. The argument is closely related to the discussion in section 1.3 regarding the short- and long-time scales. Let us consider one Fourier component of this instantaneous transverse velocity field,

$$\Delta v_x(\mathbf{r}, t = 0) = a(\mathbf{k}_T) \exp(i\mathbf{k}_T \cdot \mathbf{r}), \quad (5.4)$$

where the wave vector \mathbf{k}_T is orthogonal to the velocity direction x and $a(\mathbf{k}_T)$ is the Fourier transform of the velocity field. For a generic, structureless fluid the viscosity determines the decay of transverse components of the instantaneous velocity field. For such a system one expects this perturbation to decay as [20]

$$\Delta v_x(\mathbf{r}, t) = a(\mathbf{k}_T) \exp(-k_T^2 \nu_0 t) \quad (5.5)$$

where ν_0 is the kinematic viscosity of the fluid. For a given wave vector the perturbation therefore decays on a time scale $t_\nu \sim 1/k_T^2 \nu_0$, while the time it takes a particle to diffuse a distance of the order of its own radius is of the order $t_D \sim a^2/D$, where a is the particle radius and D the diffusion coefficient. The diffusion coefficient can be estimated from the Stokes-Einstein equation (equation 1.1). If we now consider, for illustrative purposes, the case of a micron sized particle dispersed in water at room temperature then we find that $t_D \sim 1\text{s}$ and $t_\nu \sim 100/k_T^2\text{s}$. The high frequency condition, *i.e.* that $t_\nu \ll t_D$, is therefore satisfied so long as $k_T \gg 10\text{cm}^{-1}$. Thus, there exists a large range of values of k_T , corresponding to real lengths much greater than the dimensions of the colloidal particles, where we can safely neglect the effects of Brownian motion and consider the configuration of particles to be essentially "frozen".

If we examine equation 5.5 we see that it further gives us a means of achieving the goals we set out in the introduction. We can simply examine the time dependent response of the suspension to an initial velocity perturbation of the form given in equation 5.4. We would not however expect the decay of such a perturbation to simply follow equation 5.5. It only applies for a simple structureless fluid. On length scales of the order of the colloidal particle radius a suspension cannot be considered structureless. We expect, however, that on length scales long compared to the size of the particles ($k_T \ll 1/a$) the behaviour of a structureless fluid will be recovered with the suspension viscosity ν_ϕ (henceforth the fact that we are looking at the high frequency viscosity will be implied) appearing as the viscosity in equation 5.5. In the opposite limit ($k_T \gg 1/a$) we would conversely expect that the decay of the perturbation will be so rapid that the particles in the suspension will not have time to feel each others presence. Consequently the apparent viscosity will be less than the small wave vector value. There will thus, one expects, be a wave vector dependent viscosity characterizing the decay of transverse velocity fluctuations. Only by looking for the (small k_T) limiting value can we calculate the suspension viscosity. The smallest value of the wave vector that can be studied in a simulation is of course

determined by the system size, so this will necessitate using the algorithmic and computational strategies described in chapter 3. By establishing the wave vector dependence of the viscosity we can also address our second question; on what length scales does a suspension behave like a simple fluid. For a simple model fluid the viscosity is independent of wave vector. If and when we recover this behaviour in a suspension we can, interpreting a wave vector as an inverse characteristic length, determine on what spatial length scales simple fluid behaviour is recovered.

5.3 Calculating the wave vector dependent viscosity

The method we used involved three dimensional simulations of configurations of hard spheres embedded in the simple lattice-Boltzmann model fluid (the solvent). The initial configurations of colloidal spheres were generated using a Poisson process and further compressed under equilibrium conditions, using a standard Monte Carlo method [17], in case of concentrated suspensions. Using the lattice-Boltzmann model (for the solvent), spontaneous fluctuations are absent. Thus, in the absence of any externally imposed fluctuations, a colloidal particle in a Boltzmann fluid does nothing. Fluctuations can be reinstated in the lattice-Boltzmann model by adding a suitable random noise term to the stress tensor [18], but we have chosen a different approach. According to Onsager's regression hypothesis the decay of a fluctuation which we impose on the (otherwise) purely dissipative system should be the same as the decay of a spontaneous fluctuation in the real fluctuating system. The advantage of following the decay of an imposed, rather than spontaneous, fluctuation is that it does not involve adding any additional noise to the system and so the results are relatively free from statistical error. A philosophically similar procedure was applied in reference [19] to study diffusion in suspensions. In this work, however, as outlined above, the fluctuation we need to impose corresponds to one Fourier component of the transverse velocity field *i.e.* we apply an initial velocity perturbation of the form

$$v_x(\mathbf{r}, t = 0) = A \exp(i\mathbf{k}_T \cdot \mathbf{r}) \quad (5.6)$$

where A is a constant, to both the fluid and the colloidal particles. We then calculate the correlation function

$$C_\nu(t) = \sum_{i=1}^{N_l} v_x(\mathbf{r}_i, 0)v_x(\mathbf{r}_i, t) + \sum_{j=1}^{N_p} v_x(\mathbf{r}_p, 0)v_x(\mathbf{r}_p, t) \quad (5.7)$$

where N_l is the number of lattice sites outside the spheres, N_p the number of colloidal spheres and \mathbf{r} the position vector of either the lattice site (subscript l) or the centre of the particle (subscript p). In keeping with our high frequency, (or short time) assumption the positions of the particles do not change during the course of the simulation. The mass of the particles was set equal to the mass of the equivalent volume of fluid and the method described in Chapter 4 was used to remove the

effects of the internal fluid. One expects *a priori* that the function $C_\nu(t)$ will decay as [20]

$$\frac{C_\nu(t)}{C_\nu(0)} = \exp(-k_T^2 \nu_\phi(\mathbf{k})t) \quad (5.8)$$

where we have, on the basis of the argument given in the preceding section, introduced $\nu_\phi(k_T)$, a wave vector dependent viscosity. Hence, in principle one can extract $\nu_\phi(k_T)$ by calculating $C_\nu(t)$. Such an approach remains of course phenomenological in that it assumes $C_\nu(t)$ decays as predicted by equation 5.8. This remains to be shown. Even if it is the case, we still need to simulate small enough wave vectors to enable us to establish the limiting $k_T \rightarrow 0$ behaviour of the viscosity.

Viewed simply as a means of calculating the viscosity, the approach outlined above has a number of advantages. The obvious alternative would be to look for the steady state response to an constant external perturbation (see section 2.4). The disadvantage with this approach is that the time required for a system to reach a steady state increases dramatically as the system size increases. System size is an important consideration for two reasons. Firstly, hydrodynamic interactions are long ranged and finite size effects on transport coefficients can be large [21]. Secondly, the system size determines the minimum value of k_T which can be studied and only in the limit of k_T approaching zero can one expect $\nu_\phi(k_T)$ to approach the limiting value ν_ϕ (the true, in our case high frequency, viscosity). If we are merely interested in extracting the viscosity then it is obviously important that we can simulate wave vectors small enough such that, to a good approximation, $\nu_\phi(k_T) = \nu_\phi$ or, alternatively, that one can extrapolate reliably to this limit. An analogous linear response technique for calculating the viscosity can be applied in molecular dynamics simulations and extracting a reliable estimate of the zero wave vector value can indeed be problematic [17]. It is clear that we must anticipate having to simulate large systems to obtain a reliable estimate for the viscosity. Using the steady state approach this also implies having to perform long simulations to ensure the steady state is reached. Using the lattice-Boltzmann approach Ladd [18], for example, reported having to simulate for hundreds of thousands of time-steps before the steady state response to an imposed shear was observed. In contrast, if equation 5.8 does hold then it provides a convenient means of extracting the wave vector dependent viscosity because one only has to establish the rate of decay of $C_\nu(t)$. This should require a relatively small number of time-steps and, furthermore, one does not expect this number to depend on system size. Another obvious alternative method for calculating the viscosity is to introduce thermal fluctuations into the lattice-Boltzmann system and calculate the stress-stress correlation function. The stress-stress correlation function is related to the viscosity by a Green-Kubo formula similar to that which relates the velocity autocorrelation function to the diffusion coefficient (equation 2.26). The disadvantage of this approach is that the thermal fluctuations introduce additional noise into the system, so extensive time averaging is required. More seriously, the fluctuating lattice-Boltzmann model lacks true equipartition and this introduces an element of uncertainty regarding the true temperature of the system (which is needed to relate the stress-stress correlation function to the viscosity). Taken as a whole,

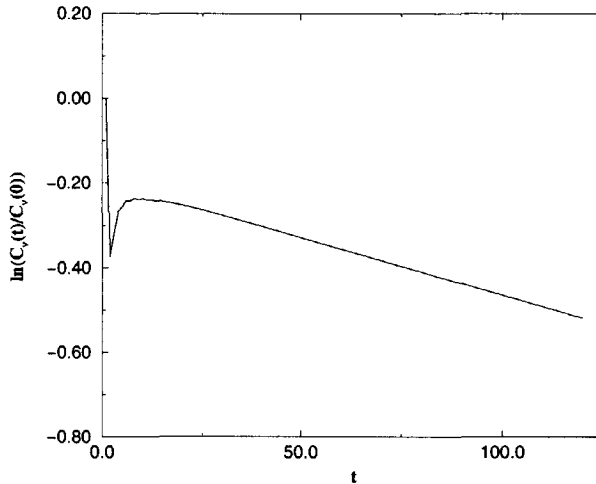


Figure 5.1: Log-linear plot of the correlation function $C_\nu(t)$ (defined in the text) as a function of time. The data refer to a simulation of a system of 1956 spheres of nominal radius 2.5 lattice units, the spheres occupying a volume fraction of 25%. The reduced wave vector ($k_T a$) was equal to 0.2.

the method we propose here, viewed purely as a means of calculating the viscosity, seems to have several computational advantages. Given that we also gain additional information, the dependence of the viscosity on the wave vector, it is our preferred method for studying the viscosity.

5.4 Results

5.4.1 Typical decay of the correlation function

Applying the methodology outlined above, a typical example of the results we obtain for the correlation function $C_\nu(t)$ is plotted in linear-log form in figure 5.1. These particular results are for a suspension consisting of 1956 spheres at a volume fraction of 25% and the function has been averaged over 10 configurations. The dimensionless wave vector k^* (defined as $k_T a$, where a is the particle radius) was equal to 0.2. In the simulation, the radius of one sphere was nominally equal to 2.5 lattice spacings. The particle radius in these lattice units is an important parameter because it basically determines the spatial resolution of the simulation. Increasing this radius leads to a better resolution of the hydrodynamic interactions between spheres which are almost touching (the lubrication forces), at the expense of bigger system sizes. One sees from the figure that, after the decay of some short lived initial transients, an exponential decay is observed (the plot becomes linear). Thus, we find the decay which we expected and we can use equation 5.8 to calculate a wave vector dependent

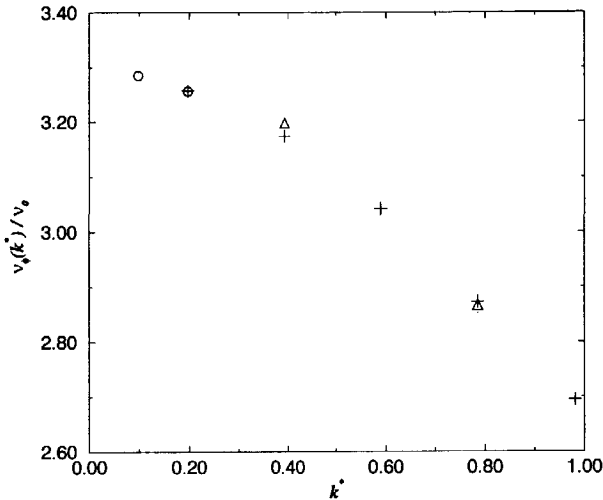


Figure 5.2: The k -dependent viscosity for a simulation of a suspension of colloidal spheres which occupy a volume fraction $\phi = 0.35$. The symbols correspond to systems of 21904 spheres (circles), 2738 spheres (pluses) and 342 spheres (triangles). The statistical errors are of the order of, or less than, the symbol size.

viscosity. We also note that the number of time-steps required before we can establish the form of the exponential decay is relatively few (~ 100) whereas for steady state calculations on much smaller systems (reference [22]) the number of steps required was hundreds of thousands. This confirms the suggestion we made in section 5.3 that this is a much more efficient method for calculating the viscosity.

5.4.2 Determining the limiting suspension viscosity

Repeating the simulations for various values of the wave vector, we calculated the wave vector dependent viscosity by fitting an exponential to the post-transient decay of $C_\nu(k, t)$ and using equation 5.8. To illustrate the dependence of the viscosity on k^* we focus on one particular intermediate volume fraction, $\phi = 0.35$. In figure 5.2 the wave vector-dependent viscosity is plotted as a function of k^* . The results were again averaged over ten independent configurations and these results are for a sphere of radius of 4.5 lattice units. This simulations were repeated with a larger value for the radius ($a = 6.5$), but, at this particular volume fraction, the values obtained for $\nu_\phi(k^*)$ were not significantly different, indicating that a radius of 4.5 gave adequate resolution. The conclusion one can draw from figure 5.2 is that the limiting ($k^* = 0$) value has almost been reached for the smallest wave vector we have studied ($k^* = 0.098$). With the aid of a small extrapolation, based on a polynomial fit to the data shown in figure 5.2, we can therefore obtain an accurate value for ν_ϕ . The uncertainty in the extrapolation is in fact of the same order as the statistical

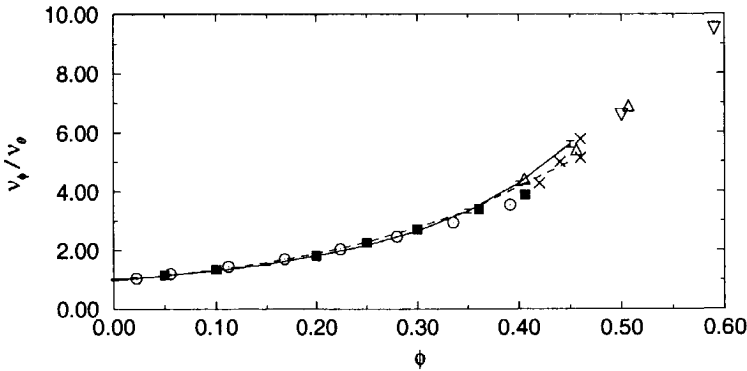


Figure 5.3: The high frequency suspension viscosity, ν_ϕ as a function of volume fraction ϕ . The solid line is a spline through the numerical values calculated by Ladd. The dashed line is the theoretical result due to Beenakker. The crosses are the experimental results of van der Werff et al.. The remaining symbols are the numerical results described in this work using spheres of nominal radius 2.5 (circles), 4.5 (squares), 6.5 (upward triangles) and 8.5 (downward triangles). The statistical errors are of the order of, or smaller than, the symbol size.

error associated with averaging over a number of configurations.

5.4.3 The suspension viscosities for different volume fractions

By following this procedure, we have calculated the high frequency viscosity over the range of volume fractions $0 < \phi < 0.59$. The highest value is very close to the maximum possible for a random packing of hard spheres $\phi = 0.63$. The values we obtained are plotted in figure 5.3. In the figure we also show the effect of changing the spatial resolution (the radius, in lattice units, of the sphere). Clearly this needs to be increased as the volume fraction increases but not dramatically. At a volume fraction of 50%, spheres of radii 6.5 and 8.5 give results which differ only by a few percent; a difference which is not statistically significant. However, at these high volume fractions smaller spheres are clearly not adequate. In the figure we have also plotted accurate numerical results [21], the theoretical prediction due to Beenakker [6] and the results of experimental measurements by van der Werff et al. [7]. The agreement between all three is very good. However, at a volume fraction of 45% our results are in somewhat better agreement with the theory than those of Ladd. In addition our results for higher volume fractions do not appear to increase as rapidly with increasing volume fraction as the trend suggested by Ladd's results (which only extend to $\phi = 0.45$) would indicate. It is therefore possible that the theoretical values are quite good even at volume fractions higher than 45%. Unfortunately, the values quoted in reference [6] only extend up to $\phi = 45\%$ so this we can only summarize.

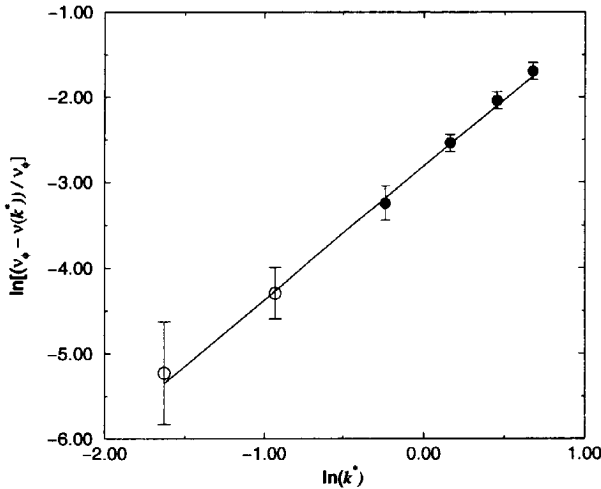


Figure 5.4: Log-log plot of the difference between the wave vector dependent viscosity, $\nu_\phi(k^*)$, and the suspension viscosity ν_ϕ as a function of the reduced wave vector k^* . The data refer to simulations of a suspension of 21904 (open symbols) and 2738 (filled symbols) spheres, occupying a volume fraction of 35%. The solid line is the result of a linear least-squares fit to the data.

5.4.4 The wave vector dependence of the viscosity

If we now return to the wave vector dependence of the viscosity (figure 5.2) we remarked that at the smallest wave vector we studied ($k^* = 0.098$), $\nu_\phi(k^*)$ was almost, but not quite, equal to ν_ϕ . There is still a statistically significant difference. What is somewhat surprising is that there is any measurable discrepancy at all. This value of k^* corresponds to dimensionless wavelengths, $\lambda^* (= l/a)$, of about 60, *i.e.* real space lengths which are very much greater than the typical separation between colloidal particles. Indeed, the theory of Beenakker [6] predicts that we should see no wave vector dependence for $k^* < 1$. It also appears that ν_ϕ is approached relatively slowly with decreasing k^* . In order to analyze this more quantitatively we have also analyzed the data shown in figure 5.2 by plotting, in log-log form $(\nu_\phi - \nu_\phi(k^*))$ as a function of k^* (figure 5.4). The plot appears to be linear. A linear fit to the data yielding a slope of 1.55 ± 0.05 . This, interestingly, is very similar to observations made by Evans [23] who performed a similar analysis for a soft sphere fluid and Alley and Alder [24] who performed a similar calculation for a hard sphere fluid. They found small k^* behaviour compatible with the form

$$\nu_\phi(k^*) = \nu_\phi - ck^* \frac{3}{2} \quad (5.9)$$

with c a positive constant. In fact, if one compares figure 5.4 with the equivalent plot for a hard sphere fluid then the similarity is not just qualitative but quantitative. For example, at $k^* = 1$ we find $\nu_\phi(k^*)/\nu_\phi = 0.8$ whereas for the hard sphere fluid it

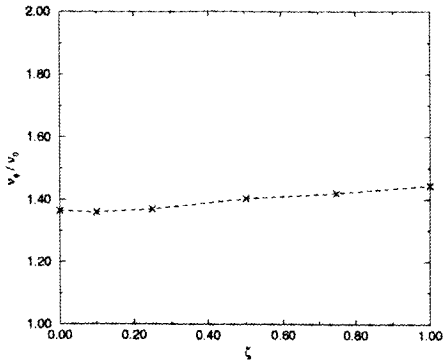


Figure 5.5: The high frequency bimodal suspension viscosity ν_ϕ in the dilute regime. Here $\phi = 0.10$ and the size ratio is 2.6. The viscosities are plotted as a function of ζ (defined in the text). The crosses are the lattice-Boltzmann results. The statistical errors are of the order of, or smaller than, the symbol size. The accuracy in the sphere representation is shown by the difference in viscosity for the radii 2.5 and 6.5

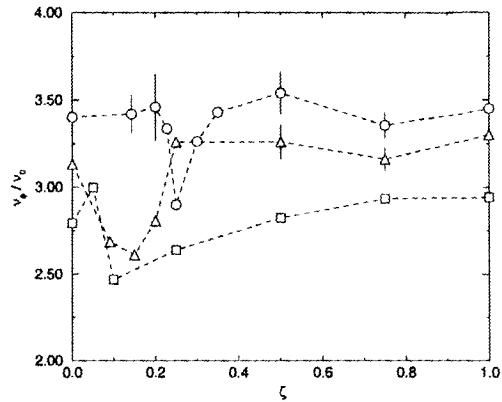


Figure 5.6: The high frequency bimodal suspension viscosity ν_ϕ at $\phi = 0.30$, $\phi = 0.33$ and $\phi = 0.35$, as a function of ζ . The size ratio is 2.6. The squares correspond to systems of $\phi = 0.30$, the triangles correspond to $\phi = 0.33$ and the circles have $\phi = 0.35$. The statistical errors are of the order of, or smaller than, the symbol size. The accuracy in the sphere representation is shown by the difference in viscosity for the radii 2.5 and 6.5.

is about 0.75. Given that the two systems are quite different (in a hard sphere fluid there is no solvent, the particles undergo ballistic motion between direct collisions) the similarity is surprising.

5.4.5 The viscosity of bimodal suspensions

Exactly the same methodology applied to study the viscosity of monodisperse suspensions can be used to study bimodal suspensions of hard spheres. We take a binary mixture of hard spheres which differ in size and again generate initial configurations using standard Monte Carlo techniques. The simulations then proceed as before. The correlation function is still found to decay exponentially and from this we extract the wave vector dependent viscosity. This is then extrapolated to the limit of small k^* . The regime we are considering is clearly still the same, *i.e.* low shear rate and high frequency. We have calculated the viscosity of bimodal suspensions in both the dilute regime and at intermediate volume fractions. For bimodal suspensions, in addition to the volume fraction, we need to specify the size ratio for the two species. For the results reported here, one sphere has a radius 6.5 lattice units and the value for the other particle radius is 2.5. This gives a size ratio 2.6 for the particles. Again the results were averaged over 10 independent configurations.

Initially, we considered the effects on the suspension viscosity in the dilute regime. To specify the composition of the bimodal system it is useful to define the volume fraction ϕ , as the total volume fraction occupied by colloidal particles (large and small) and the mixing volume fraction ζ defined as the relative volume occupied by the small spheres

$$\zeta = \frac{v_S}{v_S + v_B} \quad (5.10)$$

where v_B is the volume density of big spheres and v_S the volume density of small spheres. First we consider a volume fraction of 10%. We have calculated the viscosity for mixing volume ratios of $\zeta = 10\%$, $\zeta = 25\%$, $\zeta = 50\%$ and $\zeta = 75\%$. Over the whole range, it seems that there is no statistically significant viscosity difference (see figure 5.5) for the bidisperse system as compared to the monodisperse system. The dilute regime theory of Jones [15] predicts that we should see a reduction in the viscosity and that the viscosity has a minimum when the volume fraction is evenly split between the two sizes of particles ($\zeta = 0.5$). As figure 5.5 shows, we see no evidence for this. It is still possible, for this dilute system, that the effect is too small to measure within the accuracy of the lattice-Boltzmann technique. Conversely, if any effect is present it is too small to be of any practical importance.

There are two possible routes for enhancing the effect of bidispersity. One is to make the size ratio between the particles much larger. The other is to go to more concentrated suspensions. Increasing the size ratio implies simulating bigger particles and therefore bigger systems (to measure the value of the viscosity $\nu(k^*)$ at the same dimensionless wave vector k^*). Alternatively (and more conveniently) we can simulate higher volume fractions. Given that we are restricted in the size ratios we can study, we have chosen to calculate bimodal suspension viscosities for some intermediate volume fractions.

Moving to higher volume fractions we find that substantial viscosity reductions can indeed be observed. The results for overall volume fractions $\phi = 0.30, 0.33$ and 0.35 are plotted in figure 5.6, as a function of the mixing volume ratio ζ . The amount by which the viscosity is reduced is about 15%, at this size ratio. Interestingly, at the lower of the three volume fractions, this is the viscosity reduction we would expect if the suspension viscosity were determined by solely the volume fraction of large spheres. It is as if the small particles contribute nothing to the suspension viscosity. Experimentally, it is universally observed that in a concentrated suspension the addition of a small volume of small particles replacing large particles, such that the total volume fraction occupied by the colloidal particles remains constant, results in a noticeable viscosity reduction [25, 26, 27]. This is consistent with what we observe. One also sees from the figure that the minimum of the viscosity, with respect to mixing volume ratio, occurs on the side rich in large particles. Experimentally, this asymmetry in the reduction of the viscosity as a function of mixing volume ratio is also typical [28, 29, 30]. Again this is in contrast with the low density theory of Jones [15], according to which the minimum occurs when the volume fraction is evenly split between the two sizes of particles. Interestingly, our observation is very similar to that of Chang and Powell [16], who performed a two-dimensional

Stokesian Dynamics simulation over a range of volume fractions. They always found the minimum for the viscosity at around 25% small and 75% large particles. This is in rough correspondence with what we observe. We can go farther to say that, for a given ratio of particle sizes, the minimum viscosity initially appears for suspensions rich in large particles, but that, as the volume fraction increases, this minimum shifts towards suspensions of more equal composition. Furthermore, for a fixed value of the size ratio, the composition with the minimum viscosity appears to be very sensitive to the total volume fraction (see figure 5.6).

5.5 Discussion

5.5.1 Monodisperse colloidal suspensions

We have described a method for calculating, within the lattice-Boltzmann framework, the high frequency, low shear rate viscosity of a colloidal suspension. The method seems to have some advantages over those previously employed in that it only requires the dynamics of the suspension be simulated for a very short period of time. The values for the viscosity that we have calculated using this approach are, up to volume fractions of 45%, in good agreement with other simulations, experiment and theory. We have also extended the calculations up to volume fractions approaching the maximum possible for random (that is “glass-like” as opposed to “solid-like”) configurations of spheres. A comparison with theory at these higher volume fractions would clearly be desirable. This would allow one to establish to what extent the theory breaks down at higher volume fractions - at 45% it still works remarkably well. A comparison with experiment would also be desirable as it would establish if, at sufficiently high volume fractions, our approximation of colloidal particles as perfect hard spheres breaks down. In reality the colloidal particles studied experimentally are only approximately hard spheres (they have polymer coats and interact via a short-ranged electrostatic interaction). One might expect that eventually, at high enough volume fractions, the hard sphere approximation would break down and some difference would become apparent.

Finally, we examined the wave vector dependence of the viscosity. We found that the low k^* limit was approached relatively slowly with decreasing k^* , in a manner very similar to that observed for simple model “atomic” fluids. The k^* dependence was apparent at wavelengths much smaller than the theory contained in reference [6] would suggest. This means that the suspension can only be expected to behave like a simple (continuum) Newtonian fluid on spatial lengths scales very much greater than the size of the colloidal particles. This may be relevant if one considers a suspension flowing in some constricted geometry with dimensions not much larger than the colloidal particles themselves. An example would be the flow of a suspension through a tube that we discussed earlier. For tube flow we may well expect that the suspension will behave as if it had a somewhat lower viscosity than in a bulk sample, if the diameter of the tube does not exceed that of the colloidal particles by at least an order of magnitude. This remains to be examined. Finally, it is worth

commenting on the similarity between the k^* dependence we found for a suspension and that found in a hard sphere fluid. A hard sphere fluid is most fundamentally different from a suspension in that, on the length scales of the particles making up the fluid, the fluid cannot be treated as a continuum. One might therefore expect that any deviations between the dynamics of a hard sphere fluid and the dynamics of a continuum Newtonian fluid (for instance a k^* dependent viscosity) would originate from this discrete nature of the fluid. However, this is not true for a suspension because the solvent, on the length scale of the colloidal particles, does appear as a continuum. Deviations from simple Newtonian fluid behaviour in the suspension can only originate from the complex nature of the hydrodynamic interactions between the particles and the non uniform distribution of the particles. The observation that the (small) k^* dependence of the viscosity in a suspension is very similar to that of a hard sphere fluid suggests that, in a simple "atomic - like" fluid, the k^* dependence of the viscosity has its origins more in the structure of the fluid than in the hydrodynamics. The static properties of a hard sphere fluid are identical to those of a colloidal suspension of hard spheres although the dynamics are very different.

5.5.2 Bidisperse colloidal suspensions

At a moderate volume fraction, the values we have calculated for the viscosity of bimodal suspensions showed the commonly observed viscosity reduction phenomenon. We considered the viscosity as a function of the mixing volume ratio. For these, high frequency viscosities, there are only theoretical results expected to be valid in the dilute regime with which to compare. Unfortunately, at low volume fractions, where these theories should be valid, the viscosity reduction effect was either non-existent or too small (for the size ratio we used) to be measurable. A comparison with theory for the intermediate volume fractions would clearly be desirable but the fact that we only observe this effect at intermediate volume fractions is indicative of the fact that it is a many-body effect. This being the case, it is difficult to invoke a simple "intuitive" explanation for the viscosity reduction. Nonetheless we find good qualitative agreement with experiment. Specifically, at intermediate volume fractions we found a significant viscosity reduction and when we studied this as a function of the mixing volume ratio, the minimum of the viscosity always showed up for compositions rich in large particles. Experiments measure the real "Newtonian" viscosity which consists of a high frequency component and a Brownian component, due to Brownian motion of the particles. Only the former is calculated here. Although this short-time or high frequency component is important and has to be determined, it is not as yet known to what order Brownian motion contributes. By analogy with the monodisperse case, it would be reasonable to assume that, at the volume fractions we studied, the Brownian contribution will be small and that our results are reasonably representative of the true Newtonian viscosity.

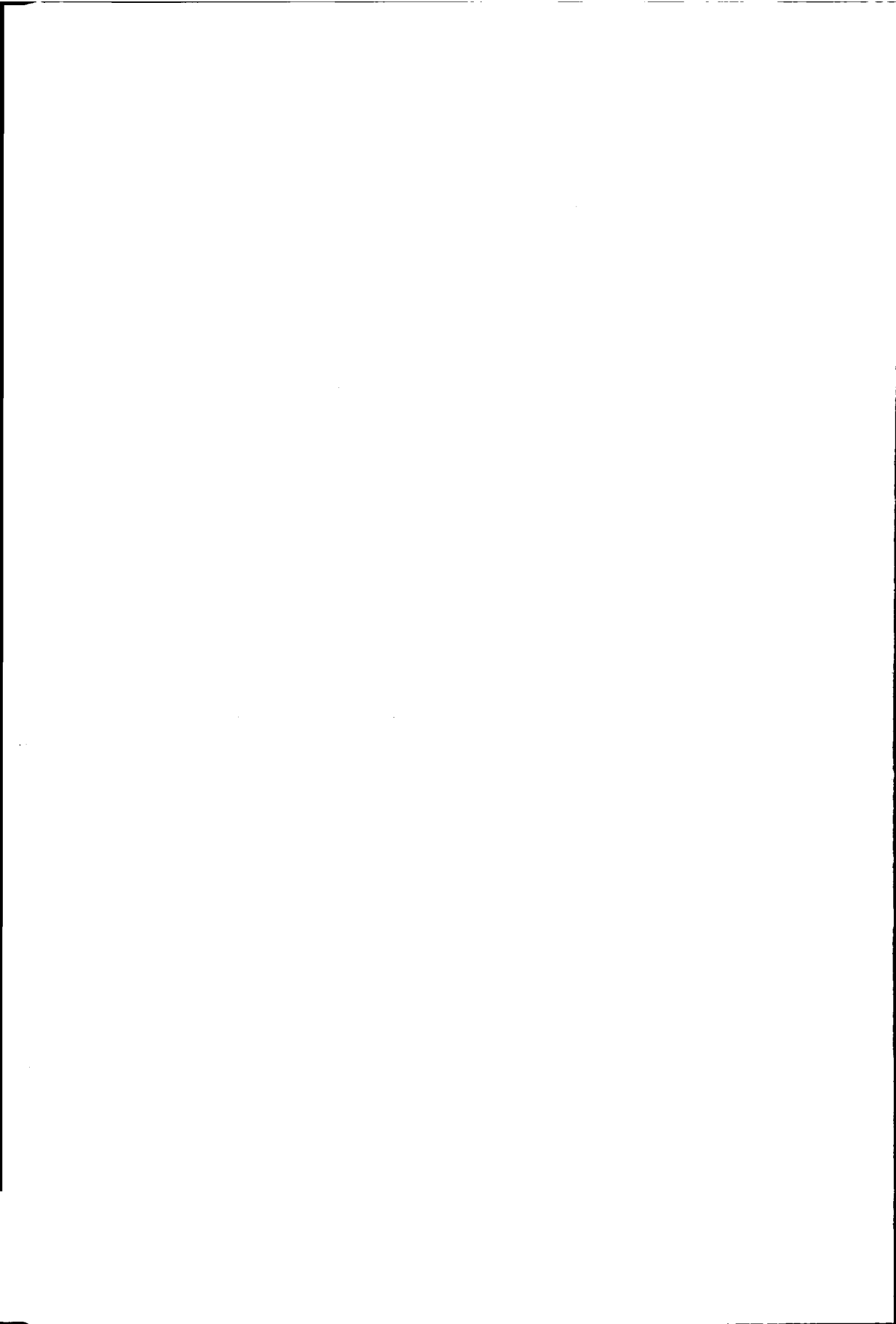
To study the viscosity reduction effects for bimodal suspensions in the regime of most practical importance, it would be necessary to make the size difference between

the two types of particles very much larger. Within the lattice-Boltzmann scheme there are two problems associated with this. Firstly, a bigger size ratio implies that the problem space grows as the difference of the radius to the power of three. With this, the decay time for the system gets larger with the difference of the radius squared. Secondly, at high volume fractions ($> 40\%$), where the viscosity reduction effect is probably bigger, spheres of small radii are clearly not adequate. This will lead to an extra increase in the size of problem space to keep the size ratio the same. It is for these reasons that we considered only moderate volume fractions and size ratios. Nonetheless, we succeeded in observing the viscosity reduction effect and identifying some of its features. To our knowledge this is the first time this has been achieved in three dimensional simulations. To be able to study the high volume fraction and high size ratio regime, further hardware and or algorithmic improvements are needed.

Bibliography

- [1] L.D. Landau and E.M. Lifshitz, *Fluid Mechanics* (Addison-Wesley), London (1959).
- [2] A. Einstein, *Ann. Physik.* **19**, 289 (1906).
- [3] J.M. Peterson and M. Fixman, *J. Chem. Phys.* **39**, 2516 (1963).
- [4] G.K. Batchelor and J.T. Green, *J. Fluid Mech.* **56**, 401 (1972).
- [5] D. Bedeaux, R. Kapral and P. Mazur, *Physica* **88A**, 88 (1977).
- [6] C. W. J. Beenakker, *Physica* **128A**, 48 (1984).
- [7] J.C. van der Werff, C.G. de Kruif, C. Blom and J. Mellema, *Phys. Rev A* **39**, 795 (1989).
- [8] M.R. Stapleton, D.J. Tildesley & N. Quirke, *J. Chem. Phys.* **7**, 4456 (1990).
- [9] B. D'Aguanno, R. Klein, J.M. Mendez-Alcaraz and G. Naegele, In *Complex Fluids* (ed. L. Garrido), Springer (1993).
- [10] A.T.J.M. Woutersen & C.G. De Kruif, *J. Rheol.* **37**, 681 (1993).
- [11] G. Bossis and J.F. Brady, *J. Chem. Phys.* **91**, 1866 (1989).
- [12] J.F. Brady, *J. Chem. Phys.* **99**, 567 (1993).
- [13] R. Verberg, I.M. de Schepper and E.G.D. Cohen, *Phys. Rev. E* **55**, 3143 (1997).
- [14] C.P. Lowe and A.J. Masters, *J. Chem. Phys.* (in press 1999).
- [15] R.B. Jones, *Physica* **212A**, 43 (1994).
- [16] C. Chang and R.L. Powell, *J. Fluid Mech.* **253**, 1 (1993).
- [17] M.P. Allen and D.J. Tildesley, "*Computer simulation of liquids*", Oxford University Press, Oxford (1987).
- [18] A.J.C. Ladd, *J. Fluid Mech.* **271**, 285 (1994).
- [19] C.P. Lowe and D. Frenkel, *Phys. Rev.* **E54**, 2704 (1996).
- [20] J.-P. Hansen and I. R. McDonald, "*The theory of simple liquids*", Academic Press, London (1986).
- [21] A.J.C. Ladd, *J. Chem. Phys.* **93**, 3483 (1990).
- [22] A.J.C. Ladd, *J. Fluid Mech.* **271**, 311 (1994).
- [23] D.J. Evans, *Mol. Phys.* **47**, 1165 (1982).

- [24] W.E. Alley and B.J. Alder, *Phys. Rev.* **A27**, 3158 (1983).
- [25] K. Sweeny & R. Geckler, *J. Appl. Phys.* **25**, 1135 (1954).
- [26] J.S. Chong, E.D. Christiansen & A.D. Baer, *J. Appl. Poly. Sci.* **15**, 2007 (1971).
- [27] S.C. Goto & H. Kuno, *J. Rheol.* **26**, 387 (1982).
- [28] R.J. Farris, *Trans. Soc. Rheol.* **12**, 281 (1968).
- [29] N.L. Ackerman & H.T. Shen, *AIChEJ.* **25**, 327 (1979).
- [30] S.C. Goto & H. Kuno, *J. Rheol.* **28**, 197 (1984).



6 The role sound plays in propagating hydrodynamic interactions

6.1 Introduction

6.1.1 The nature of hydrodynamic interactions

As a colloidal particle moves it induces flow fields in the solvent. These flow fields are both influenced by, and influence, the motion of its neighbours. In a concentrated suspension these "hydrodynamic" interactions between the colloidal particles modify the transport coefficients relative to their values in the dilute limit. Understanding colloidal suspensions therefore implies understanding hydrodynamic interactions. Compared to the intermolecular forces between individual molecules in a simple fluid, hydrodynamic interactions between colloidal particles differ in several respects. Whereas the former are essentially instantaneous, colloidal particles influence one another only via the fluid occupying the space between them. These interactions cannot be considered instantaneous. The speed at which they propagate depends on the properties of the fluid itself. Generally this transient regime can be probed experimentally (by for instance, diffusing wave spectroscopy [1, 2]). More formally, hydrodynamic interactions are a consequence of momentum transfer between particles by way of the fluid. Consider, for example, a colloidal particle i that, at a given instant in time has momentum $\mathbf{p}_i(0)$. As time goes by the velocity of the particle will be thermalized by collisions with the solvent molecules. The initial momentum will thus be dissipated through the system and "felt" by the particle's neighbours. Transport of momentum can take place via two mechanisms generally operating on very different time scales. The first is the diffusion of momentum transverse to the original direction. The second is the propagation of a sound wave longitudinal to the original direction. Theoretical approaches developed thus far [3, 4] only take into account the first, diffusive, mechanism. Incorporating the effects of sound propagation at the many particle level would be a daunting task. Nonetheless, there are cases in which the second, sonic, mechanism can be shown

to be relevant [5, 6]. Furthermore, the suggestion has been made that sound propagation may explain apparent discrepancies between computer simulation results and experiments probing the time dependence of the hydrodynamic interactions. In this chapter our aim is to establish, by computer simulation, precisely what role sound plays in propagating hydrodynamic interactions.

6.1.2 A single particle in a compressible fluid

To begin with it is useful to consider a case where considerable theoretical progress can be made. Namely, a single colloidal particle. This serves as a useful means of illustrating the relative characteristics of the two propagation mechanisms. The analysis of the single particle case begins with the observation that the equation of motion for the colloidal particle takes the form of a generalized Langevin equation [7, 8, 9]

$$\frac{dp_\alpha(t)}{dt} = -\frac{1}{m} \int_0^t \gamma(t-s)p_\alpha(s)ds + R(t) \quad (6.1)$$

where m is the mass of the particle and p_α one Cartesian component of the particle momentum. The convolution on the right hand side expresses the change in the velocity of the particle at time t in terms of its previous history through the (as yet) unknown memory function $\gamma(t)$. The second term, $R(t)$, is a stochastic force orthogonal to the momentum (*i.e.* $\langle p_\alpha(t)R(t) \rangle = 0$), introduced to ensure that the correct equilibrium properties are recovered. In order to study the decay of velocity fluctuations, it is useful to introduce the velocity autocorrelation function, $C(t)$. In terms of one component of the instantaneous velocity $v_\alpha(t)$ this is defined as

$$C(t) = \langle v_\alpha(0)v_\alpha(t) \rangle \quad (6.2)$$

The solution to equation 6.1 for the Laplace transform of the velocity autocorrelation function (denoted by the tilde) in terms of the transform variable z , reads

$$\tilde{C}(z) = \frac{\langle v_\alpha^2 \rangle}{z + \tilde{\gamma}(z)/m} \quad (6.3)$$

As it stands equation 6.3 is not very useful because we do not know the memory function $\tilde{\gamma}(z)$. However, given the equations of motion describing the dynamics of the solvent and imposing the correct boundary conditions on the surface of the particle, $\tilde{\gamma}(z)$ can in principle be calculated. The simplest assumption is that the motion of the solvent can be described by the *incompressible* Navier-Stokes equations. In this case the pressure and velocity, fields $p(\mathbf{r}, t)$ and $\mathbf{u}(\mathbf{r}, t)$ satisfy

$$\begin{aligned} \frac{\partial \mathbf{u}(\mathbf{r}, t)}{\partial t} &= \nu_0 \nabla^2 \mathbf{u}(\mathbf{r}, t) - \frac{1}{\rho_0} \nabla p(\mathbf{r}, t) \\ \nabla \cdot \mathbf{u}(\mathbf{r}, t) &= 0 \end{aligned} \quad (6.4)$$

where ρ_0 is the equilibrium density and ν_0 the kinematic viscosity of the fluid. For colloidal particles in equilibrium the non-linear term is extremely small and so

has been neglected. Assuming that the fluid velocity matches the colloidal particle velocity at its surface (a stick boundary condition), for a spherical particle of radius a this problem can be solved analytically [10] to yield

$$\tilde{\gamma}(z) = 6\pi\rho_0\nu_0a \left(1 + \frac{1}{9}z^* + \sqrt{z^*} \right) \quad (6.5)$$

where z^* is the dimensionless transform variable za^2/ν_0 . Substituting this result into solution of the generalized Langevin equation gives an expression for the dimensionless VACF,

$$\frac{\nu_0\tilde{C}(z^*)}{a^2C(0)} = \left[z^* + \frac{9\rho^*}{2} \left(1 + \frac{1}{9}z^* + \sqrt{z^*} \right) \right]^{-1} \quad (6.6)$$

where ρ^* is the ratio of the mass of fluid displaced by the particle to the mass of the particle itself *i.e.* $\rho^* = 4\pi a^3\rho_0/3m$. In practice, for stable suspensions the particles are nearly neutrally buoyant ($\rho^* = 1$), otherwise the system would separate under gravity. Equation 6.6 implies that, for a given value of ρ^* , the normalized VACF is a unique function of the dimensionless time $\tau_\nu = t\nu_0/a^2$. Values of τ_ν of the order unity characterize the time it takes transverse momentum to diffuse a distance the order of a particle radius. This is in turn controlled by the viscosity so we subsequently refer to this as the viscous time scale. A notable feature of equation 6.6 is that, taking the limit of large z^* and performing the inverse transformation to obtain the short time behaviour of the VACF, one finds a discontinuous drop in the value from unity at $t = 0$ to a value $(1 + \rho^*/2)^{-1}$ at an infinitesimal time later. This so called “added mass” effect is an artefact of assuming that the fluid is completely incompressible. A proportion of the initial momentum is carried away by the propagation of a sound wave. For a neutrally buoyant particle the normalized VACF drops instantaneously to a value of 2/3, reflecting the fact that 1/3 of the momentum is carried away by sound propagation and that, in an incompressible fluid, this happens instantaneously. In practice fluids are not, of course, completely incompressible. Sound propagates on a time scale set by the speed of sound through the system. To allow for the finite speed of sound, one needs to proceed as above, but solve the more complex *compressible* Navier-Stokes equations instead

$$\begin{aligned} \frac{\partial\rho_0(\mathbf{r},t)}{\partial t} + \rho_0\nabla\cdot\mathbf{u}(\mathbf{r},t) &= 0 \quad (6.7) \\ \frac{\partial\mathbf{u}(\mathbf{r},t)}{\partial t} + \frac{c_s^2}{\rho_0}\nabla\rho_0(\mathbf{r},t) - \nu_0\nabla^2\mathbf{u}(\mathbf{r},t) - \left(\frac{\nu_0}{3} + \nu_B\right)\nabla\nabla\cdot\mathbf{u}(\mathbf{r},t) &= 0 \end{aligned}$$

where ν_B is the bulk viscosity, and with c_s the speed of sound. Despite the greater complexity, this problem can nonetheless be solved [11]. Assuming the dynamics of the fluid are given by equation 6.7, and again imposing a stick boundary condition, an expression can be derived for the frequency dependent friction coefficient (equation 4.13) and hence the VACF.

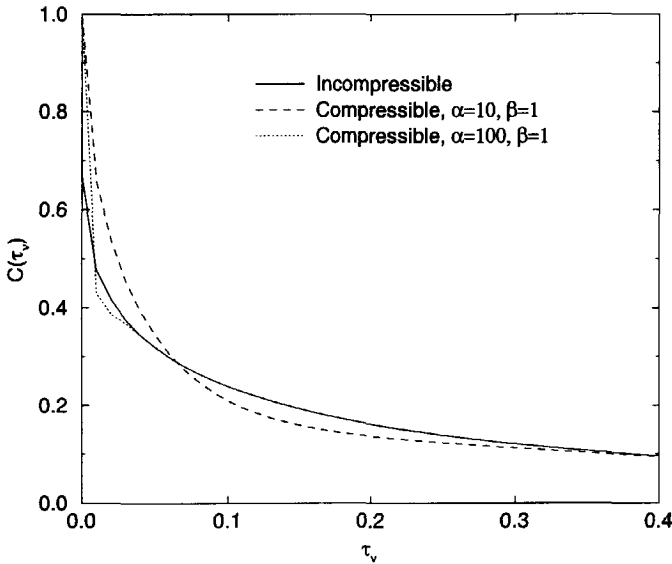


Figure 6.1: The normalized VACF for a single, neutrally buoyant, colloidal sphere in an incompressible and compressible fluid. The compressible result is shown for two different values of the compressibility factor α . In both cases the bulk viscosity is assumed equal to the shear viscosity. Note that the rapid short time decay in the compressible case replaces the discontinuity at $t = 0$ in the incompressible case. At longer times the results become identical

The solution to our problem is now more complicated (see section 4.3.2) because it involves the two additional parameters associated with sound propagation, c_s and ν_B . These are most conveniently incorporated into the analysis by defining, in addition to the viscous time, a “sonic” time $\tau_s = tc_s/a$ and a viscosity ratio $\beta = \nu_B/\nu_0$. For most fluids the latter is of the order unity. As for the sonic time, values of the order unity characterize the time it takes a sound wave to travel a distance the order of a particle radius. To give a feel for the two time scales involved, it is useful to consider real times in a “typical” suspension. A typical system we consider to be particles of radius $1\mu\text{m}$ dispersed in water at room temperature. This being the case we have $\tau_\nu \sim 1$ when $t \sim 10^{-6}\text{s}$, whereas $\tau_s \sim 1$ when $t \sim 10^{-9}\text{s}$. The ratio of the two $\alpha = \tau_\nu/\tau_s = ac_s/\nu_0$ takes the value $\alpha \sim 1000$. Clearly, on the scale of a colloidal particle sound propagates momentum much more rapidly than does viscous diffusion. In terms of the viscous and sonic time scales, the principle characteristics of the VACF in a compressible fluid can now be summarized as follows. Real times, where given, correspond to the typical system described above.

- At short times, $t \ll a/c_s$ ($t \ll 10^{-9}\text{s}$), the normalized VACF depends only on c_s/a and is a unique function of the dimensionless “sonic” time scale

$\tau_s = tc_s/a$. This very rapid decay replaces the discontinuity found for the incompressible case and reflects the period during which the particle generates the sound wave.

- At intermediate times $t \sim a/c_s$ ($t \sim 10^{-9}$) there is a “mixed” region where the viscous time, sonic time, and viscosity ratio are all relevant. This reflects the period where the sound wave is separating away from the particle.
- For longer times $t > a/c_s$ ($t > 10^{-9}$) the result reduces to the incompressible result above (equation 6.6). The sound wave has departed and consequently compressibility plays no role.

In summary, by going from an incompressible to a compressible model for the fluid, we get rid of the discontinuity in the VACF at very short times. Further, we find that for times $\tau_s > 1$ we could have saved ourselves the trouble because the incompressible result suffices. This is illustrated in figure 6.1 where we have plotted the VACF predicted by compressible theory, for a neutrally buoyant particle with $\alpha = 10$ and $\alpha = 100$, along with the incompressible result.

6.1.3 Sound in a concentrated suspension

While the above discussion serves as a useful guide to the relevant parameters and time scales for a compressible fluid, it only applies for a single particle. What we are interested in is a suspension, for which there are many particles. The question then arises, what role does sound play in a suspension? We have already seen that the hydrodynamic interactions between particles are a result of momentum transfer and that a significant proportion of that momentum is carried off by sound propagation. Therefore, in principle, part of the interactions can develop on the fast sonic time, rather than the slow viscous time. There are several reasons to establish whether such a mechanism is present. Firstly, it is the separation of the relative time scales for the various processes operating in suspensions that underlies theoretical treatments. A detailed discussion of this was given by Masters [12]. Secondly, if sound can be neglected (the solvent is assumed *incompressible*) then the size of colloidal particles becomes essentially irrelevant. The results for any correlation function can be expressed as universal functions of the dimensionless parameters outlined above (equation 6.6 for example). On the other hand, if sound propagation does play a role this is no longer true. The radius of the particles enters in the expression for the compressibility factor α . Thus, if sound plays a role, correlation functions for particles of different sizes differ fundamentally. They cannot simply be scaled onto each other. This is important because the compressibility can vary considerable between different systems that could still lay claim to be called colloidal. For instance, we quoted a value $\alpha \sim 10^3$ for our typical system of a micron sized particle suspended in water. We further commented that this implied sound transported momentum on times scales very short compared to viscous diffusion. There is nothing special about one micron though. Particles with sizes in the range $1nm < a < 10\mu$ satisfy the criterion of being atomically large but macroscopically

small. Further, particle spanning this entire range are synthesized and used in experiments. Usually the radius is chosen to suit the problem under study or the technique being applied. This in turn implies a range of compressibilities in the range $1 < \alpha < 10^4$. That is ranging from sound propagation and viscous diffusion occurring on similar time scales to the regime where the latter is much slower.

Despite the fact that sound propagation might be an important mechanism for propagating interactions in a suspension, until relatively recently the tacit assumption was that it is not. One reason for this might simply be wishful thinking. Constructing an incompressible theory for the propagation of hydrodynamic interactions is difficult enough without the additional complication of compressibility. There are, however, two more substantial reasons. First, as outlined above, it is largely irrelevant for a single particle. Second, at sufficiently long times, it definitely cannot play a role. This is simply because the integral of a correlation function is related to the zero frequency response. The zero frequency response to an external perturbation is the same for a compressible or an incompressible fluid. Thus, the speed of sound does not enter into the expression for the diffusion coefficient of a single particle whether the fluid is compressible or not (see section 2.4). The question then becomes, when does it become irrelevant rather than if. More recently experimental theoretical and computer simulation results have suggested that the effects of sound propagation may be manifest on viscous time scales. As we have seen, for a single particle, this is not the case. Firstly, experiments were reported [13, 14] probing the transient behaviour of the mean square displacement at short times ($\tau_\nu \sim 1$). By comparing the short time dynamics of particles in a concentrated suspension with those of an isolated particle, Zhu *et al.* [13] found that all the experimental data could be plausibly collapsed onto the single-particle curve if the time was rescaled in units of a^2/ν_ϕ , where ν_ϕ is the kinematic viscosity of the suspension. The conclusion was, that even on time scales where $\tau_\nu \sim 1$, a colloidal suspension behaves like an “effective fluid”, by which we mean a fluid with the viscosity of the suspension. This was surprising because, if the hydrodynamic interactions develop on the viscous time scale, one would expect that the suspension can only behave as an effective fluid on time scales $\tau_\nu \gg 1$. Computer simulations performed by Ladd [15, 16] appeared to confirm this, although more detailed simulations [17], and theoretical work [4] suggested that effective fluid regime was only reached on longer times $\tau_\nu \gg 1$. Nonetheless, these observations led to Español *et al.* [18, 19] to re-examine the role of sound propagation and suggest that the speed of sound may play a role in determining the time scale at which the hydrodynamic interactions propagate. This might, it was suggested, make effective fluid behaviour possible on very short time scale. A similar explanation was invoked to explain a discrepancy between experimental work and computer simulations *vis a vis* the collective dynamics of simulations. In the simulations, Ladd observed collective correlation induced by sound propagation but these were ascribed to excessive compressibility in the simulation model. More recently, for a colloidal particle confined in a medium with a fixed geometry, it was demonstrated that the effects of sound propagation persist well beyond the sonic time scale and into the viscous diffusion regime [5]. So

much so, compressibility actually determines the long time form of the decay of the VACF. This is because, in a confined geometry (which dissipates momentum), the sound wave generated by a particle ceases to propagate and dissipates by a diffusive mechanism instead [6]. If the sound wave no longer disappears away with its quota of momentum, it is not surprising that its effects linger on beyond the normal sonic time.

Given the above, a detailed study of the role sound plays in a suspension is clearly in order. This is our aim here. We wish to establish in what regimes the effect of sound propagation can be safely neglected and conversely where not. To do so we have chosen to study, rather than the velocity autocorrelation function, the more general wave vector dependent current-current correlation function $J(k, t)$, defined as

$$J(k, t) = \frac{1}{N} \left\langle \sum_{i=1}^N \sum_{j=1}^N [\hat{\mathbf{k}} \cdot \mathbf{v}_i(t) \mathbf{v}_j(0) \cdot \hat{\mathbf{k}}] \exp [i\mathbf{k} \cdot (\mathbf{r}_i - \mathbf{r}_j)] \right\rangle \quad (6.8)$$

where k is the wave vector. The reasons for choosing to study this function are twofold. First, it gives an insight into collective correlations. That is, the ability of the instantaneous velocity of one particle to subsequently influence the motion of its neighbours. There is no analogue of this process in the case of a single particle so the inference that sound does not influence this function cannot, by analogy, be drawn. The second reason is that the suggestion has already been made that this quantity is indeed influenced by sound propagation [20, 21].

6.2 Calculating the current-current correlation function

The procedure we used was as follows. We generated a configuration of hard spheres using standard Monte-Carlo techniques and “embedded” them in a lattice-Boltzmann fluid. This, as we have discussed in chapter 4, is a model compressible fluid. Because spontaneous fluctuations are averaged out in the lattice-Boltzmann fluid we need to introduce velocity fluctuations in the system to calculate the wave vector dependent current-current correlation function (equation 6.8). One way is to do so is to drive fluctuations in the stress tensor of the fluid and thus maintain the model colloidal particles at some prescribed temperature [22]. The other is to impose velocity fluctuations on the colloidal particles and study the decay [23] of these fluctuations in an otherwise dissipative system. According to Onsager’s regression hypothesis these two methods should be equivalent. For reasons of computational expediency we have chosen the latter. We have seen in chapter 4, that, if the model colloidal particles contain internal fluid, there are certain artefacts associated with internal sound propagation. We will be looking for the effects of sound propagation in a suspension largely by studying scaling behaviour and these artefacts complicate the analysis considerably. We have therefore adopted the procedure described in chapter 4 to remove the effects of the internal fluid. Thus we generated initial

velocities, $\mathbf{v}_i(0)$, for the colloidal particle from a Gaussian distribution with a fixed variance. The subsequent velocities $\mathbf{v}_i(t)$ are calculated by simply letting the system evolve in time. The correlation function can then be calculated by simply substituting these quantities into equation 6.8 and taking the ensemble average over different initial configurations of particles and statistically independent initial values of the velocity. In practice we do both at the same time by repeating the calculation with different configurations each with a set of initial velocities drawn independently from Gaussian distributions. At least 40 independent configurations were used. The statistical errors in the time integral of $J(k, t)$ were then of the order of 10%, which is just about adequate for our present purposes. It would have been desirable to use more extensive ensemble averaging, say 500 configurations, but the computational demands would have been excessive.

One small point in calculating the correlation function (equation 6.8) is that we do not constrain the total momentum in the system to be zero because this introduces an artificial anticorrelation between the velocity of an individual particle and the velocities of its neighbours. However, since we have a nett momentum in the system the correlation function does not, for a finite system size, decay to zero. To correct for this we perform the calculation in a frame of reference where the total solvent momentum remains zero. This has the effect of scaling the velocities from $\mathbf{v}_i(t)$ to $\mathbf{v}'_i(t)$, where, by definition

$$\mathbf{v}'_i(t) = \mathbf{v}_i(t) - \frac{\Delta \mathbf{p}(t)}{V \rho_0} \quad (6.9)$$

Here $\Delta \mathbf{p}(t)$ the total momentum in the solvent phase at time t and V the volume of the system. By using values of $\mathbf{v}'_i(t)$ rather than $\mathbf{v}_i(t)$, the correlation function, starting from a system with nett momentum, decays to zero and is independent of system size [17].

In order to separate out the contribution from collective motions from that of the single particle motion, it is useful to split the wave vector dependent current-current correlation function into the (normal) velocity autocorrelation function, $C(t)$ and an interaction velocity correlation function $J_I(k, t)$. Thus we have $J(k, t) = C(t) + J_I(k, t)$, where, by definition (see equation 6.8) $J_I(k, t)$ is:

$$J_I(k, t) = \frac{1}{N} \left\langle \sum_{i=1}^N \sum_{j \neq i}^N \left[\hat{\mathbf{k}} \cdot \mathbf{v}_i(t) \mathbf{v}_j(0) \cdot \hat{\mathbf{k}} \right] \exp[i\mathbf{k} \cdot (\mathbf{r}_i - \mathbf{r}_j)] \right\rangle \quad (6.10)$$

By considering the properties of $J(k, t)$ and $C(t)$ we can deduce some of the features we expect to characterize the interaction correlation function. The integral over all times of $J(k, t)$ defines the wave vector dependent collective diffusion coefficient, $D(k)$. In the limit $k \rightarrow 0$ this should approach the (short time) collective diffusion coefficient, D_c . In the limit $k \rightarrow \infty$ terms with $i \neq j$ average to zero, $J(k, t)$ reduces to the velocity autocorrelation function and so $D(k)$ approaches the single particle or self diffusion coefficient D_s , (equation 1.6). In terms of transport coefficients,

the integral of $J_I(k, t)$ over time is equal to the difference between the wave vector dependent collective diffusion coefficient and the self diffusion coefficient.

$$\int_0^{\infty} J_I(k, t) dt = D(k, t) - D_s \quad (6.11)$$

Given the above, we expect that as $k \rightarrow \infty$ the integral of $J_I(k, t)$ will be zero, whereas in the limit $k \rightarrow 0$ it will be equal to the largest interactive contribution part of the collective diffusion coefficient $D_c = D - D_s$. The collective diffusion coefficient can be calculated (to a good approximation) theoretically [24] and has also been calculated numerically [20, 25]. Both concur that $D \ll D_s$, so we expect that, as $k \rightarrow 0$, the integral of $J_I(k, t)$ will be a negative quantity.

6.3 Results

6.3.1 The effect of sound propagation on single particle motion

We will begin by considering the effect of sound propagation on the motion of an individual particle in a dense suspension. To this end, we consider only the self part of $J(k, t)$, that is the velocity autocorrelation function $C(t)$. Measuring all quantities in units such that the lattice spacing and time-step are equal to unity, we took a suspension with volume fraction $\phi = 0.25$ and calculated the VACF for spheres with three different radii, $a = 2.5, 4.5$ and 6.5 . The solvent viscosity ν_0 , speed of sound c_s , and bulk viscosity ν_B were kept at constant values of $1/6, 1/\sqrt{2}$ and $1/30$ respectively. This means that for these three simulations the compressibility factor $\alpha (= ac_s/\nu_0)$ took the values $10.6, 19.1$ and 36.0 . We are therefore making the suspension more incompressible by increasing the size of the particles. Physically this is because the viscous time is proportional to a^2 whereas the sonic time is proportional to a . Therefore sound travels a characteristic distance a in a proportionately shorter time if we increase the particle radius. The reasons this is our preferred method for changing the compressibility factor are firstly that there are strict stability conditions on the speed of sound. This cannot be varied much. Secondly, although the viscosity can be chosen freely, the particles have an effective radius which depends on the viscosity. The value $\nu_0 = 1/6$ gives effective radii very similar to the nominal radii but, as the fluid viscosity varies either side of $1/6$, this becomes increasingly untrue. Furthermore, the memory reduction scheme, described in chapter 3, is most effective for this particular viscosity. We therefore prefer to vary a . The down side of this is that we require proportionately larger systems. However, for these three sizes of particles we have been able to simulate systems large enough to allow us to calculate the VACF up to sufficiently long times and still limit the calculations to times less than that required for sound to cross the simulation box. The periodic boundary conditions applied at the faces of the simulation box cannot, therefore, influence the results. If such a procedure is not adopted there is a pronounced perturbation to

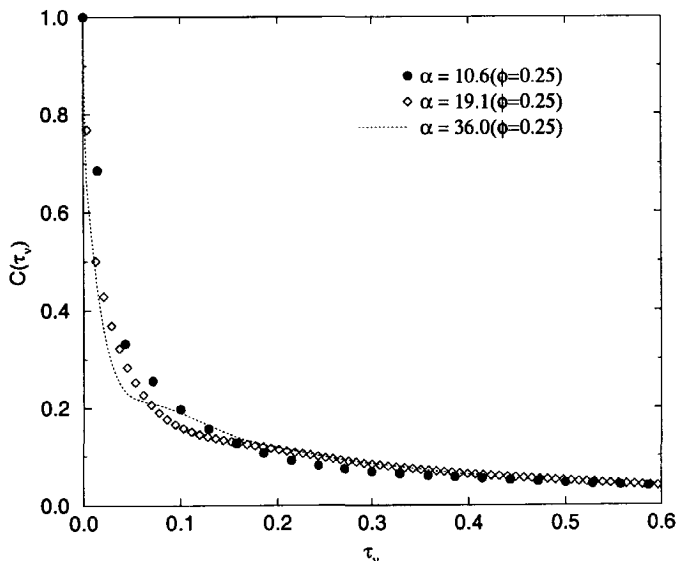


Figure 6.2: The velocity autocorrelation function for the self part, $C(t)$, at three different compressibilities of a suspension of volume fraction $\phi = 0.25$. These three different compressibilities are obtained by varying only the radii: $a = 2.5, 4.5$ and 6.5 . Other parameters responsible for the compressibility were kept constant and are given in the text.

the decay of the VACF as a particle gets hit by the sound wave generated by its periodic images.

The results we obtained for the normalized VACF, as a function of the viscous time scale τ_ν , are plotted in 6.2. Plotting the data in this form makes that the effects of compressibility are simple to spot. Any difference between the curves (apart from numerical errors, which are relatively small even for $a = 2.5$, see chapter 4) must be attributable to sound propagation. If the fluid is incompressible then, in these dimensionless terms we are basically simulating the same system (equation 6.6). Clearly, at short times the VACF for the three systems are not identical. However, at longer times the three functions do converge indicating that sound is playing no role. Furthermore, the time at which the functions become indistinguishable shifts to shorter times as we decrease the compressibility (increase α). More quantitatively we find that the VACF calculated for $\alpha = 10.6$ becomes indistinguishable from the other two (higher) values of α for $\tau_\nu > 0.40$, whereas the VACF calculated for $\alpha = 19.1$ becomes indistinguishable from that calculated at $\alpha = 36.0$ for times $\tau_\nu > 0.20$. We saw in section 6.1.2 that, for the single particle case, the effects of compressibility can be neglected on time scales long compared to the sonic time τ_s , that is $t > a/c_s$. In terms of the viscous time this condition corresponds to $\tau_\nu > \nu_0/c_s a$ or $\tau_\nu > 1/\alpha$. Therefore, in terms of the viscous time the effects of compressibility become negligible after a time which scales as $1/\alpha$. The behaviour

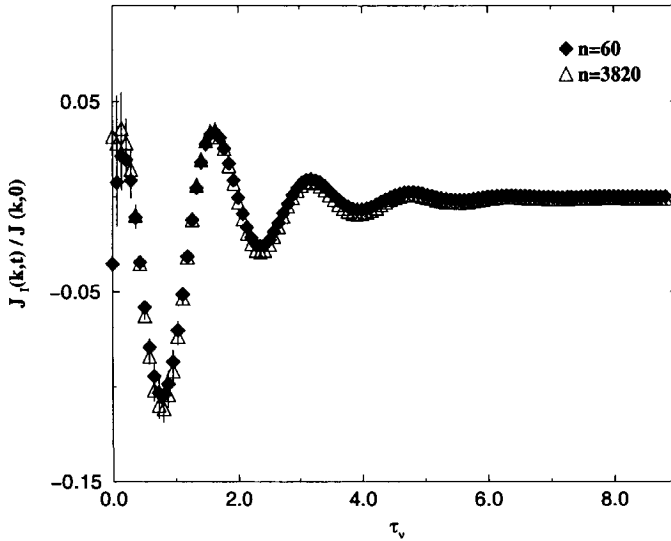


Figure 6.3: The interaction part of the normalized current-current correlation function, $J_I(k, t)/J_I(k, 0)$, for two different system sizes. The simulation data are for a 60 sphere simulation system (diamonds) and a 3820 sphere simulation system (triangles). The dimensionless wave vector k^* is .6283 in both cases. The other parameters are given in the text. The functions are statistically indistinguishable

we noted above is quite consistent with this also being the case in a suspension. On increasing α from a value of 10.6 to 19.1 (a factor of 1.8) the time at which incompressible behaviour is observed decreases by a factor of approximately 2.0. Given the uncertainty involved in establishing a precise value for the incompressible time, this difference cannot be regarded as significant. It is interesting to note that the incompressible time not only scales in the same way as for the single particle case but is also quantitatively almost identical. Examining the Bedeaux and Mazur result (figure 6.1) for a single particle, the incompressible time is, to a good approximation $\tau_\nu \approx 4/\alpha$. Extrapolating the same behaviour to a suspension, one would predict an incompressible time of $\tau_\nu = 0.38$, for the system with $\alpha = 10.6$, and $\tau_\nu = 0.21$ for the system with $\alpha = 19.1$. This compares with values 0.4 and 0.2 respectively calculated from the simulation results. The most obvious conclusion we can therefore draw from figure 6.2 is that, in a suspension, the role of sound propagation on the velocity autocorrelation function is rather trivial. It is remarkably similar to the single particle case in that it influences the decay on the short sonic time scale. On the longer viscous time scale sound appears irrelevant and an incompressible theory could adequately describe the dynamics.

<i>set</i>	<i>a</i>	<i>a_{eff}</i>	ν_0	α	Γ_0	<i>N</i>	$L \times L \times L$	<i>nr_{runs}</i>
R1	1.5	1.5	1/6	6.3	1/4	3820	60 × 60 × 60	40
R2	2.5	2.5	1/6	10.5	1/4	3820	100 × 100 × 100	40
R3	4.5	4.5	1/6	18.9	1/4	3820	180 × 180 × 180	40
R4	8.5	8.5	1/6	35.7	1/4	477	170 × 170 × 170	40
R5	4.5	4.7	1/48	157.9	1/18	119	47 × 47 × 94	40
R6	4.5	4.79	1/96	321.9	1/24	120	48 × 48 × 96	40

Table 6.1: The various parameters associated with the six simulations.

6.3.2 Calculating the interaction contribution

Turning our attention to the interaction part of the transverse current-current correlation function $J_I(k, t)$ we found it useful to adapt our approach in two respects. Firstly, by comparing the results for simulations on different system sizes we found that, in contrast to the VACF, the periodic boundary conditions did not influence the results significantly, even on time scales long compared to the time taken by a sound wave to cross the simulation box. We were therefore able to calculate $J_I(k, t)$, free from finite size artefacts, up to longer times and using smaller systems. This is illustrated in figure 6.3, where we have plotted the normalized interaction correlation function for a system of 60 and 3820 spheres of radius 1.5 lattice sites. The volume fraction was 25%. Because of the periodic boundary conditions we can only use wave vectors commensurate with the periodic box. With these two system sizes we can simulate the same wave vector in both cases. Other than the system size, these simulations are therefore identical. As the figure shows, the results for the two systems are indistinguishable. This is despite the fact that, for both systems, the time range plotted greatly exceeds the time it takes a sound wave to cross the simulation box. It should be noted that the other possible time scale on which we might expect to observe finite size effects, the time it takes transverse momentum to diffuse across the simulation box, is not reached. However, this is a much less serious restriction. All the simulations we subsequently report also satisfy the condition.

Secondly, in order to gain a reasonable degree of insight into the role of sound propagation, the compressibility factor needed to be varied to a greater extent than was practical by varying the particle size alone. It was necessary, in addition, to vary the viscosity. For simulations where the viscosity differed from the value 1/6 (used thus far in the simulations outlined above), the particle radii were assigned to be the effective, viscosity dependent, radii (a_{eff}) calculated by Ladd [16]. Six sets of simulations were carried out in total, all at a volume fraction of $\phi = 0.25$. The values of the parameters associated with these simulations, which we denote by *R1*, *R2*, ..., *R6*, are summarized in table 6.1. Here, the sound wave attenuation coefficient Γ_0 is defined as $(4\nu_0/3 + \nu_B)$. It defines the rate of damping for sound waves propagating through the solvent. The number of colloidal particles is denoted *N* and the number of configurations by *nr_{runs}*. The final column gives the dimen-

sions L of the simulation box. For the cubic systems we averaged over over wave vectors directed along each of the three directions of the coordinate axes (giving 120 independent correlation functions). For the non-cubic systems, only wave vectors directed parallel to the long axis were used.

6.3.3 General features of the interaction correlation function

In figure 6.4 we have plotted $J_I(k, t)$, calculated for various values of the dimensionless wave vector $k^* = ka$, for run *R4*. This simulation had a compressibility factor $\alpha = 36$ and, as such, corresponds to particles of radius $a \sim 25nm$ suspended in water *i.e.* small colloidal particles. The most notable feature is clearly the pronounced oscillation. This phenomenon was also observed in computer simulations performed by Ladd *et al.* [20]. Ladd *et al.* further concluded that these oscillations were sonic in origin, but that they were an artefact of the excessive compressibility of the model they were using. The model was, in all but detail, the same as the lattice-Boltzmann scheme we are using here. What we are interested in is whether these oscillations can really be considered artefacts. To begin with we re-iterate that the results shown in figure 6.4 are parametrically correct for small colloidal particles. This simulation can only be regarded as excessively compressible if we are interested in larger particles. In figure 6.5 we show the equivalent plot for run *R6*. This simulation had a compressibility factor $\alpha = 325$, approximately an order of magnitude greater. As such it corresponds to particles of radius $a \sim 250nm$ suspended in water. This could reasonably be described as an average colloidal particle. As figure 6.5 shows, we still observe oscillations although they are characterized (at a given value of k^*) by a higher frequency and more rapid damping than was the case for $\alpha = 36$. Taking figures 6.4 and 6.5 together it appears that these oscillations are not necessary artificial, but rather, they are sensitive to the compressibility of the system. The fact that their characteristics depend on the compressibility factor shows that they must be sonic in origin. If the solvent were incompressible this behaviour could not be observed, figures 6.4 and 6.5 would be identical. A further point illustrated by figures 6.4 and 6.5 is that that both the frequency and damping of the oscillations depend on the wave vector.

In order to come to any conclusion as to whether this effect will be relevant in the analysis of experimental results, it is necessary to establish the scaling with respect to the wave vector. There are two reasons for this. First, experimentally it is not possible to measure the correlation function $J(t)$ itself. It is only possible to measure its time integral (as in photo-correlation spectroscopy), or a quantity closely related to the time interval. The contribution these oscillations make to the integral of the correlation function and the time scale over over which this contribution will be significant, will depend on the amplitude, frequency and rate of damping. Second, the time regime probed by experiments depends on the wave vector. Longer wave vectors are, for instance, characterized by longer decay times for correlation functions of position. Thus, experimentally, decreasing the wave vector normally implies probing longer times. If the oscillations in $J(k, t)$ increase in magnitude

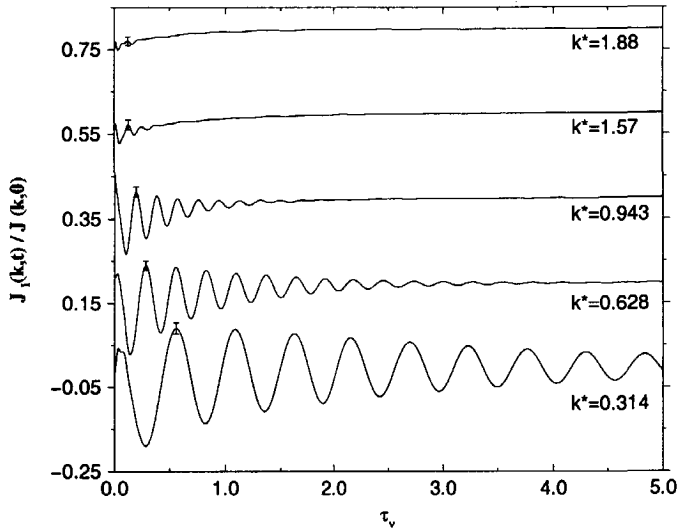


Figure 6.4: The dimensionless interaction correlation function $J_I(k, t)/J(k, 0)$, for Run 4, calculated for various values of the reduced wave vector k^* .

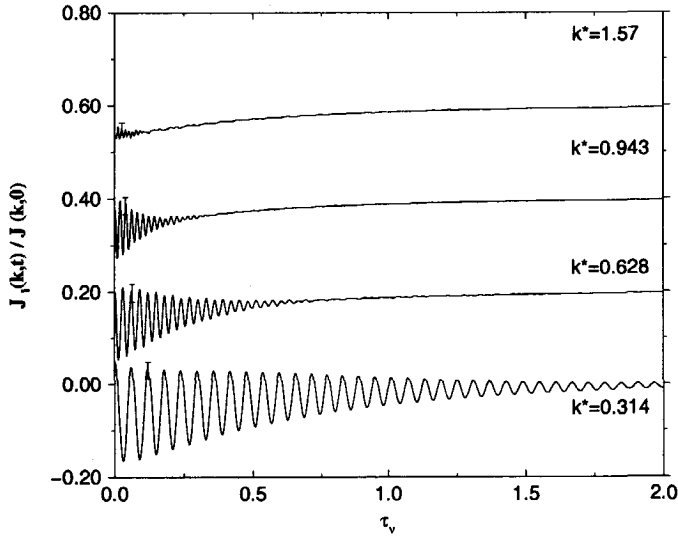


Figure 6.5: The dimensionless interaction correlation function $J_I(k, t)/J(k, 0)$ for Run 6, calculated for various values of the reduced wave vector k^* .

with decreasing wave vector, but correspondingly decay over shorter times, their effect may not be relevant.

A convenient reference point for analyzing the wave vector dependent current-current correlation function is what one may term "classic hydrodynamic" behaviour. For a one component, isothermal, compressible fluid whose behaviour can be described by the compressible Navier-Stokes equations (equation 6.7), the contribution to $J_I(k, t)$ from sound propagation, $J_i^s(k, t)$, is of the form [26]

$$J_i^s(k, t) = \frac{k_B T}{2m\pi} \cos(kc_s t) \exp(-\Gamma_0 k^2 t) \quad (6.12)$$

The full form of $J_i^s(k, t)$ in the frequency, domain is given in reference [26]. Equation 6.12 is obtained by taking the inverse transformation for frequencies $\omega \ll c_s k$ so can only be expected to hold for times $\tau_s k^* \gg 1$. In a suspension, $J_i^s(k, t)$ can in general only be one component of the total interaction function $J_I(k, t)$. We know this because the integral over all time of $J_I(k, t)$ at small k , is not zero. As noted above, this integral is equal to the difference between the total diffusion coefficient and self diffusion coefficient ($D(k) - D_s$), (as equation 6.12 implies) and in the limit of $k \rightarrow 0$ represents the collective part of the diffusion coefficient D_c . Furthermore, as we pointed out in section 6.1.3, this quantity ($D(k) - D_s$), cannot depend on the compressibility of the fluid. There must therefore be an "incompressible" contribution to $J_I(k, t)$, *i.e.* a component that is independent of the compressibility of the solvent. This is clearly illustrated in both figures 6.4 and 6.5, particularly at short times, where $J_I(k, t)$ oscillates about a negative non-zero value. To try to separate out the effects of the compressible component of $J_I(k, t)$ it is convenient to work with the relative amplitudes of successive oscillations rather than absolute values. We therefore define the following quantities.

- A frequency ω defined $2\pi/\Delta t$, where Δt is the time between successive maxima (or minima) in the oscillations. From the first maximum (or minimum) onwards we find that this value is constant, in agreement with equation 6.12. Equation 6.12 further predicts that $\omega = ck$.
- A dimensionless "initial" amplitude $A_0^* = A_0 m / 2\pi k_B$, where A_0 is defined as the difference between the first minimum of $J_I(t)$ and the first maximum. According to equation 6.12, $A_0^* = \exp(-\Gamma_0 k^2 \pi / \omega) (1 + \exp(-\Gamma_0 k^2 \pi / \omega))$. If $k^2 \Gamma_0 \pi / \omega \ll 1$ (the decay of the oscillations is slow compared to the frequency) this can be expanded in the simpler form,

$$A_0^* \simeq 2 - k^2 \Gamma_0 \pi / \omega + \mathcal{O}k^4 \quad (6.13)$$

- A dimensionless time-dependent amplitude, $A^*(t_l)$ defined as

$$A^*(t_l) = |J_I(t_l - \Delta t/4) - J_I(t_l + \Delta t/4)| m / 2\pi k_B T \quad (6.14)$$

where $l = 1, 2, \dots$, is an integer and $t_l = l\Delta t/2 + \Delta t/4$. According to equation 6.12 this should decay as,

$$2A^*(t_l) = \exp(-k^2 \Gamma_0 t_l) (\exp(-k^2 \Gamma_0 \pi / 2\omega) + \exp(k^2 \Gamma_0 \pi / 2\omega)) \quad (6.15)$$

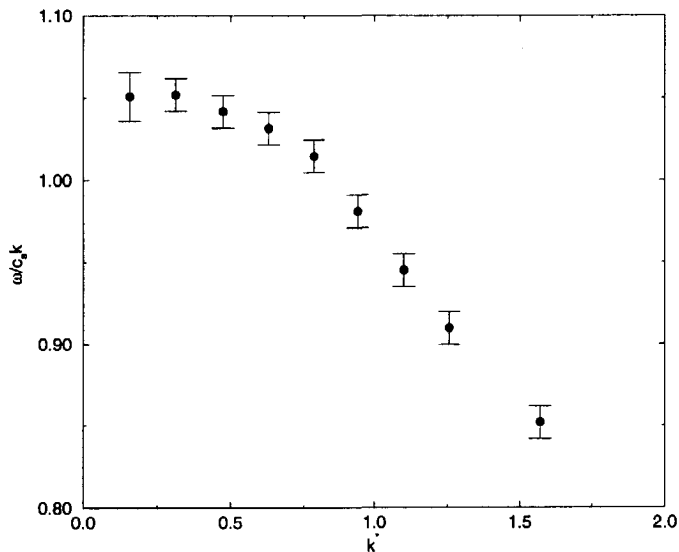


Figure 6.6: The (dimensionless) frequency of the oscillations observed in the interaction correlation function plotted as a function of the reduced wave vector ($k^* = ka$). This data corresponds to run *R4*. Data for the other runs showed the same behaviour.

Again, so long as $k^2\Gamma_0\pi/\omega \ll 1$, this can be expanded in a simpler form

$$A^*(t_i) \simeq \exp(-k^2\Gamma_0 t_i) + \mathcal{O}k^4 \quad (6.16)$$

We will take these characteristics in turn and examine to what extent they describe the results we find in a suspension, beginning with the frequency.

6.3.4 The frequency of the sound induced correlations

In figure 6.6 we have plotted the dimensionless frequency $w^* = \omega/c_s k$ as a function of the dimensionless wave vector k^* . According to classic hydrodynamic theory, this function takes a value of unity, independent of wave vector. As figure 6.6 shows, the dimensionless frequency of the oscillations displays a weak dependence on the wave vector, but becomes independent of k for $k^* < 0.5$. That is, we recover hydrodynamic behaviour on sufficiently long length scales. However, careful analysis of figure 6.6 shows that, in this limit, the dimensionless frequency does not quite asymptote to unity. The value we find is $\lim_{k \rightarrow 0} \omega/c_s k = 1.05 \pm 0.01$.

We now note, however, that there are two primary objections to applying the classic theory (equation 6.12) to a suspension. First, there is an ambiguity as to the values we should input for the transport coefficients. In the above analysis we have taken the speed of sound to be the speed of sound in the solvent, that is, the speed of sound in the dilute limit. Of course, as with, for instance the viscosity, we do not

necessarily expect the speed of sound in a suspension to be equal to the speed of sound in the solvent. Second, it takes no account of the structure of the fluid.

One possible explanation for the low frequency asymptote differing from unity concerns the former. Simply, the speed of sound in the suspensions $c_{s\phi}$ is slightly greater than that in the solvent, specifically $c_{s\phi}/c_s = 1.05$. We have independently confirmed that this is the case by measuring directly the speed of sound in the simulation system. Specifically, we examined the time at which sound induced perturbations to the decay of the VACF, resulting from the periodic boundary conditions, were observed. By comparing with the dilute limit, this analysis gives a value $c_{s\phi}/c_s = 1.05$. As a point of reference, the suspension viscosity ν_ϕ is equal to $2.17\nu_0$ at this volume fraction, so this is a rather weak dependence. Nonetheless, the asymptotic behaviour we observe for the frequency of the oscillations, at long wave lengths, is consistent with classic hydrodynamic theory if we replace a transport coefficient characteristic of the solvent (c_s) with a transport coefficient characteristic of the suspension ($c_{s\phi}$).

If we now turn to the wave vector dependence, this is most likely to be a consequence of the structure present in the fluid. This (in Fourier space) is most conveniently probed by the static structure factor $S(k)$

$$S(k) = \frac{1}{N} \left\langle \sum_i \exp(i\mathbf{r}_i \cdot \mathbf{k}) \sum_i \exp(-i\mathbf{r}_i \cdot \mathbf{k}) \right\rangle \quad (6.17)$$

At sufficiently small wave vectors the static structure factor (SSF) approaches a constant value, reflecting the fact that, on sufficiently long length scales, the suspension appears essentially homogeneous. For hard spheres at this volume fraction (see for example reference [27]), the SSF becomes essentially independent of k for $k^* < 0.5$, in line with our estimate for the wave vectors for which we observe classic hydrodynamic behaviour. Thus, the wave vector dependence we observe in $\omega/c_s k$ at short wave lengths is consistent with the structure of the suspension, not accounted for in the simple theory, playing a role.

We finally note that generalizing the hydrodynamic result by defining a wave vector dependent speed of sound $c_s(k)$, such that $\omega/c_s(k)k = 1$, the data we have plotted in figure 6.6 is consistent, at short wave lengths with $c_s(k) < c_s$. That is, a wave vector dependent speed of sound less than the speed of sound in the solvent (the region where $\omega/c_s k < 1$). Although this is somewhat counter intuitive, the same phenomenon - on lengths scales where the structure of the fluid cannot be neglected - is observed in simple atomic fluids [28, 29]. It can be accounted for by more sophisticated theories [30]. It should also be pointed out, however, that in simple atomic fluids, the wave vector dependence of the speed of sound is significantly more pronounced. The suspensions we consider here follow classic hydrodynamic behaviour to a far better approximation than do simple fluids.

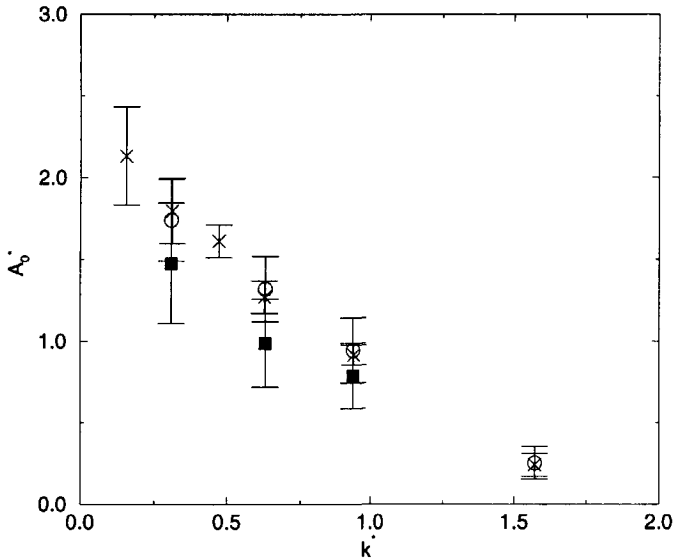


Figure 6.7: The dimensionless initial amplitude A_0^* (defined in the text) of the oscillations observed in the interaction correlation function, plotted as a function of dimensionless wavelength ($k^* = ka$). The data correspond to runs R2, R4 and R6.

6.3.5 The initial amplitude of the correlations

Moving on to the second characteristic of classic hydrodynamic behaviour, the dimensionless initial amplitude A_0^* , is plotted in figure 6.7. It is clear from figures 6.4 and 6.5 that the period of the oscillations is significantly less than the decay rate, so we are justified in comparing our results with the small k expansion (equation 6.13). Examining figure 6.7 we see that the dimensionless initial amplitude is approaching the value 2 as $k \rightarrow 0$, so again we are recovering classic hydrodynamic behaviour in the limit of long wave lengths. However, there is a clear k dependence, with the amplitude decreasing roughly linearly with increasing wave vector. The k dependence is not quadratic, so it cannot be accounted for by the $\mathcal{O}(k^2)$ term appearing in equation 6.13 (which simply reflects the relatively trivial change in the value of exponential decay envelope between the first minimum and first maximum). The k dependence we observe therefore represents behaviour not accounted for by simple hydrodynamics, again manifesting itself on length scales where the structure of the suspension cannot be neglected. One further point illustrated by figure 6.7 is that, following the trend, the amplitude of the oscillations tends to zero at a value $k^* \sim 2$. That is, we observe no collective effects at all for $k^* > 1.75$. Presumably this reflects the fact that the minimum separation of $2a$ between particles essentially defines a maximum wave vector at which particles can interact via sound propagation. Again, the theory outlined above takes no account of this effect.

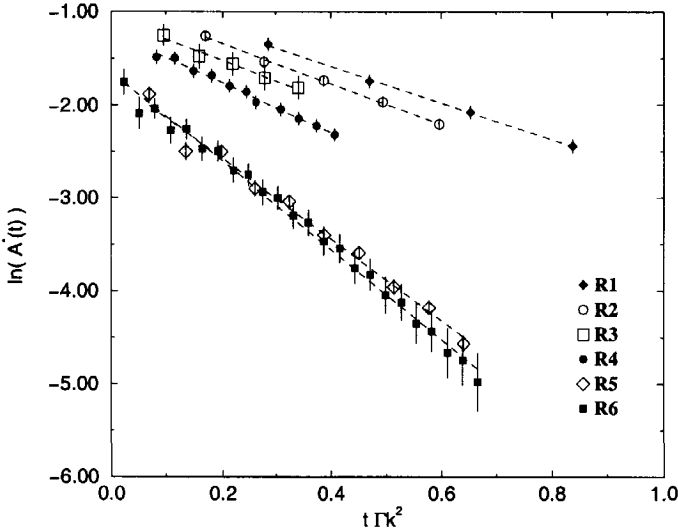


Figure 6.8: Linear-log plot of the dimensionless time-dependent amplitude $A^*(t)$ of the oscillations in the interaction correlation function (defined in the text), as a function of dimensionless time $t\Gamma_0 k^2$. The reduced wave vector k^* was equal to 0.314. Data for all six runs is shown.

set	R1	R2	R3	R4	R5	R6
Γ_ϕ/Γ_0	2.1	2.2	2.0	2.6	4.8	4.4

Table 6.2: The apparent the sound wave attenuation coefficient of the suspension, Γ_ϕ , relative to the solvent value Γ_0 .

6.3.6 The rate of decay of sound induced correlations

Having examined the factors determining the frequency and initial amplitude of the sound induced oscillations, all that remains is to establish what determines the subsequent rate of decay. In figure 6.8 we have plotted, at a reduced wave vector $k^* = 0.314$, the dimensionless time-dependent amplitude as a function of a dimensionless time $t\Gamma_0 k^2$, for all six simulations. Hydrodynamically, this plot should be linear with a slope equal to unity. As figure 6.8 shows, the data are, to a good approximation, linear. The amplitude of the oscillations decays exponentially. However, if we calculate the slopes, by linear regression, the values are not unity. Following the same reasoning applied for the speed of sound, it seems sensible to interpret this as indicating that the sound wave attenuation coefficient in the suspension Γ_ϕ is not the same as the solvent value Γ_0 . That is, we expect the amplitude of the oscillations to decay as $\exp(-\Gamma_\phi k^2 t)$. Having made this assumption, we can calculate values for Γ_ϕ consistent with the data shown in figure 6.8. These values are summarized in table 6.2. As the table shows, for the first four systems (R1, R2, R3, R4) the ratio

Γ_ϕ/Γ_0 takes a roughly constant value between 2.0 and 2.6. For these simulations, the solvent viscosity is greater than the bulk viscosity so, to a first approximation, we can neglect the bulk viscosity and thus $\Gamma_0 \sim 4\nu_0/3$. If we further interpret Γ_ϕ as depending on the suspension viscosity ν_ϕ and the suspension bulk viscosity $\nu_{B\phi}$, *i.e.* $\Gamma_\phi = 4\nu_\phi/3 + \nu_{B\phi}$, this condition corresponds to $\Gamma_\phi/\Gamma_0 = \nu_\phi/\nu_0$ (so long as $\nu_{B\phi}/\nu_B \leq \nu_\phi/\nu_0$). The value of ν_ϕ for suspensions of hard spheres is known. Accurate multipole calculations performed by Ladd [25] give a value $\nu_\phi/\nu_0 = 2.17$ at this volume fraction. The values we obtained for the ratio Γ_ϕ/Γ_0 ($\sim \nu_\phi/\nu_0$) from the first four simulations are roughly equivalent to this value (see table 6.2). It should be noted that, because these simulations use spheres of different radii, the numerical errors are not the same. We expect the run R4, where the radius of the spheres was 8.5 lattice units, to be the most accurate. This simulation gives a value $\Gamma_\phi/\Gamma_0 = 2.6$, somewhat higher than the value quoted above. It is nonetheless clear from table 6.2 that the most anomalous results are those for runs R5 and R6. These runs are characterized by a bulk viscosity greater than the viscosity, and a bulk viscosity similar to the viscosity, respectively. The obvious explanation for this is that the ratio $\nu_{B\phi}/\nu_B$ behaves significantly differently to the ratio ν_ϕ/ν_0 . If we take the values of Γ_ϕ/Γ_0 for these two runs and solve for the two viscosity ratios we find $\nu_\phi/\nu = 2.3$ and $\nu_{B\phi}/\nu_B = 4.8$. If we now return to run R6 and examine the correction due to the non-negligible bulk viscosity then, substituting this value for ν_B we find that $\Gamma_\phi/\Gamma_0 = 2.5$, in better agreement with the value we calculated (2.6). Taken as a whole, our results are therefore consistent with the sound wave attenuation coefficient in the suspension taking the form $\Gamma_\phi = 4\nu_\phi/3 + \nu_{B\phi}$, if $\nu_{B\phi}/\nu_B \sim 4.8$, suggesting that the bulk viscosity of the suspension has a stronger dependence on the volume fraction than does the shear viscosity. It would be useful to test this hypothesis by calculating $\nu_{B\phi}$ directly. Unfortunately, as of yet we have not succeeded in doing so. The above must therefore remain a working hypothesis.

6.3.7 The effect of sound propagation on the wave vector dependent collective diffusion coefficient

We now turn our attention to the contribution the oscillations do, or do not, make to the time integral of $J_I(k, t)$. According to equation 6.12, the compressible contribution to the correlation function makes, on average, no contribution to the time integral. It merely induces oscillations about the incompressible contribution. In figure 6.9 we have plotted the time integral of $J_I(k, t)$, at a reduced wave vector $k^* = 0.314$, as a function of the viscous time scale. Data for five of the six runs are plotted figure 6.9. Data from run R5 is omitted for clarity (it follows the same trend). As the figure shows, for the data obtained from the least compressible simulation (R6), the frequency of the oscillations in $J_I(t)$ is so high that they hardly influence the time integral of the correlation function. The striking thing is, for all the other data where the effects of the oscillations are non negligible, the time integrals clearly oscillate about the same underlying function as run R6. This is despite the fact that, between runs R1 and R6, the compressibility factor varies by a factor of 50. It is

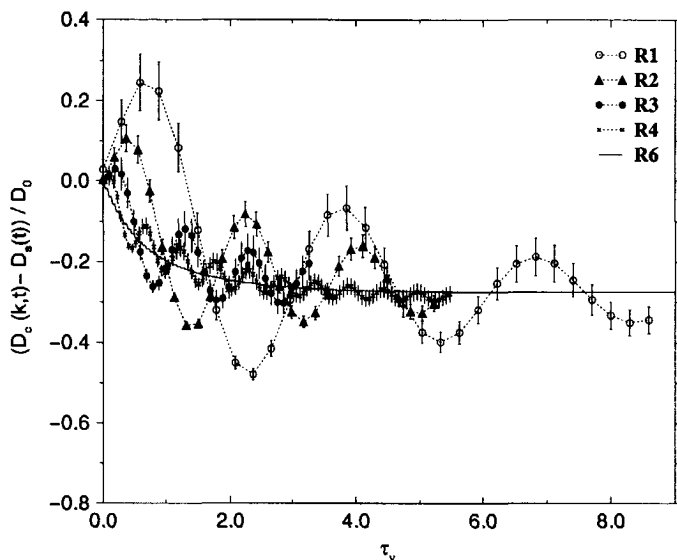


Figure 6.9: Dimensionless time integral of the interaction correlation function. The dimensionless wave vector was 0.314. The results for run *R5* are omitted for clarity.

therefore clear that the correlation function consists of a compressible component which oscillates about zero, and therefore contributes nothing, on average, to the integral, and incompressible component, determined entirely by τ_ν . Although we only show results for $k^* = 0.314$, where the statistical errors are minimal, the same was true for all the wave vectors we studied.

6.4 Discussion

Having carefully examined the role sound plays propagating hydrodynamic interactions, we arrive at the following conclusions. On the dynamics of a single tagged particle in a suspension, the effect of sound is relatively trivial. Sound propagation only influences the dynamics on time scales of the order of the time it takes a sound wave to propagate a distance the order of a particle radius. At longer times, the dynamics of the particle become completely independent of the parameters associated with compressibility. An incompressible theory could, in principle, describe the motion. This is exactly the same kind of behaviour one observes for an isolated colloidal particle. Thus, as far as one particle is concerned, the rest of the suspension behaves in the same way as a simple solvent. This means that sound propagation cannot induce the relatively rapid onset of “effective fluid” behaviour, observed in experiments. Rather, it is more likely that, as speculated in references [4] and [17], this behaviour is more apparent than actual.

If, however, we consider collective motions, that is the ability of one particle to influence the velocity of others, the situation is more complicated. We observe oscillations in the longitudinal current-current correlation function that are clearly the result of sound propagation between the colloidal particles. These oscillations are not restricted to the very short times, characteristic of sound propagating a typical distance in the suspension. Rather, in the limit of small wave vectors ($k \ll 1/a$) the criteria by which these oscillations will be negligible, our results imply, is that $t \gg 1/(k^2\Gamma)$ should be satisfied. Thus, at sufficiently small wave vectors, the influence of sound propagation will always be significant. If we return to our original question, can hydrodynamic interactions propagate at the speed of sound? The answer is, yes. More strictly, a part of the interaction of one particle with its neighbours is governed by the speed of sound and the sound wave attenuation coefficient. Since these are quantities characteristic of sound propagation, this clearly implies a sonic propagation of hydrodynamics interactions. This may seem a little daunting. It would imply that a complete understanding of hydrodynamic interactions would require the development of a full, many body, compressible theory. However, our simulations show that although sound propagation is playing a role, it can be understood relatively simply. At sufficient small wave vectors (the simulations suggest roughly $ka < 0.1$) the effect of sound in a suspension is the same as the effect of sound propagation in a simple fluid. In other words, if one views a colloidal suspension on length scales very much greater than the size of the particles, it behaves in the same way as a generic "structureless" fluid would behave. This can be understood quite simply in terms of what one may term classical hydrodynamics. The only modification required was that the transport coefficients be characteristic of the suspension (speed of sound, bulk and shear viscosity), rather than the solvent. Our simulations suggested that the speed of sound, for a suspension where the colloidal particles occupy 25% of the available volume, is approximately 1.05 times the value for the solvent. The bulk viscosity, on the other hand, appears to be 4.8 times the solvent value. Relative to other transport coefficients, this applies a very weak dependence on volume fraction for the former and a very strong dependence for the latter. The scattering of sound waves by the particles is, it seems, a more effective means of dissipating density fluctuations than propagating them.

We concluded above that hydrodynamic interactions can propagate at the speed of sound. Here we add the caveat that it depends somewhat on what we take as the definition of a hydrodynamic interaction. Our results show that the motion of one particle can influence another by sound propagation. However, we might prefer to define a hydrodynamic interaction as the motion of one particle influencing another *on average*. If we took this definition we would come to a different conclusion. Looking at the integrated influence of sound propagation we found no effect. On average sound does nothing but induce wiggles about the incompressible result. It is still, therefore, the viscous diffusion mechanism that determines the time scale on which the interactions have a net effect - the "relaxation" time scale on which the transport coefficients asymptote. Consequently, we find no evidence to support the speed of sound propagation mechanism suggested by Ladd *et al.* to explain the

different relaxation times observed in computer simulations and experiment. The origin of this discrepancy remains unknown.

Based on our results we can nonetheless speculate as to when sound induced oscillations should be observable experimentally. To do so we return to the time-dependent transport coefficients. The quantity measured experimentally, in photo-correlation spectroscopy for example, is the dynamic structure factor $S(k, t)$. The decay of the dynamic structure factor, to lowest order in k is given by,

$$S(k, t) = S(k, 0) \exp \left(-k^2 \int_0^t D(k, t') dt' \right) \quad (6.18)$$

where

$$D(k, t) = \int_0^t J(k, t') dt' \quad (6.19)$$

If we approximate the non-oscillatory components of $J(k, t)$ by their asymptotic values (valid for times $t > a^2/\nu_0$) we have

$$\int_0^t D(k, t) \simeq D(k, t)t + \int_0^t \int_0^{t'} J_i^s(k, t'') dt'' dt' \quad (6.20)$$

In order for the oscillations in the second term to be experimentally observable the condition

$$\frac{\int_0^t \int_0^{t'} J_i^s(k, t'') dt'' dt'}{D_0 t} \sim 1 \quad (6.21)$$

should be satisfied. Here D_0 is the Stokes-Einstein diffusion coefficient characteristic of the dilute limit. Substituting the hydrodynamic result for $J_i^s(k, t)$ (equation 6.12) and performing the double integration this corresponds to the condition

$$t \sim \frac{\nu_0}{(c_s k^*)^2} \quad (6.22)$$

We have also taken the limit that $k^* \ll \alpha$ but, as we have seen, for any colloidal suspension the compressibility factor α is greater than unity so this only corresponds to the condition $k^* < 1$. The latter restriction is in any case necessary for the simple hydrodynamic result to be valid. The conclusion we therefore arrive at is that sound induced oscillations in the dynamics structure should be observable at short times. To see how short we can substitute values for c_s and ν_0 typical of water at room temperature. This yields $t < 10^{-10} s$ at $k^* = 10^{-1}$, which is rather short, or more reasonably $t < 10^{-6} s$ at $k^* = 10^{-3}$. We should also point out that the dynamic structure factor decays on a time scale $t \sim 1/(k^2 D(k))$ and that, unless the colloidal particles are very small ($a \sim 1 nm$), the time regime defined by equation 6.22 is very much shorter. Thus, any effects of sound propagation on the dynamic structure factor would show up as rapid oscillation about the initial value, rather than any modulation of the decay.

Bibliography

- [1] D.J. Pine, D.A. Weitz, P.M. Chaikin and B. Herbolzheimer, *Phys. Rev. Lett.* **60**, 1134 (1988).
- [2] S. Fraden and G. Maret, *Phys. Rev. Lett.* **65**, 512 (1990).
- [3] S.T. Milner and A.J. Liu, *Phys. Rev.* **E48**, 449 (1993).
- [4] H.J.H. Clercx, *Phys. Rev.* **E56**, 2950 (1997).
- [5] M.H.J. Hagen, I. Pagonabarraga, C. P. Lowe and D. Frenkel, *Phys. Rev. Lett.* **78**, 3785 (1997).
- [6] I. Pagonabarraga, M.H.J. Hagen, C.P. Lowe and D. Frenkel, *Phys. Rev.* **E 59**, 4459 (1999).
- [7] H. Mori, *Prog. Theor. Phys.* **34**, 399 (1965).
- [8] B. J. Berne and G. D. Harp, *Adv. Chem. Phys.* **17**, 63 (1970).
- [9] J.M. Deutch and I. Oppenheim, *Faraday Discuss. Chem Soc.* **83**, 1 (1987).
- [10] J. A. McLennan, "Introduction to Non-equilibrium Statistical Mechanics", Prentice Hall, Englewood Cliffs, New Jersey (1989).
- [11] D. Bedeaux and P. Mazur, *Physica* **78**, 505 (1974).
- [12] A.J. Masters, *Mol. Phys.* **57**, 303 (1986).
- [13] J.X. Zhu et all, *Phys. Rev. Lett.* **68**, 2559 (1992).
- [14] M.H. Kao, A.G. Yodh and D.J. Pine, *Phys. Rev. Lett.* **70**, 242 (1993).
- [15] A.J.C. Ladd, *Phys. Rev. Lett.* **70**, 1339 (1993).
- [16] A.J.C. Ladd, *J. Fluid Mech.* **271**, 311 (1994).
- [17] C.P. Lowe and D. Frenkel, *Phys. Rev.* **E54**, 2704 (1996).
- [18] P. Español, M.A. Rubio and I. Zúñiga, *Phys. Rev. E* **51**, 803 (1995).
- [19] P. Español, *Physica A* **214**, 185 (1995).
- [20] A.J.C. Ladd, H. Gang, J.X. Zhu and D.A. Weitz, *Phys. Rev.* **E52**, 6550 (1995).
- [21] A. J. C. Ladd, H. Gang, J. X. Zhu and D. A. Weitz, *Phys. Rev. Lett.* **74**, 318 (1995).
- [22] A. J. C. Ladd, *J. Fluid. Mech.* **271**, 285 (1994).
- [23] M.H.J. Hagen, D. Frenkel and C. P. Lowe, *Physica A*, in press (1999).

- [24] C.W.J. Beenakker and P. Mazur, *physica* **126A**, 349 (1984).
- [25] A.J.C. Ladd, *J. Chem. Phys.* **93**, 3484 (1990).
- [26] J. P. Hansen and I. R. McDonald, *Theory of simple liquids*, Academic Press Limited, 2nd edition (1990).
- [27] J.-P. Boon and S. Yip, "*Molecular Hydrodynamics*", McGraw-Hill, New York (1980).
- [28] K. Sköld and K. E. Larsson, *Phys. Rev.* **161**, 102 (1967).
- [29] A. Rahman, in "*Neutron Inelastic Scattering*" **1**, International Atomic Energy Agency, Vienna, 561 (1968).
- [30] C.-H Chung and S. Yip, *Phys. Lett.* **50A**, 175 (1974).



Summary

The lattice-Boltzmann method is a simulation method to study colloidal particle dynamics. In this method the colloidal particles are incorporated in a discrete lattice-Boltzmann fluid model by simple Eulerian discretized equations of motion. To represent the complex, collective particle dynamics properly, several ten thousands of colloidal particles, implying an astronomic number of solvent molecules to deal with as well, must be included in the simulation, which is perfectly possible within the lattice-Boltzmann technique. An additional advantage is that the full time regime can be studied. These advantages do not come cheap; the calculations require large computer resources. Besides, an accurate and robust method for simulating the motion of truly solid colloidal particles with the same density as the fluid is still lacking.

The most powerful computers nowadays have a parallel architecture. Due to the parallel nature of the lattice-Boltzmann scheme a parallel calculational scheme will speed up the calculations. Therefore the code is parallelized and the scalable performance is tested as a function of the number of processors for two given parallel computer systems.

The first part of this thesis describes two algorithm improvements. The first concerns a way to greatly reduce the demand for memory, affecting both main memory and hard disk. This storage reduction is particularly effective when the collision operator associated with a kinematic fluid viscosity of $1/6$ is used, resulting in a storage reduction of more than 75%, with which most of our simulations are carried out. This being the case allows the system sizes to grow by a factor of four. We have shown that this storage reduced algorithm is efficient and highly parallel scalable.

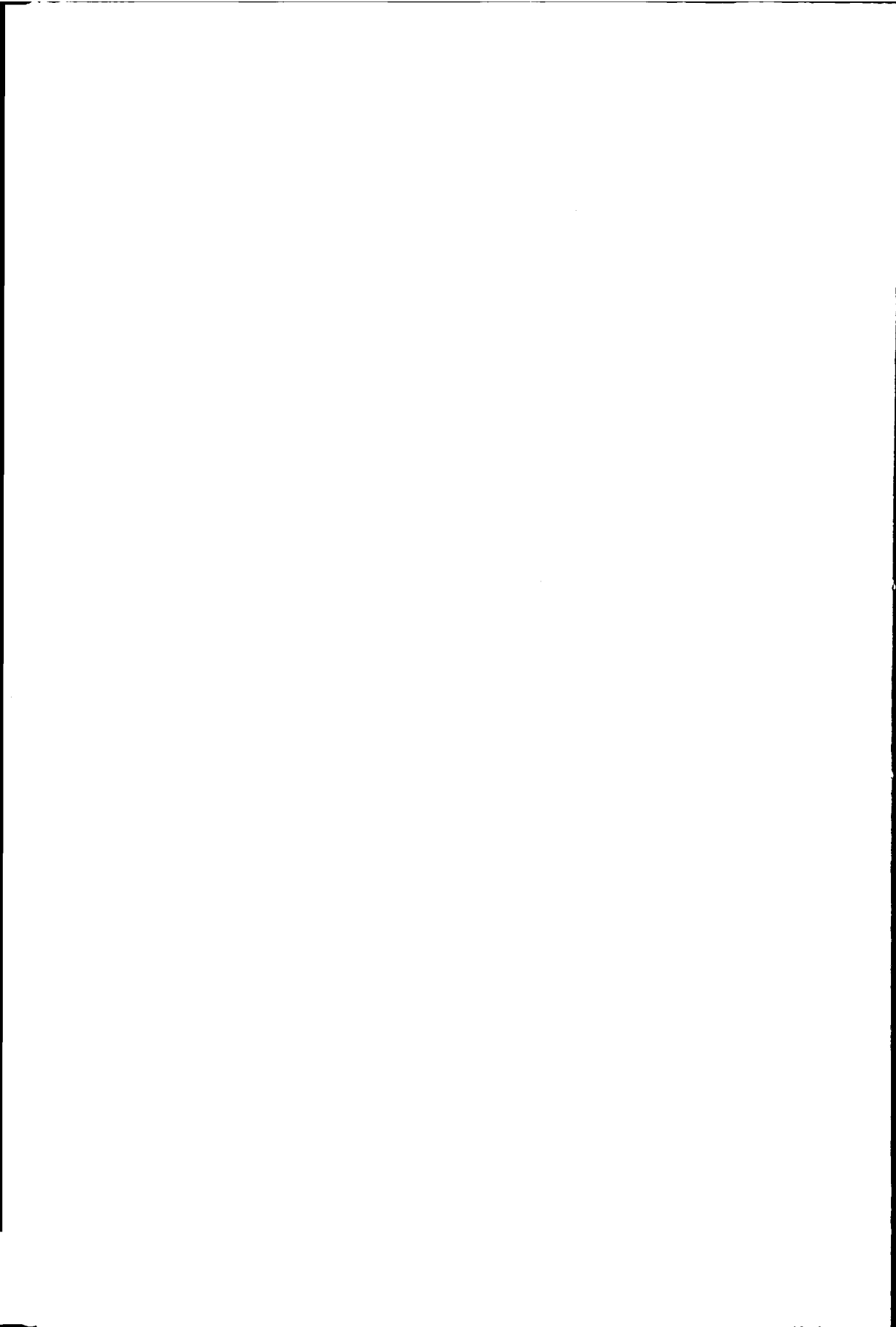
The second algorithm improvement deals with a method for truly solid particle motion, incorporated in the lattice-Boltzmann fluid. The method removes the effect of the internal fluid. It has been demonstrated that the correct time-dependent rotational and translational dynamics of a single solid particle were recovered. For a concentrated suspension we have showed that an additional inertia from the internal fluid contributed to the effective density ratio of the suspension and that the

kinematic viscosity does not display the same dependence on volume fraction as it should. It has been shown that the new method recovers the correct kinematic viscosity up to high volume fractions.

The second part of this thesis is devoted to two applications that have been studied using this storage reduced and removed effect of internal fluid algorithm. The first concerns calculating a transport coefficient, namely the high frequency low shear rate viscosity for both monodisperse and bimodal hard sphere suspensions, using a method that only requires the dynamics to be simulated for a very short period of time. For monodisperse suspensions we found good agreement with other simulations, experiment and theory for volume fractions up to 45%. Furthermore, we examined the wave vector dependence of the viscosity and found that simple Newtonian fluid behaviour appears at spatial length scales very much greater than the size of the colloidal particles, i.e. $k^* < 0.1$, indicating that one may expect a somewhat lower viscosity when considering for example tube flow. Finally, the similarity found for the k^* dependence of a suspension and that of a hard sphere fluid suggests that the k^* dependence of a simple atomic fluid has its origin more in the structure than in the hydrodynamics. For bimodal suspensions at moderate volume fractions and size ratio 2.6, the commonly observed viscosity reduction has been shown, with its minimum showing up for compositions rich in large spheres. To our knowledge the first time this has been achieved in three dimensional simulation. To study higher volume fractions and higher size ratios further hardware and or algorithmic improvements are needed.

The second application is investigating the role sound plays in propagating hydrodynamic interactions. It appears that on the dynamics of a single particle in a suspension, the effect of sound is negligible. Already on time-scales of ~ 1 ns and longer, the dynamics of the particle becomes completely independent of the compressibility theory and an incompressible theory could, in principle, describe the motion. When considering collective motions the situation seems more complicated. We observed oscillations in the longitudinal current-current correlation function that are clearly the result of sound propagation between the colloidal particles. These oscillations are not restricted to the very short sonic times. For small wave vectors ($k \ll 1/a$) the criteria by which these oscillations will be negligible, our results imply $t \gg 1/(k^2\Gamma)$. Thus at small enough wave vectors the influence of sound propagation will always be significant. However, although sound is playing a role it could be understood relatively simple. For small enough wave vectors (roughly $ka < 0.1$) simple fluid behaviour has been recovered again and thus on length scales very much greater than the size of the particles, the suspension behaves in the same way as a generic "structureless" fluid would behave. The only modification required was that the transport coefficients (speed of sound, bulk and shear viscosity) of the solvent have to be replaced by the values of the suspension. It has been shown that, at a volume fraction of 25%, the speed of sound is 1.05 times the value for the solvent and the bulk viscosity 4.8 times the solvent value. This means a relative weak dependence on volume fraction for the former and a relative strong dependence for the latter. Looking at the integrated influence of sound propagation it appeared

that on average sound does nothing but induce wiggles about the incompressible result. It is still the viscous diffusion mechanism that determines the relaxation time scale on which the transport coefficients asymptote. Speculating as to when the sound induced oscillations should be observable experimentally, we concluded that any sound effects would show up as rapid oscillations unless the colloidal particles are very small ($a \sim 1nm$).



Samenvatting

De rooster-Boltzmann methode is een geschikte simulatie methode om de dynamica van colloïdale deeltjes in evenwicht te bestuderen. Deze colloïdale deeltjes zijn via simpele Euleriaanse bewegingsvergelijkingen geïntegreerd in een zeer gediscretiseerd vloeistofmodel, wat de rooster-Boltzmann methode is. Omdat de dynamica tussen de colloïdale deeltjes zeer complex en collectief van aard is, zijn systeemgroottes van enkele tienduizenden colloïdale deeltjes vereist. Dit is zeer goed mogelijk met de rooster-Boltzmann methode die het bijbehorende astronomische aantal vloeistof moleculen op geschikte wijze behandelt. Een bijkomend voordeel is dat het gehele, natuurlijke tijdsverloop bestudeerd kan worden. Deze voordelen hebben hun prijs; de berekeningen vergen veel computertijd en geheugenruimte. Daarnaast ontbreekt een nauwkeurige en robuuste methode voor de beweging van echte ondoorlaatbare zwevende harde bollen nog steeds.

De krachtigste computers van deze tijd hebben een parallelle architectuur. Vanwege de uiterst parallelle natuur van de rooster-Boltzmann methode zal een parallel rekenschema de berekeningen behoorlijk versnellen. Daarom is de computercode geparalleliseerd en de parallelle prestaties getest op schaalbaarheid als functie van het aantal processoren. Dit is gedaan voor twee gegeven parallelle systemen.

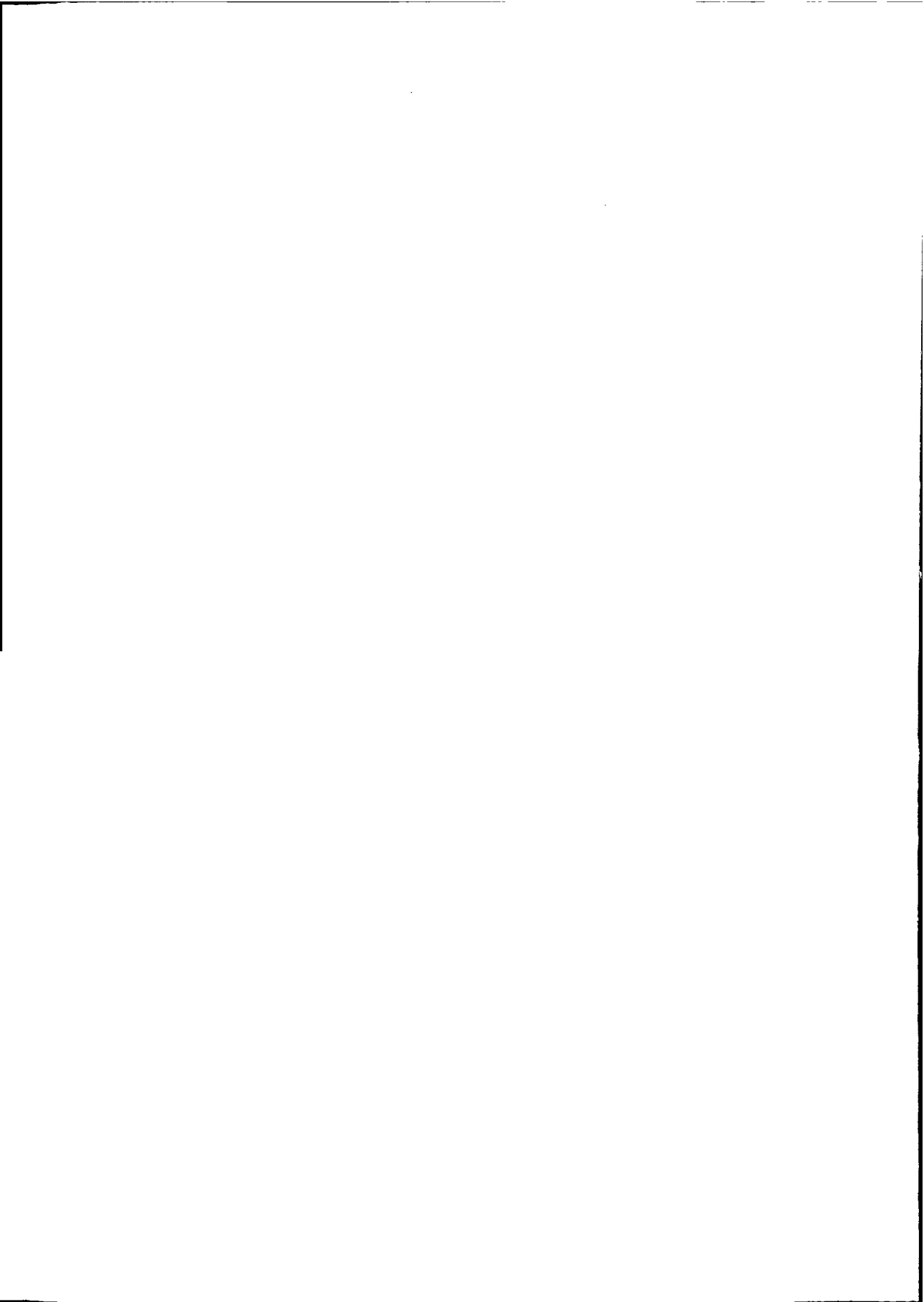
Het eerste deel van dit proefschrift beschrijft twee algoritmiek verbeteringen. De eerste betreft een manier om het gigantische geheugengebruik van deze methode terug te dringen, zowel voor het werkgeheugen als de harde schijf. Dit werkt vooral in het geval de botsingsregels voor de kinematische viscositeit van $1/6$ voor de vloeistof worden gebruikt, een viscositeit waarmee verreweg de meeste simulaties zijn uitgevoerd. In dit geval kan het geheugengebruik met meer dan 75% worden teruggebracht. En dus kan de systeemgrootte verviervoudigd worden en daarmee ook het aantal te simuleren colloïdale deeltjes. Vervolgens worden de prestaties van dit parallelle en opslaggereducente algoritme besproken.

De tweede algoritme verbetering betreft de beweging van de colloïdale deeltjes in de rooster-Boltzmann vloeistof. De methode verwijdert het onnatuurlijke effect dat de interne vloeistof in de bol zou kunnen hebben, zoals een extra traagheidskracht

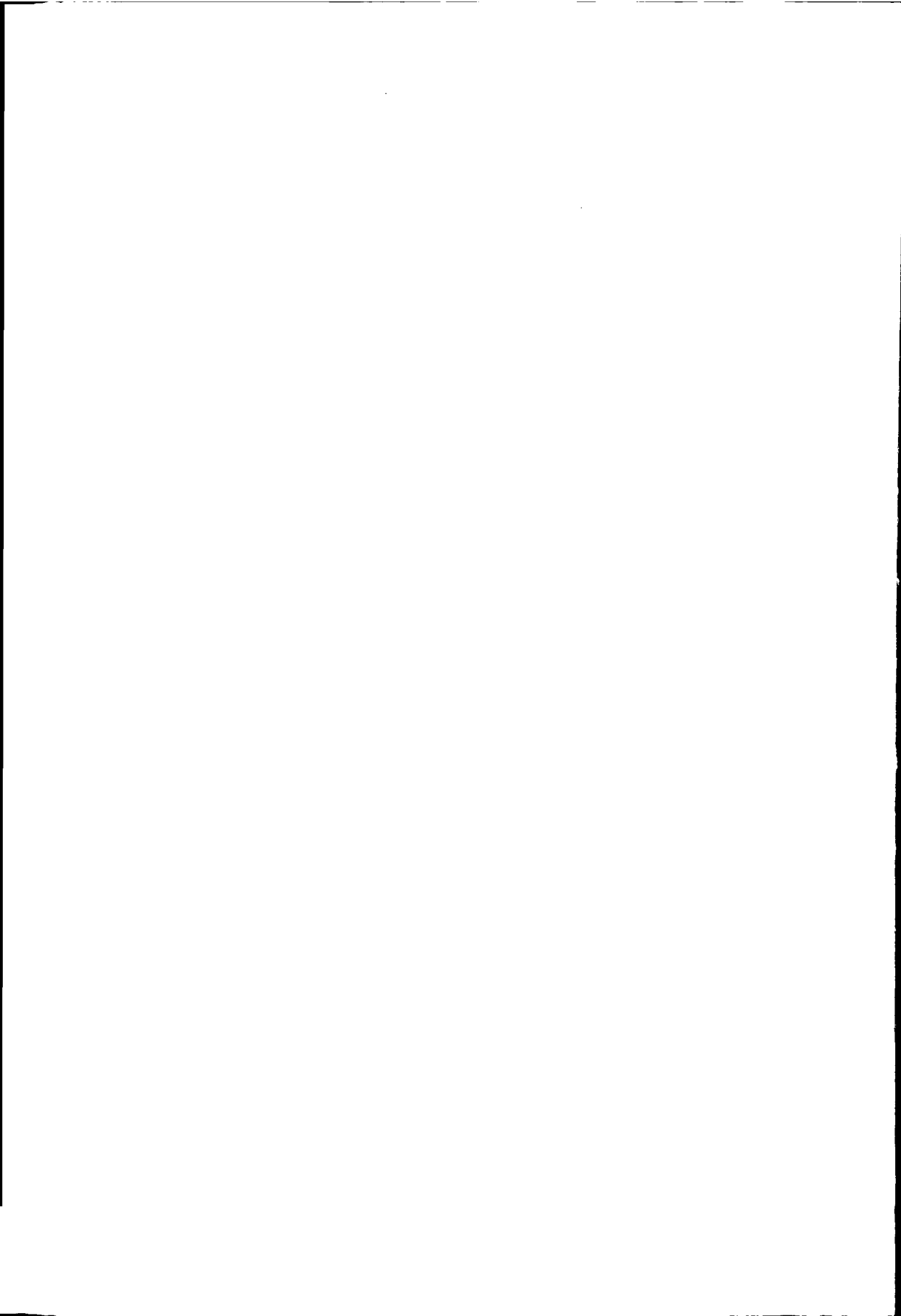
vanwege de extra massa. De berekeningen wijzen uit dat de correcte, tijdafhankelijke rotatie en translatie snelheden worden gevonden met deze nieuwe methode. Voor een geconcentreerde suspensie blijkt dat de interne vloeistof zorgt voor een andere kinematische viscositeits afhankelijkheid van de deeltjesconcentratie dan zou moeten. Met de nieuwe methode wordt de juiste kinematische viscositeit verkregen tot hoge deeltjesconcentraties.

In het tweede deel van dit proefschrift worden twee toepassingen behandeld die zijn bestudeerd met dit opslaggereduceerde algoritme en waarin het effect van de interne vloeistof is verwijderd. De eerste toepassing is een berekening van een transport coefficient, namelijk de viscositeit voor korte tijden en onder lage schuifspanning, zowel voor monodisperse als bidisperse systemen, gebruikmakend van een meetmethode die alleen de simulatie van de dynamica op zeer korte tijden behoeft. Voor monodisperse systemen vertonen de berekeningen goede overeenkomsten met theory en experiment, tot hoge deeltjesconcentraties (45%). Vervolgens hebben we de golfengte afhankelijkheid getoetst en gevonden dat puur Newtoniaans vloeistof gedrag optreedt op lengteschalen die veel groter zijn dan de colloïdale deeltjes zelf, dat is $k^* < 0.1$. Dit geeft aan dat we een lagere viscositeit kunnen verwachten in bijvoorbeeld cilinder stroming. Tot slot volgt een overeenkomst met een harde bol vloeistof voor de golfengte afhankelijkheid van de viscositeit. Deze overeenkomst suggereert dat de oorzaak van de golfengte afhankelijkheid gezocht moet worden in de structuur van de vloeistof en niet in de hydrodynamische interacties. Voor bidisperse systemen met relatieve grootteverhouding 2.6 en een redelijke deeltjesconcentratie (30% – 35%), vertonen de rooster-Boltzmann simulaties zichtbare viscositeitsreducties. Het minimum hiervan bevindt zich steeds aan de kant van grote concentraties van grote deeltjes. Voor zover bekend is dit niet eerder bereikt in een drie dimensionale simulatie. Echter om hogere concentraties en grotere grootteverhoudingen te simuleren zijn verdere hardware- en of algoritmeaanpassingen nodig.

De tweede toepassing is het bepalen welke rol geluid en daarmee de compressibiliteit van de suspensie, speelt in de voortplanting van hydrodynamische interacties. Het blijkt dat voor een geïsoleerd deeltje in een suspensie dit effect verwaarloosbaar is. Reeds vanaf zeer korte tijden ~ 1 ns raakt de dynamica van het deeltje compleet onafhankelijk van de compressibiliteits theory en zou een incompressibele theory, waarbij wordt aangenomen dat de geluidssnelheid oneindig is, in principe voldoen. Echter, wanneer we de collectieve bewegingen van de deeltjes beschouwen is de situatie veel gecompliceerder. Er doen zich oscillaties voor in de longitudinale snelheids correlatie functies van de deeltjes die duidelijk een resultaat zijn van geluidspropagatie tussen de deeltjes. Deze oscillaties duren langer dan de tijd die geluid nodig heeft om een deeltjesdiameter af te leggen. Onze berekeningen wijzen uit dat deze oscillaties voor kleine golfvectors ($k \ll 1/a$) pas verwaarloosbaar zijn voor tijden $t \gg 1/(k^2\Gamma)$. Dit betekent dat voor kleine golfvectors de invloed van geluidspropagatie altijd significant is. Gelukkig kan de geluidspropagatie eenvoudig worden voorgesteld. In het geval van kleine (ruwweg $ka < 0.1$) golfvectors treedt effectief vloeistof gedrag op, wat betekent dat de suspensie zich gedraagt als een pure, simpele atomaire vloeistof. Het enige vereiste is wel dat de vloeistofparameters ver-

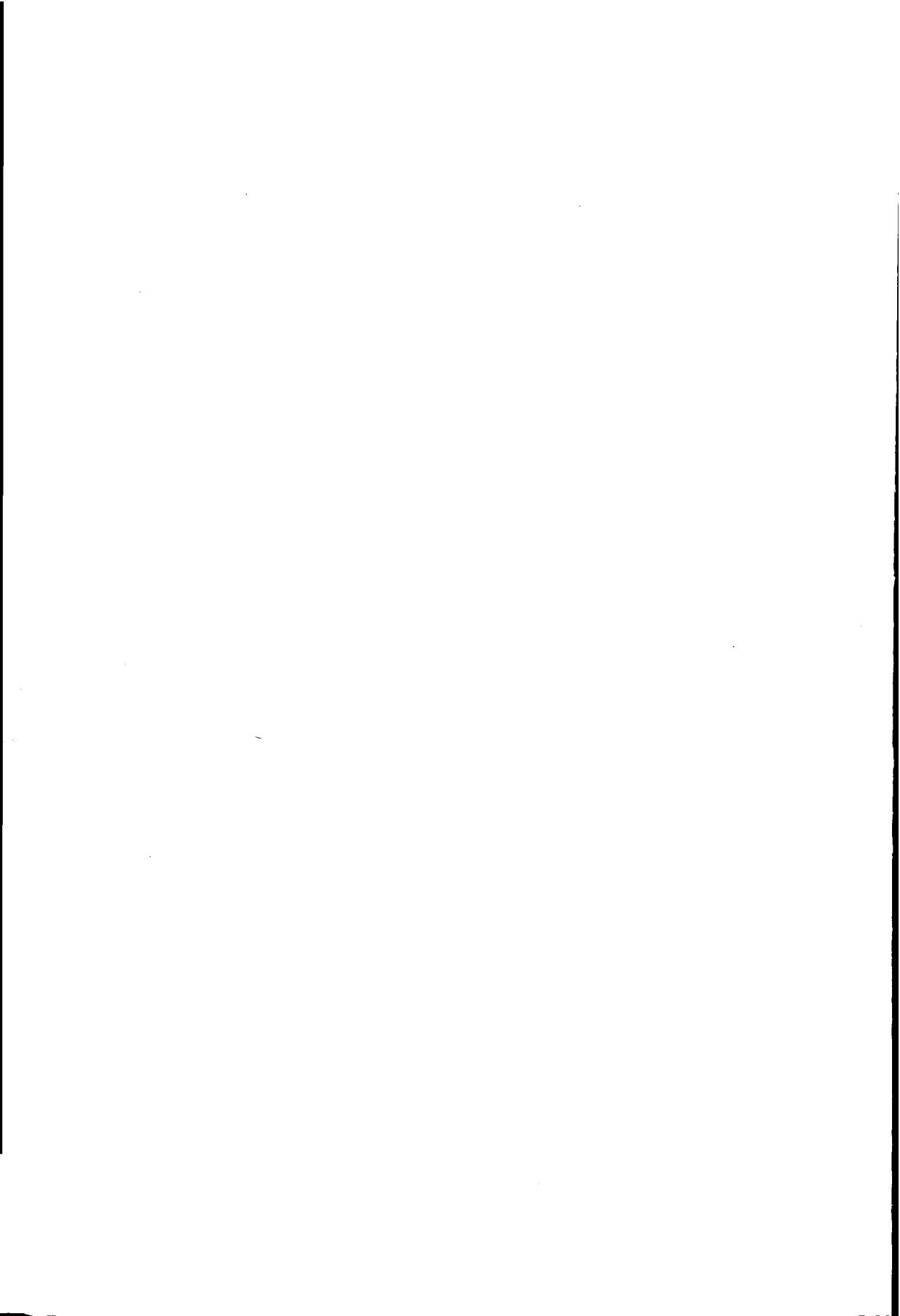


vangen dienen te worden door de suspensieparameters. Bij een deeltjesconcentratie van 25% blijkt de geluidssnelheid 1.05 keer de vloeistofsnelheid te zijn en de bulk viscositeit 4.8 keer de vloeistof waarde. Dit betekent een relatief zwakke afhankelijkheid van de concentratie voor de geluidssnelheid en een relatief sterke voor de bulk viscositeit. Wanneer we naar de geïntegreerde effecten van geluidspropagatie kijken blijkt dat geluid slechts kleine oscillaties veroorzaakt rondom het incompressibele resultaat. Het blijft nog steeds het diffusiemechanisme dat bepalend is voor de asymptotische benadering van de transport coëfficiënten. Concluderend kunnen we stellen dat geluidseffecten zich voordoen in de vorm van snelle oscillaties rondom het incompressibele resultaat en meetbaar worden voor kleine colloïdale deeltjes ($a \sim 1nm$).



Epilogue

Finis coronas opus. It is really finished now. At this place I like to thank everybody who has contributed to the completion of this thesis. In the first place I like to thank Simon de Leeuw, my promotor, for adopting me when he became a professor of the computational physics group, for the freedom he gave me in my research and for critically reading the manuscript. Secondly, I'd like to thank Loek Bakker, "toegevoegd promotor", for the fruitful and plentiful discussions we had about the computer algorithm and everything, the high-tech working environment he took care off and for his never ending optimistic view on life. It was a special time. Next, I thank Christopher Lowe for sharing his knowledge and experiences, and for improving the quality of this thesis by getting rid of all the nonsense which I put in. Without him the results would not be there or much later. I want to thank all my colleagues, especially the present and previous members of the computational physics group for their participation in bringing this project to a good end and all other ways they have contributed to this thesis. In particular I would thank Berend van Wachem, Marcel Molenaar and Frans van Gool for their fruitful collaboration. HP α C is kindly acknowledged for providing computing time and support. Also I'd like to thank Frans Berwald for providing support on the DEMOS. Maria thank you for taking care of official stuff for me. I am grateful to Servaas van der Heijden who supported me debugging some sunday afternoons, when incidentally the parallel code crashed. I thank my parents for kicking me into the world some odd years ago and always supporting me after that. I'll finish by thanking all my friends for allowing me to be absent (mentally as well as physically) the last few years. Last but not least I would like to thank Harry Pennekamp, who supported me fully through the last years and I trust many years to come.



Curriculum Vitae

On may 12th 1969, I was born in Beesel (limburg), in The Netherlands. After receiving the "Gymnasium B" degree at the "Bisschoppelijk College Broekhin" school in Roermond, I started studying Applied Physics at the Delft University of Technology. The batchelor degree I received in september 1989 and after completing the compulsory part with main subjects on physics and informatics, I started my research year of which the subject was the design and implementation of a special-purpose computer to accelerate lattice-gas simulations a lot compared to the expensive and commercial available general-purpose supercomputers, supervised by dr. ir. A.F. Bakker. I completed this study in december 1993. In January 1994, I started working as a PhD student. This PhD research was performed within the Computational Physics group of the Delft University of Technology, supervised by prof. dr. S.W. de Leeuw and in cooperation with dr. C.P. Lowe. The results of this research have been described in this thesis.

